International Scientific-Technical and Production Journal

The Paton WELDING JOURNAL

November 2005 # 11

English translation of the monthly «Avtomaticheskaya Svarka» (Automatic Welding) journal published in Russian since 1948

Founders: *E.O. Paton Electric Welding Institute of the NAS of Ukraine*
International Association «Welding»

Publisher: *International Association «Welding»*

Address:
E.O. Paton Electric Welding Institute,
International Association «Welding»,
11, Bozhenko str., 03680, Kyiv, Ukraine
Tel.: (38044) 287 67 57
Fax: (38044) 528 04 86
E-mail: journal@paton.kiev.ua
http://www.nas.gov.ua/pwj

State Registration Certificate
KV 4790 of 09.01.2001

Subscriptions:
$324, 12 issues per year,
postage and packaging included.
Back issues available.

CONTENTS

TO THE ISSUE OF INTERMITTENT SOLIDIFICATION OF WELD METAL*

V.I. MAKHNENKO and **G.Y. SAPRYKINA**
E.O. Paton Electric Welding Institute, NASU, Kiev, Ukraine

The issue of intermittent solidification of the weld pool metal is considered, which was very actively discussed by specialists in 1970s. The authors propose, without laying claim to comprehensive solution, a phenomenological model of the readily observed facts.

Keywords: *arc welding, weld pool, intermittent solidification, phenomenological model, weld metal, laminar structure, latent heat*

In fusion welding quality of a weld metal frequently depends upon conditions of primary solidification, especially for such structural materials as aluminium alloys and austenite steels. Primary solidification of a weld metal of these materials determines the degree of local chemical heterogeneity, grain size, risk of hot crack formation, etc. That's why the issues of primary solidification of the weld pool metal attracted [1, 2, etc.] and continue to attract at present [3–5, etc.] rather high attention of researchers. One of the least clear issues of primary solidification of the weld pool metal is so called intermittent solidification observed in special experiments [2, 5, 6], traces of which may be rather easily seen on simple microsection metallographic specimens of a weld metal. Examples of traces are shown in Figure 1, *a–d*, and intermittent solidification — in Figure 1, *e, f*. In Figure 1, *a–d*, layers of solidification separated by boundaries, in which solidification rate equals zero, are seen.

In low-carbon steel after γ–α transformation in a weld metal solidification layers are, naturally, seen less clearly. In Figure 1, *e, f*, the results of rapid filming at a specific moment (condition) of a weld pool made it possible for the authors to observe process of intermittent solidification depending upon a welding speed. Observed in [1] real rates of solidification essentially differ from the classical ideas, which proceed from Figure 2 at

$$v_{mean} = v_w \cos \alpha, \qquad (1)$$

where v_{mean} is the mean rate of solidification according to the «classical» mechanism.

There is no for a time being explanation to this fact, which cardinally changes our ideas on primary solidification of a weld pool. In this work an attempt is made to find explanation of this within the framework of a phenomenological model of the process.

Proposed phenomenological model of a weld pool metal solidification. The proposed model is based on the assumption that in the zone of sufficiently high temperature gradients the «classical» mechanism of solidification, when speed of the transformation front movement is determined by change of a spatial position of the temperature $T_{sol} \approx T_S + T_L/2$ (T_S is the solidus temperature; T_L is the weld metal liquidus temperature), is forced out by the «martensite» mechanism, at which solidification starts at a certain overcooling, i.e. at the temperature $T_{st} < T_{sol}$, and finishes at a respective overheating, i.e. at the temperature $T_{fin} > T_{sol}$.

So, within the temperature range T_{st}–T_{fin} solidification process is irreversible and proceeds at a rather high rate (as well as martensite transformation of austenite in steels at temperatures below T_{st}). Mean rate of solidification front movement according to the «martensite» mechanism v_m should be associated with solidification rate v_{sol} according to the condition (1) $v_m = v_{sol}\xi_m$, where $\xi_m \geq 1.0$. As far as solidification process is connected with emission of latent heat, temperature at the solidification front may increase, thus creating prerequisite for a stop, if it achieves temperature T_{fin}. There is an approximate dependence from [4], by which it is possible to estimate temperature increment $\Delta T(h)$ at the end of the solidification layer of h thickness, i.e.

$$\Delta T(h) = \frac{q_{lat}}{c}\sqrt{\frac{h v_m}{\pi a}} - w\frac{h}{v_m} + G h, \qquad (2)$$

where $\Delta T(h) = T_{fin} - T_{st}$; q_{lat} is the latent heat of solidification, J/g; c is the heat capacity, J/(g·°C); a is the thermal diffusivity of a material, cm^2/s; w is the cooling rate in the solidification zone, °C/s; G is the temperature gradient in the same zone, °C/cm (w and G are macroscopic characteristics in absolute magnitude). Parameter w changes from zero in a fusion zone to, approximately, T_{melt} $(v/2a)$ in tail part of the weld pool, which moves at a speed v. Gradient of temperatures G is vise versa maximal in the fusion zone and minimal in tail part of a weld pool (gradient of temperatures near boundary of fusion on the side of liquid part of a weld pool is meant). If liquid metal

*On the basis of materials of the Second International Conference «Mathematical Modelling and Information Technologies in Welding and Related Processes» (September 13–17, 2004, Katsiveli, Crimea, Ukraine).

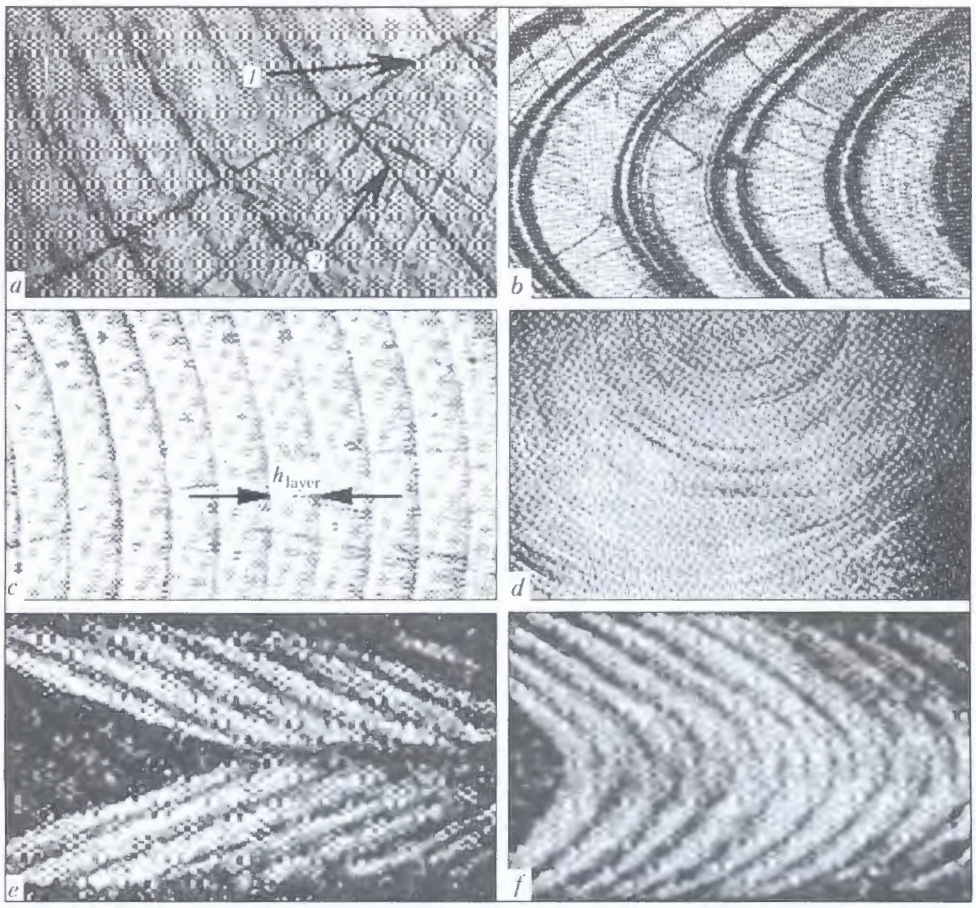

Figure 1. Laminar structure of metal of welds performed by fusion welding: *a*, *b* — aluminium AV000 [5, 6]; *c* — pure aluminium [6]; *d* — low-carbon steel [2]; *e*, *f* — steel Kh18N10T at v_w = 31.3 and 11 m/h, respectively [1]; *1* — boundary of columnar crystallites; *2* — traces of solidification fronts; h_{layer} — thickness of solidification layer

is energetically mixed in a weld pool, it is quite reasonable to consider that in equation (2) $G \approx 0$ and thickness of a layer h is determined by the dependence

$$\sqrt{\frac{hv_m}{a}} = \frac{2\sqrt{\pi}c\Delta T}{q_{lat}(1+\sqrt{1-Aw})}, \quad (3)$$

where

$$A = \frac{4\pi ac^2}{q_{lat}^2 v_m^2}\Delta T. \quad (4)$$

Dependence (3) is valid if $Aw \le 1$, otherwise process of intermittent solidification is disturbed. For tail part of a weld pool

$$w \approx T_{melt}\frac{v^2}{Aa}. \quad (5)$$

In this case condition $Aw \le 1$ is presented, respectively, in the form

$$v_m \ge v_w \frac{\sqrt{4\pi T_{melt}\Delta T}}{q_{lat}}c. \quad (6)$$

Having assumed for aluminium q_{lat} = 407 J/g, c = = 1.08 J/(g·°C), $\Delta T \approx$ 59 °C, T_{melt} = 630 °C, we shall obtain $v_m \ge v_w \cdot 1.81$.

Experimental data on solidification layers in tail part of a weld pool obtained during welding of pure aluminium without filler metal for v_w = 15 m/h are given in Figure 1, *c*, and dependence of parameter h upon various v_w — in *Figure 3*.

If we assume according to Figure 3 that speed v_w, at which intermittence is disturbed in tail part of a weld pool, equals approximately 56 m/h, then $v_m \approx$ ≈ 2.8–3.0 cm/s. Hence, $A_w = 0.365v_w^2$ at v_m = = 3.0 cm/s and, respectively,

$$h = \frac{0.3a}{3(1+\sqrt{1-0.365v_w^2})^2}. \quad (7)$$

Having substituted different values v_w in (7) at a = 0.9 cm/s^2, we'll obtain the following calculated

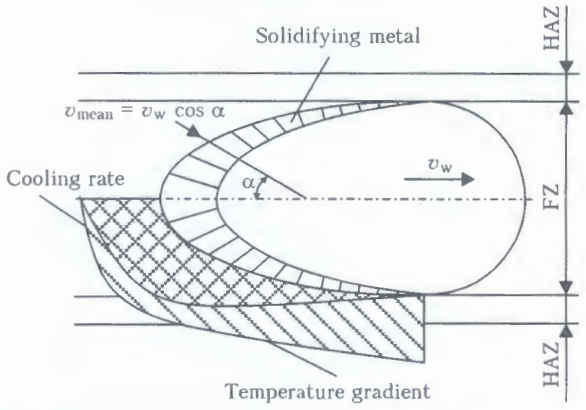

Figure 2. Scheme of moving weld pool and metal solidification

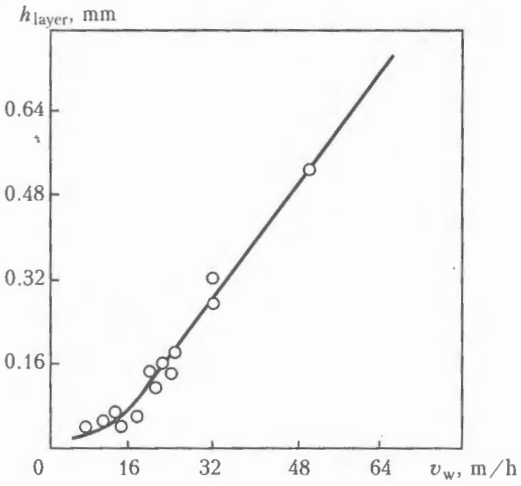

Figure 3. Influence of welding speed on thickness of solidification layer

and experimental thicknesses of solidification layers depending upon a welding speed:

v_w, cm/s	0.5	0.8	1.0	1.2	1.33	1.5
h_{calc}, mm	0.24	0.25	0.286	0.32	0.36	0.46
h_{exp}, mm	0.14	0.2	0.33	0.4	0.5	0.56

As we can see, this rather simple calculation matches quite well with the experiment from [6] for tail part of a weld pool, where temperature gradient G is not high and its contribution into h is small in comparison with the cooling rate w.

For obtaining respective estimations for a fusion zone, in which the gradients are high, numeric algorithm was used, the essence of which consists in the following.

Solidification process was considered within a special interval $l = 3(T_L - T_S)/G$. Solidification rate according to the «martensite» mechanism significantly exceeds solidification rate according to the «classical» mechanism, i.e. $v_m >> v_{mean}$, whereby at the front latent heat of solidification q_{lat} is emitted.

Temperature field in the process of considered solidification is determined within a section $0 < x < l$ as a result of the following problem solution:

$$\frac{\partial}{\partial x}\left(\lambda \frac{\partial T}{\partial x}\right) + Q(x, t) = c\gamma\left(\frac{\partial T}{\partial t} + \theta\right), \qquad (8)$$

where $Q(x, t) = \dfrac{q_{lat} v_m \gamma}{\Delta x}$ in the point $x = v_m t$, and in the rest points $Q(x, t) = 0$.

Equation (8) is solved under the following conditions:

Table 1. Thermophysical properties of steel Kh18N10T and aluminium alloy AMg6 [7–9]

Material	T_S, °C	T_L, °C	$q_{lat}\gamma \cdot 10^{-6}$, J/m^3	λ, W/(m·°C)	$c\gamma \cdot 10^{-6}$, J/(m^3·°C)	a, m^2/s
Kh18N10T	1410	1490	2093	1.84	4.6	0.04
AMg6	570	629	879.06	0.28	2.93	0.96

Table 2. Parameters of intermittent solidification for steel Kh18N10T

G, °C/cm	h_{layer}, cm	Δt_{sol}, s	Δt_{stop}, s	G, °C/cm	h_{layer}, cm	Δt_{sol}, s	Δt_{stop}, s
v_m = 0.5 cm/s				v_m = 2.0 cm/s			
500	0.01	0.02	0.1	500	0.0025	0.00125	0.0284
1000	0.0095	0.0185	0.054	1000	0.0025	0.00125	0.0207
1500	0.01	0.02	0.048	1500	0.0025	0.00125	0.0153
2000	0.01	0.02	0.038	2000	0.0025	0.00125	0.013
2500	0.0095	0.019	0.031	2500	0.0025	0.00125	0.0113
3000	0.011	0.022	0.028	3000	0.0025	0.00125	0.0105
3500	0.0115	0.023	0.0255	3500	0.0025	0.00125	0.009
4000	0.0115	0.0237	0.0237	4000	0.0025	0.00125	0.0085
v_m = 1.0 cm/s				v_m = 3.0 cm/s			
500	0.005	0.005	0.053	500	0.0015	0.0005	0.0186
1000	0.0045	0.0045	0.0331	1000	0.0015	0.0005	0.0128
1500	0.0050	0.0050	0.028	1500	0.0015	0.0005	0.0102
2000	0.0045	0.0045	0.0215	2000	0.0015	0.0005	0.0087
2500	0.0045	0.0045	0.0185	2500	0.0015	0.0005	0.0075
3000	0.0045	0.0045	0.0165	3000	0.0015	0.0005	0.0068
3500	0.0045	0.0045	0.0158	3500	0.0015	0.0005	0.006
4000	0.0045	0.0045	0.014	4000	0.0015	0.0005	0.0056

Table 3. Parameters of intermittent solidification for aluminium alloy AMg6

G, °C/cm	h_{layer}, cm	Δt_{sol}, s	Δt_{stop}, s	G, °C/cm	h_{layer}, cm	Δt_{sol}, s	Δt_{stop}, s
v_m = 0.5 cm/s				v_m = 2.0 cm/s			
150	0.4	0.8	0.54	150	0.068	0.034	0.212
250	0.71	1.42	–	250	0.07	0.035	0.16
350	0.51	1.02	–	350	0.07	0.033	0.128
450	0.4	0.8	–	450	0.07	0.035	0.11
500	0.35	0.74	–	500	0.073	0.037	0.107
1000	0.18	0.36	–	1000	0.12	0.06	0.1
1500	0.12	0.24	–	1500	0.12	0.06	–
2000	0.09	0.18	–	2000	0.09	0.045	–
v_m = 1.0 cm/s				v_m = 3.0 cm/s			
150	0.15	0.15	0.36	150	0.05	0.017	0.157
250	0.15	0.15	0.26	250	0.05	0.017	0.124
350	0.15	0.15	0.2	350	0.05	0.017	0.099
450	0.28	0.28	0.21	450	0.05	0.017	0.087
500	0.3	0.3	0.066	500	0.05	0.017	0.081
1000	0.18	0.18	–	1000	0.05	0.017	0.05
1500	0.12	0.12	–	1500	0.08	0.027	0.066
2000	0.09	0.09	–	2000	0.08	0.027	0.053

$$t = 0;\ T = T_S + Gx \text{ at } 0 < x < l/3,\quad T = T_L \text{ at } l/3 < x < l; \tag{9}$$

$$t > 0;\ T = T_S - \theta t \text{ at } x = 0,\quad T = T_L - \theta t \text{ at } x = l. \tag{10}$$

At $t = l/3$, $v_m = t^*$, i.e. process of a layer solidification finishes; if $T(1/3, t^*) < T_L$ then $t_{stop} = 0$; if $T(1/3, t^*) > T_L$ then calculation is continued till the moment t^{**}, when $T(1/3, t^*) = T_L$.

Duration of a solidification front movement stop is determined according to $\Delta t_{stop} = t^{**} - t^*$.

In the article results of calculation for the fusion zone during solidification for steel Kh18N10T and aluminium alloy AMg6 are presented.

Calculation was carried out at constant thermal physics characteristics in considered area of temperatures (see Table 1).

By means of a shown algorithm calculated data were obtained and consolidated in the Tables 2 and 3.

CONCLUSIONS

1. For describing process of solidification layer formation solidification model should be used based on the «martensite» mechanism of solid phase formation, at which emission of latent solidification heat q_{lat} enables the solidification front stop.

2. Mathematical model of intermittent solidification of a weld metal is developed, which allows calculating parameters of intermittent solidification (Δt_{stop}, Δt_{sol}, h_{layer}) at assigned G and v_m.

3. Approbation of the model was carried out for structural materials (steel Kh18N10T and aluminium alloy AMg6). The results obtained coincide with experimental data with sufficient accuracy.

1. Dyatlov, V.I., Abralov, M.A., Shnajder, B.I. (1967) Primary solidification of molten pool in welding of small thickness metals. *Avtomatich. Svarka*, **1**, 26–30.
2. Petrov, G.L. (1961) On problem of liquating impurity distribution in crystallized weld metal. In: *Transact. of the M.I. Kalinin Leningrad Polytechnic Inst.*, **216**, 83–101.
3. (1991) *Welding and materials to be welded*. Vol. 1: Weldability of materials. Ed. by E.L. Makarov. Moscow: Metallurgiya.
4. Makhnenko, V.I. (2002) Prospects of development of mathematical modelling and information technologies in welding and related processes. In: *Proc. of Int. Conf. on Mathematical Modeling and Information Technologies in Welding and Related Processes* (Sept. 16–20, 2002, Katsiveli, Crimea, Ukraine). Kiev: PWI.
5. Prokhorov, N.N. (1968, 1976) *Physical processes in metals during welding*. Vol. 1. and 2. Moscow: Metallurgiya.
6. Nikiforov, G.D. (1972) *Metallurgy of fusion welding of aluminium alloys*. Moscow: Mashinostroenie.
7. Makhnenko, V.I., Kravtsov, T.G. (1976) *Thermal processes in mechanized surfacing of parts of circular cylinder type*. Kiev: Naukova Dumka.
8. (1976) *Tables of physical values*. Refer. Book. Ed. by I.K. Kikoin. Moscow: Atomizdat.
9. Sudnik, V.A. (1991) *Prediction of welded joint quality on the base of numerical models of weld formation in fusion welding of thin-walled structures*. Syn. of Thesis for Dr. of Techn. Sci. Degree. Tula.

FEATURES OF CRACK INITIATION AND PROPAGATION UNDER THE CONDITIONS OF OFF-CENTER TENSION OF 1441 Al–Li ALLOY WELDED JOINTS

T.M. LABUR, A.Ya. ISHCHENKO, T.G. TARANOVA, V.A. KOSTIN and G.M. GRIGORENKO
E.O. Paton Electric Welding Institute, NASU, Kiev, Ukraine

Peculiarities of initiation and propagation of cracks at fracture of metal in HAZ of welded joints on aluminium-lithium alloy 1441, depending upon the thermophysical conditions of welding and volume content of precipitating phases, have been studied. It is shown that formation of fracture centres is related to increase in the volume content of coarse phases present in the metal structure. It has been established that the rate of metal cooling in fusion welding affects the value of the energy of crack initiation in the alloy.

Keywords: *fusion welding, aluminum-lithium alloy, thermophysical conditions, heat-affected zone, simulation sample, fracture mechanics, off-center tension, fractorgraphy*

Change of metal structure under the impact of the thermal cycle of welding affects the properties of welded joints and fracture characteristics [1–5]. Fracture mechanism differs considerably from the processes proceeding in the base metal. Many factors leading to formation and growth of microcracks in the structural material structure are taken into account by the theoretical models of fracture, reflecting the interrelation of the macroscopic fracture characteristics with microstructure parameters [6–15].

Researchers [16–29] note the prevalence of a tough fracture mode in aluminium alloys, the mechanism of which is related to formation of pits (voids) and their subsequent coalescence during realisation of plastic deformation. Pit size is determined by grain diameter and distance between nonmetallic inclusions (NMI). Often, however, a mixed distribution of small and large pits is found on the high-strength aluminium alloy fractures [22–27]. For structures of high-strength aluminium alloy welded joints such studies are not enough, this, possibly, being related to presence of structural zones in the welded joint, differing by the volume fraction of the phases, their shape and dimensions (Figure 1).

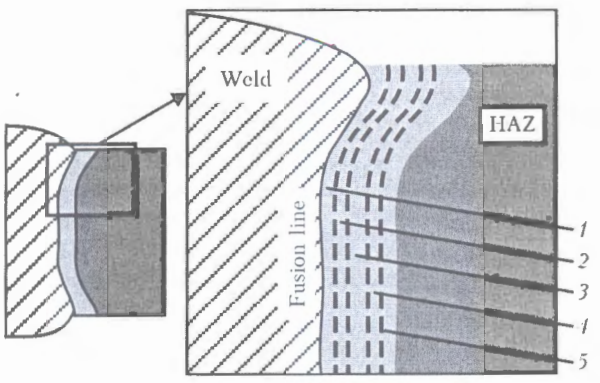

Figure 1. Schematic of welded joint with different structural zones formed in fusion welding of aluminium alloys: *1* — overheating; *2* — hardening; *3* — annealing; *4* — tempering; *5* — ageing

Weld metal is characterized by a cast structure. In the fusion zone (FZ) under the conditions of a short-term heating up to temperatures exceeding the liquidus temperature, partial welding of base metal proceeds and a small number of elongated and compact particles form. Located near FZ is a hardening zone, where dissolution of alloying elements is found at heating. Solid solution decomposition and formation of structural phases in this region of the welded joint depend on the heat source and temperature-time parameters of welding [8].

Located near the hardening zone is a region, where elongated and spherical particles of different phases form, which developed at heating up to annealing temperatures. Next comes the zone of additional ageing, where phase transformations due to an unstable state of the solid solution, result in precipitation of additional phases providing the alloy hardening. Increase of the heat input in fusion welding promotes an increase of the HAZ length from 4 to 12 mm. Quantity of strengthening phases in the grain volume is reduced, and in the intergranular gap the quantity of eutectic phases increases with increase of its width. These phases are a complex compound, consisting, as a rule, of binary and ternary alloying components.

Close attention given by the researchers to such phases in the welded joint structure is due to the fact that a number of studies [7–15] report about these phases initiating brittle fracture through microcrack initiation and subsequent coalescence at their propagation during fracture, particularly, if they are located along the grain boundaries. NMI penetrating into the alloy during the semi-finished product production have an essential role in fracture initiation. This is particularly true for Al–Li alloys, for instance, of 1441 type, containing 1.9 wt.% Li, 1.7 wt.% Cu, 0.9 wt.% Mg, 0.1 wt.% Sc and inclusions of strengthening phases of a multicomponent composition, located parallel to the direction of rolling [1–3, 10–15]. Data on the quantitative parameters of structural com-

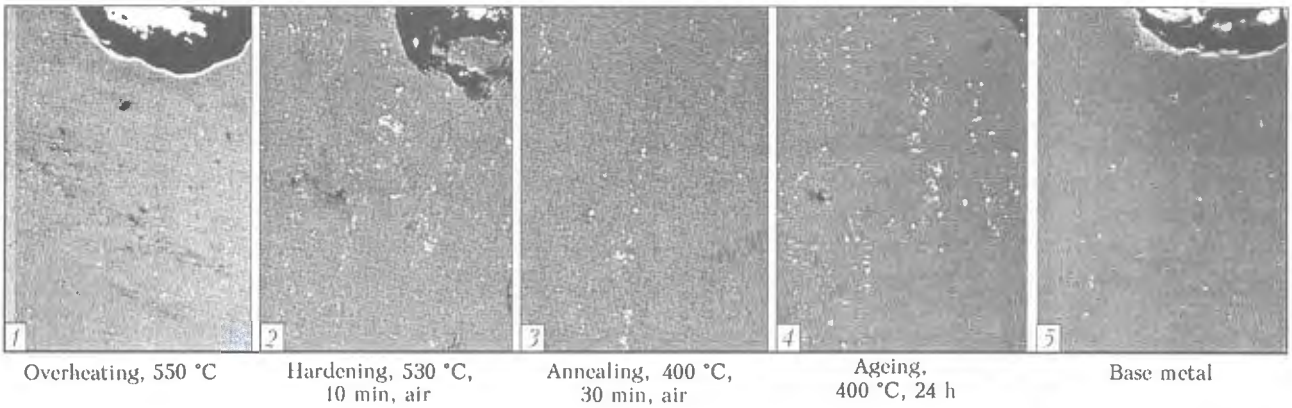

Figure 2. Influence of heating conditions simulating the HAZ in TIG welding on the averaged volume fraction of NMI: *1* — 0.42; *2* — 0.60; *3* — 0.40; *4* — 0.80; *5* — 0.25 % (×200)

ponents, the presence of which is one of the main factors of crack initiation, is lacking.

A new methodological approach is required to reveal the role of structural constituents, changing under the conditions of technological heating, in the crack formation processes in welded joint fracture. Use of quantitative and qualitative characteristics, obtained by the method of scanning microscopy, together with the fracture mechanics indices will allow interpreting the properties of the metal in individual welded joint zones, and thus, obtaining the data on the nature and individual aspects of fracture.

It appears to be rational to also study the regularities of structure formation in the heating zone in different welding processes with different heat input, as well as determine the influence of the structural and physical inhomogeneity on crack initiation and nature of their propagation by modelling on samples simulating the thermal cycle of welding.

Heating modes of such samples were selected proceeding from the thermokinetic diagram of the studied alloy transformation in tungsten-electrode argon-arc (TIG) welding, and electron beam welding (EBW), widely used in fabrication of light structures of aluminium alloys [1–10].

Semulation samples were tested under the conditions of off-center tension, this allowing, in addition to studying the structure of welded joint HAZ metal, determination of fracture resistance characteristics of its individual zones, and establishing the influence of the nature of coarse particle distribution and their volume fraction on the conditions and parameters of crack initiation and propagation.

Quantitative determination of the NMI volume fraction in the structure of the high-strength complex-alloyed aluminium alloy 1441 was performed by a computer program Image Pro30, allowing isolation of the characteristic structure elements based on the colour contrast with subsequent mathematical processing. In combination with Statistica 5.0 program, it enables processing the obtained results by applying one of the statistic approaches and plotting on their basis the graphic dependencies of the influence of NMI volume fraction on the physico-mechanical properties of the metal in different HAZ regions.

Obtained results showed that overheating of alloy 1441, occurring in welding in the FZ (Figure 2), leads to an increase of NMI volume fraction on average up to 0.422 %, increase of the quantity of elongated particles, as well as melting of base metal grains. The above phenomenon agrees well with the data of [1]. NMI volume fraction in this region of the welded joint is 1.5 to 2.5 times higher than a similar index of base metal in the initial condition (0.28 vol.%). Scatter of values is equal to about 100 %, which may be related to a considerable heterogeneity of the alloy, resulting from the incomplete recrystallization process proceeding at 550 °C for 3 s.

At sample heating up to the hardening temperature (530 °C) with soaking for 10 min and subsequent cooling in water, dissolution of alloying elements and precipitation of phase particles in the grain bulk and on their interface proceeds, this leading to an increase of NMI volume fractions by 0.18 to 0.42 %. Under the conditions of cooling in air proceeding in TIG welding, the quantity of the hardening phases increases 2 times, compared to cooling in water, simulating EBW conditions. Scatter of volume fraction of the hardening phases in the metal is reduced 3 times, which may be related to temperature-time conditions, accompanied by a fast cooling and incomplete re-distribution of alloying elements and impurities at formation of the appropriate phases.

A similar influence of heating conditions on volume fraction of the above phases was observed at cooling of the alloy with annealing temperature of 360 °C for 20 min. Lower rate of cooling in EBW, even though it causes intensive precipitation of excess phases from the oversaturated solid solution, restrains the process of coarse particle formation. Volume fraction of phases in this case is by 20 % smaller, compared to the alloy structure after cooling in air (Figure 3).

Volume fraction of NMI in the HAZ region, where the metal goes through additional ageing under the conditions of the thermal cycle of welding, increases 2 times, that according to the data of [14] is due to precipitation of ternary phases T_B ($Al_{15}Cu_8Li_2$), T_1 (Al_2CuLi), T_2 (Al_6CuLi_3), strengthening the 1441 alloy. S-phase (Al_2CuMg) also precipitates, being similar in its nature to T_1 phase, so that the highest hard-

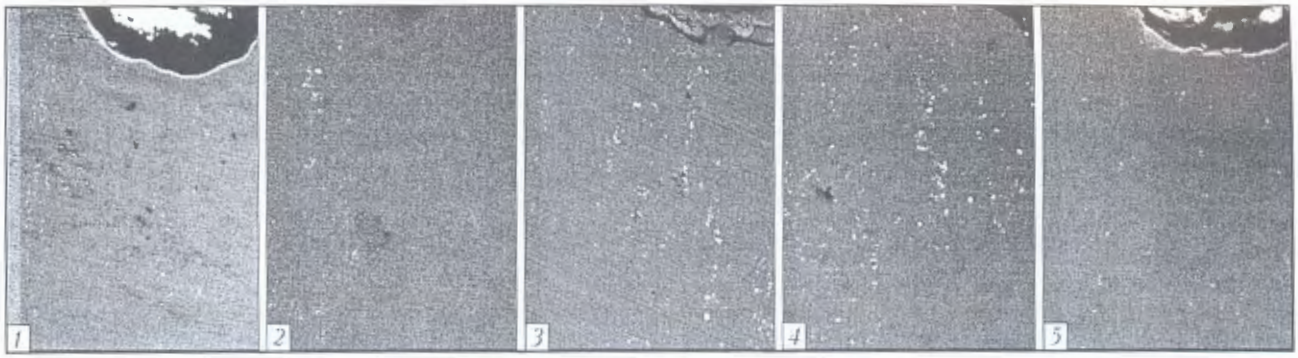

Figure 3. Influence of heating conditions simulating the HAZ in EBW on averaged volume fraction of NMI: *1* — 0.42; *2* — 0.54; *3* — 0.60; *4* — 0.80; *5* — 0.25 % (×200)

ening effect is observed. NMI volume fraction in this case is equal to 0.818 %. Precipitation of the above phases during metal ageing leads to reduction of the content of lithium, copper and magnesium in the solid solution. Scatter of values is up to 100 %.

As shown by experiments (Table), NMI volume fraction in the studied 1441 alloy has a significant influence on the fracture resistance characteristics (rated breaking stress σ_{br}; critical coefficient of stress intensity K_c; crack initiation energy J_c; specific work of crack propagation (SWCP)). Thermal conditions in place in fusion welding, have an essential influence on the nature of crack initiation and propagation at fracture. Processes of phase transformations and NMI precipitation into the intergranular space lead to formation of structural constituents of a different volume, shape and dimensions in each of the studied zones.

As is seen from the Table, the indices of brittle fracture resistance characteristics of 1441 alloy, change in this zone, depending on the heating and cooling conditions. NMI volume fraction formed in this case, not only determines the level of internal stresses in the metal, but also influences crack initiation and growth in the metal. Therefore, increase of the welding speed can be one of the possible ways to improve the fracture toughness characteristics without lowering the strength properties of welded joints on alloy 1441. Smaller quantity of NMI at heating up to 530 °C for 10 min somewhat (by 5–7 %) lowers the level of breaking stress, with K_c and J_c values increasing by 1.5 to 2 times, compared to the metal in the initial condition.

Under the annealing conditions, when complete decomposition of the solid solution and coagulation of the strengthening phases proceed in the metal, a lowering of the breaking stress level is found (see the Table). The alloy in this condition is characterized by the lowest strength (263–268 MPa) at fracture and satisfactory ductility (J_c = 8.9–9.1 J/cm^2 and SWCP = 2.6–3.1 J/cm^2). Values of stress intensity K_c vary in the range of 14.6–16.8 MPa$\sqrt{m}$, depending on the cooling rate, which influences NMI volume fraction and nature of particle distribution along the grain boundaries. Minimum level of stress intensity in 1441 alloy was found in the single-stage ageing condition (K_c = 10.3 MPa$\sqrt{m}$), this being due to formation of a large volume fraction of NMI (see Figures 2 and 3).

Fractographic analysis of 1441 alloy samples failing during testing by off-center tension, revealed that the mechanism of crack initiation and propagation is determined not only by the alloy composition, but also by temperature-time conditions of the thermal cycle of welding. Depending on that, hot cracks or coarse phase precipitates of different shape (extended, elliptical, spherical) may appear in the metal structure on the grain boundary. Non-uniform dimensions of microvoids formed at cracking of coarse phase inclusions, are indicative of stage-by-stage nature of their fracture during matrix deformation, proceeding until the fragment length has reached critical dimensions.

The fractured sample surface in overheated condition is characterized by oblique fracture, which is indicative of fracture by the mechanism of shear under tangential stresses with tough pit formation (Figure 4, *a*, *1*). Their small dimensions and presence of cleavage

Characteristics of fracture toughness of alloy 1441 depending on heating conditions (simulation of welded joint HAZ)

Conditions of alloy treatment	σ_{br}, MPa	K_c, MPa$\sqrt{m}$	J_c, J/cm^2	SWCP, J/cm^2
Overheating (FZ) (550 °C, 3 s)	372	19.4	14.2	3.7
Hardening (460 °C, 10 min)	394/372	21.6/19.4	17.0/7.2	4.8/3.7
Annealing (360 °C, 20 min)	268/263	16.8/14.6	9.1/8.9	3.1/2.6
Ageing (150 °C, 24 h)	441	10.3	8.9	1.6
Base metal	453	10.3	10.1	1.6

Note. The numerator gives the results of testing samples after heating and cooling in water, simulating the thermal conditions of EBW; the numerator — after heating and cooling in air, simulating the thermal conditions of TIG welding.

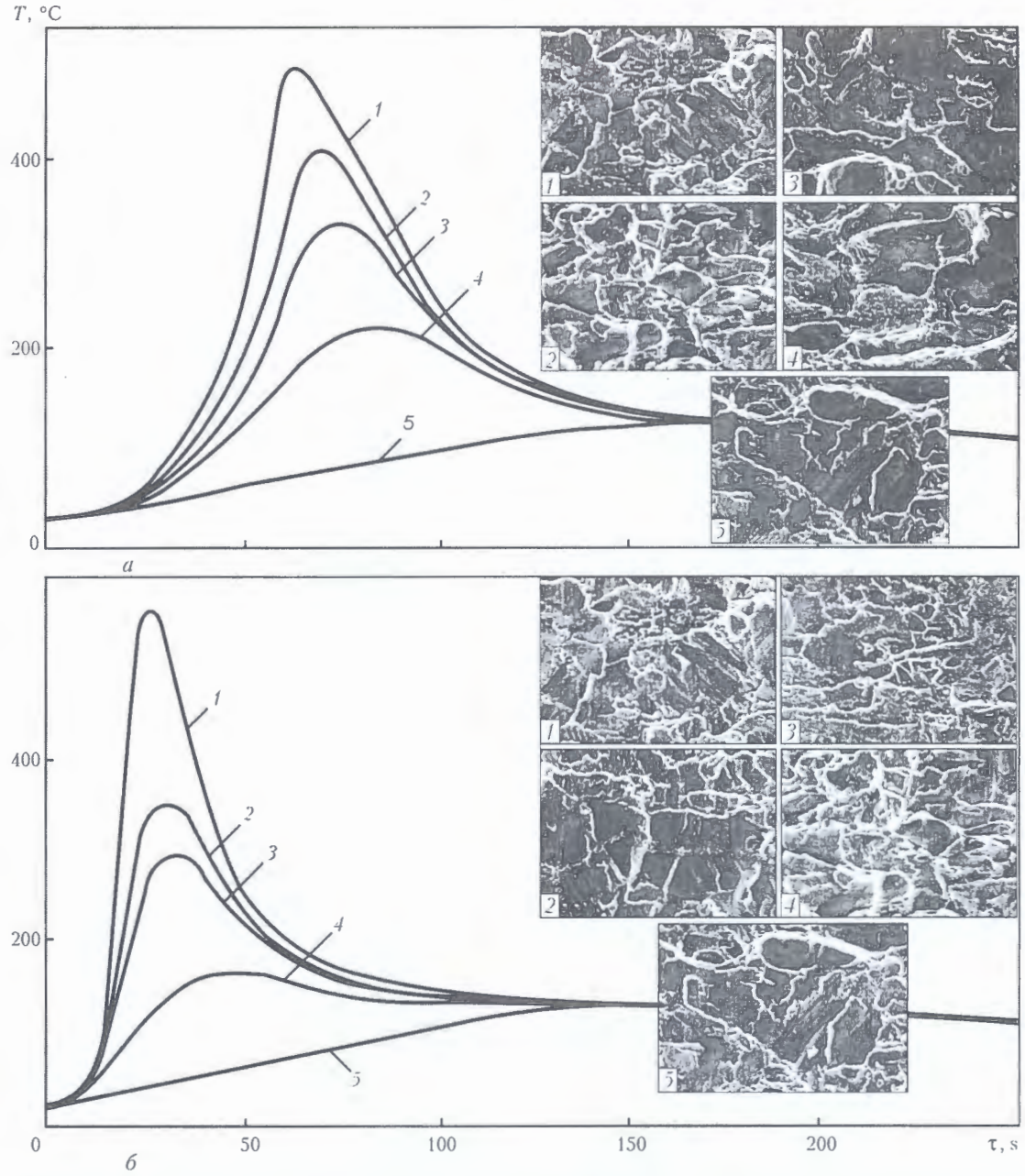

Figure 4. Influence of simulated thermal conditions of HAZ metal in TIG welding (*a*) and EBW (*b*) on the nature of fracture of samples from alloy 1441 at time of overheating τ in the zone: *1* — overheating; *2* — hardening; *3* — annealing; *4* — ageing; *5* — base metal (×500)

regions decorated by slip lines are indicative of the local nature of deformation, proceeding along the slip planes in the grain with a gradual transition to grain boundary.

The integranular gap reveals specific voids, looking like «hot cracks», formed as a result of fracture of brittle eutectics. The length of the plastic deformation zone located near the stress raiser and characterized by the properties of structural constituents, NMI, phases, which change depending on temperature-time parameters of welding, is equal to 1.83 mm. This zone contains a large number of flat regions, on the surface of which slip lines have been observed.

Hot cracks and coarse phase precipitates (Figure 4, *b*) were found in a hardened alloy cooled in air from the temperature of 530 °C and also having deformations of a local nature. In the relief of the plastic zone on grain planes, ridges were registered, having the form of bands, intersecting with deformation lines, resulting from intensive plastic deformation of grains. This is due, probably, to redistribution of stresses, where the relaxation mechanism is the grain boundary slipping [15].

At cooling of a sample heated up to hardening temperature in the water, the direction of the avalanche crack changes, which is indicative of development of a higher stress level, at which the crack initiates. In addition, this sample contains hot cracks and texture indications, which are observed in the metal cooled in air. The content of low-melting constituent in the sample fracture plane is much smaller, although the same fracture mechanism is preserved.

Plastic deformation zone is quite long (3.61 mm), more cleavage regions being present here, however; they forming the steps (Figure 4, *b*, *2*).

Heating of 1441 alloy up to annealing temperature of 360 °C with subsequent cooling in air reduces the length of the plastic zone (1.32 mm) 3 times relative to the hardened metal. Its relief is characterized by a significant quantity of cleavage regions, fringed by low ridges (Figure 4, *a*, *b*, *3*), as well as presence of shallow pores. Sample cooling in the water at simulation of the above metal state in the HAZ under the conditions of EBW reduces the extent of the ductile zone (Figure 4, *b*, *3*), in which more tough fragments appear. Now the cracks between the grains are preserved due to an increased brittleness of the eutectics formed under the heating conditions. It becomes the cracking site as a result of fracture by the mechanism of pore formation with their subsequent coalescence.

Fracture of the sample in the over-aged condition in addition to shallow pits, also contains quasi-cleavage regions, slip bands, resulting from intercrystalline fracture (Figure 4, *a*, *4*), which is indicative of a high rate of the avalanche crack propagation because of additional hardening of the metal, compared to the previous heating modes. Under such conditions the low-melting eutectics starts cracking and thus a crack initiates.

Extent of the base metal ductile zone is equal to 0.64 mm. This is smaller than in samples heated by the modes of EBW and TIG welding thermal cycles. Sample fracture has a characteristic pattern in the form of lines of a different length and orientation. They form at transition from one grain to another as a result of the change in the slip crystallography, crack traveling through the boundary surface in this region of the structure, as well as non-uniform deformation within the grain boundary. Unfavourable conditions, arising in this case, do not allow the stress to plastically relax in the intergranular gap, so that the low-melting eutectics, having a higher brittleness, becomes the initiation site of a crack, which propagates with a low energy (see the Table) in the intercrystalline mode (Figure 4, *a*, *5*).

CONCLUSIONS

1. An interrelation was established between the parameters, characterizing the fracture process in the HAZ of a high-strength complex Al–Li alloy 1441, and change of NMI volume fraction in the structure in fusion welding.

2. Metal cooling rate in fusion welding essentially influences the energy of crack initiation in the alloy. Low rate of cooling in TIG welding lowers J_c value 2.5 times after heating up to the hardening temperature.

3. The mechanism of crack initiation and propagation, as well as fractures of broken samples of alloy 1441 are determined by structural changes due to the thermophysical conditions of welding. Appearance of fracture sites is associated with increase of the volume fraction of phases precipitating in welding, and having the form of coarse precipitates located along the grain boundaries. Volume fraction of phases contained in the alloy, determines the nature of the stressed state and the associated mechanism of fracture, and also influences the fracture toughness characteristics at all the stages of crack propagation.

1. Fridlyander, I.N. (2002) Aluminium alloys in flying vehicles in the periods of 1970–2000 and 2001–2015. *Tekhnologiya Lyog. Splavov*, **4**, 12–17.
2. Fridlyander, I.N., Beletsky, V.M., Krivov, G.A. (2000) Aluminium alloys in aircraft structures. *Tekhnol. Sistemy*, **1**, 5–17.
3. Davydov, V.G. (1997) Metals science and technological investigations of aluminium-lithium alloys at the current stage. *Tekhnologiya Lyog. Splavov*, **5**, 15–25.
4. Ishchenko, A.Ya., Labur, T.M., Lozovskaya, A.V. (1995) Aluminium-lithium alloys for welded structures for aerospace engineering. *Avtomatich. Svarka*, **7**, 41–44.
5. Fujiwara, T. (2001) Technologies of light metal joining in aircraft and space engineering. *Keikinzoku Yosetsu*, 39(**3**), 1–11.
6. Kiyoto, S. (1993) Materials and joining technologies for rocket structures. *J. JWS*, 62(**8**), 46–52.
7. Ishchenko, A.Ya., Labur, T.M. (1998) Technology of welding and properties of aluminium-lithium alloy joints (Review). *Avtomatich. Svarka*, **7**, 29–33.
8. Labur, T.M., Bondarev, Andr.A., Lozovskaya, A.V. et al. (2001) Influence of welding process on fracture resistance of joints in aluminium-lithium alloys 1420 and 1460. *The Paton Welding J.*, **7**, 11–15.
9. Labur, T.M. (2003) Improvement of reliability of welded joints of aluminium-lithium structures in aerospace engineering. *Tekhnol. Sistemy*, **2**, 71–79.
10. (1998) *Welding in aircraft construction*. Ed. by B.E. Paton. Kiev: MIITsV.
11. Leshchiner, L.N., Latushkina, L.V., Fedorenko, T.P. (1994) Highly-resistant lower density alloy 1441 readily adaptable to fabrication of Al–Cu–Mg–Li system. *Tekhnologiya Lyog. Splavov*, **3/4**, 38–42.
12. Tretyak, N.G., Ilyushenko, R.V., Yavorskaya, M.R. et al. (1995) Weldability of sheet semi-finished products of alloy 1440. *Avtomatich. Svarka*, **4**, 27–30.
13. Fridlyander, I.N., Sadkov, V.V., Sandler, V.S. et al. (2000) Properties of semi-finished products of aluminium-lithium alloy 1441 readily adaptable to fabrication. *Tekhnologiya Lyog. Splavov*, **4**, 24–27.
14. Mondolfo, L.F. (1979) *Structure and properties of aluminium alloys*. Moscow: Metallurgiya.
15. Fridlyander, I.N., Chuistov, K.V., Berezina, A.L. et al. (1992) *Aluminium-lithium alloys. Structure and properties*. Kiev: Naukova Dumka.
16. Broek, D. (1980) *Principles of fracture mechanics*. Moscow: Vysshaya Shkola.
17. Vasilchenko, G.S., Kotelev, P.F. (1974) *Practical application of fracture mechanics for evaluation of structure strength*. Moscow: Nauka.
18. Botvina, L.R. (1989) *Kinetics of fracture of structural materials*. Moscow: Nauka.
19. Ivanova, V.S., Botvina, L.R., Kudryashov, V.G. (1971) Strength and ductility. Fracture under short-time loads. Tough and brittle fracture. In: *Results of science and technology*. Series: Materials Science and Heat Treatment. Moscow.
20. Kis, J.A., Smith, H.L., Romaji, H.E. et al. (1968) Fracture testing of welds. In: *Applied problems of fracture toughness*. Moscow: Mir.
21. Kishkina, S.I. (1981) *Fracture resistance of aluminium alloys*. Moscow: Metallurgiya.
22. Klevtsov, G.V. (1993) Kinetics of formation of plastic strain zones at the crack tip in fracture of structural materials in the plane-stressed and plain-strained states. *Problemy Prochnosti*, **4**, 57–63.
23. Miklyaev, P.G., Rudnitsky, E.N. (1980) Procedure of determination of parameters of anisotropic material fracture toughness. *Zavod. Laboratoriya*, 46(**3**), 265–268.
24. Neshpor, G.S., Miklyaev, P.G., Andreev, D.A. (1980) On possibility of the unification of procedure of fracture toughness determination in plane-stressed state. *Ibid.*, 261–265.
25. Gordeeva, T.A., Zhegina, I.P. (1978) *Analysis of fractures in evaluation of material reliability*. Moscow: Mashinostroenie.
26. Ivanova, V.S., Kudryashov, V.G., Konelovich, B.A. et al. (1974) Fractography and fracture toughness of aluminium and titanium alloys. *Tekhnologiya Lyog. Splavov*, **3**, 65–70.
27. (1989) *Calculations and strength testing in machine-building, classification of surface fracture (rupture) types*. Moscow: Standart.
28. Romaniv, O.N. (1981) Structural fracture mechanics as a new promising trend in the problem of metal fracture. *Fiziko-Khimich. Mekhanika Materialov*, **4**, 28–32.
29. (1982) *Fractography and atlas of fractograms*. Refer Book. Moscow: Metallurgiya.

EXPERIMENTAL SUBSTANTIATION OF METHOD FOR CALCULATION OF RESIDUAL LIFE OF PIPELINES WITH CORROSION DAMAGES

P.S. YUKHIMETS, E.F. GARF and **V.A. NEKHOTYASHCHY**
E.O. Paton Electric Welding Institute, NASU, Kiev, Ukraine

Two full-scale specimens with recesses in the form of a semi-ellipsoid and cylinder were tested to check the offered method for calculation of residual life of pipelines allowing for the surface defects. The above recesses stimulated surface corrosion damages under cycle loading by internal pressure. The results obtained proved adequacy of the developed method for estimation of residual life of pipelines comprising corrosion damages.

Keywords: *main pipelines, aging, corrosion damages, concentration of stresses, method of calculation, residual life*

Aging of pipelines, first of all the main ones, affects reliability of their operation and is often accompanied by increase of the failure rate [1].

Erosion-corrosion processes may take place as a result of long-term operation of pipelines, action of thermal and mechanical loads, and influence of the environment. As it was noted in [2], the main reason of pipelines failure within 20 years of operation is pit corrosion, amounting to 42.5 % of a total number of all registered cases.

At present requirements to safety margin in pipelines, only material of the concentration zones works above elasticity limit, while the bulk of the pipe metal is elastically deformed.

In the study geometric model of the considered surface defect in the form of semi-ellipsoid was used, axes of symmetry of which θ and z are the biggest sizes of a defect in axial, circumferential, and radial directions of a pipelines (Figure 1). Calculation of local maximal deformations is carried out in the ellipsoid apex (in the maximum point) on the basis of values of nominal stresses σ_{nom} and their concentration.

Results of fulfilled studies [3] prove that concentration of stresses in zones of corrosion damages of pipelines on their external and internal surfaces may achieve essential values, which creates threat of a cyclic elastoplastic failure, provided static strength is ensured (Figures 2–4).

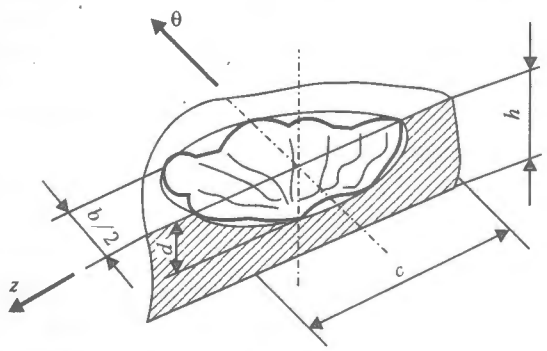

Figure 1. Scheme of surface defect in the form of semi-ellipsoid: c, b and d – length, width and depth of the defect, respectively; h – pipe wall thickness

For occurrence of a failure in a defect zone of elastic pipe steels accumulation of a respective fatigue damages is required, i.e. achievement of a certain number of loading cycles. Neglect of a possibility of low-cycle damage does not manifests itself at once, and is one of the reasons of increased number of failures, which take place as a result of a pipeline ageing.

The need to ensure maximal pipeline reliability assumes perfecting the methods for their strength analysis. In this connection a method for residual life calculation of a pipeline with corrosion damages is proposed based on a criterion of a low-cycle crack formation at loading cycles up to $1 \cdot 10^5$. This work is

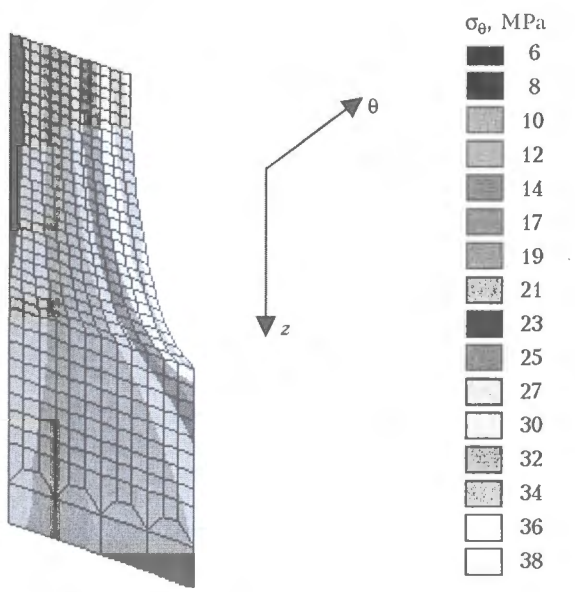

Figure 2. Distribution of circumferential stresses σ_θ over thickness of pipe wall of 322 × 7 mm size in the defect zone: half of the defect longitudinal section is on internal wall surface; c = 25 mm; b = = 35 mm; d = 1.4 mm; internal pressure P = 1 MPa (here and in Figure 3 results of the FEM calculation are given, carried out by Institute of Strength Problems, NASU, Kiev, Ukraine)

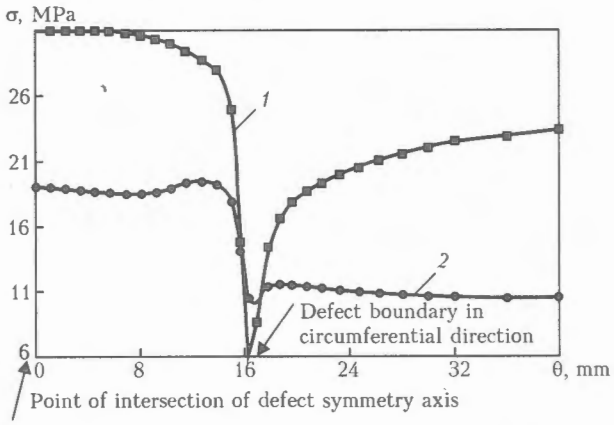

Figure 3. Distribution of circumferential σ_θ (*1*) and axial σ_z (*2*) stresses on the surface of defect along axis of symmetry θ under action of 1 MPa internal pressure in the pipe of 322 × 7 mm size (for explanations see Figure 2)

carried out for the purpose of experimental checking mentioned method.

Within the framework of used in the calculation theory of thin shells, stressed state of pipelines is presented as a plane-stressed, i.e. stresses, which act in the direction of a wall thickness, are accepted equal to zero. Asymmetry of the deformation cycle is not taken into account, because its influence on the working life under conditions of a rigid loading of elastic steels at values of asymmetry characteristic of the condition of changing loads, which act on pipelines, is insignificant. Using intensity of deformations (stress) in calculation of the values, which are invariant to the stressed state type, we assume that a deformation diagram in the zone of defects corresponds to the smooth specimen tensile diagram.

Determination of the components of various categories of stresses is performed using a rectangular coordinate system θ–*z*.

On the basis of analysis of the pipeline operation conditions maximum loading cycles were established (Figure 5).

For each main loading cycle of the *j*-th type, stress ranges of the components of nominal normal $\Delta\sigma_{zj}$ and $\Delta\sigma_{\theta j}$ and tangent $\tau_{z\theta j}$ stresses, which are used for de-

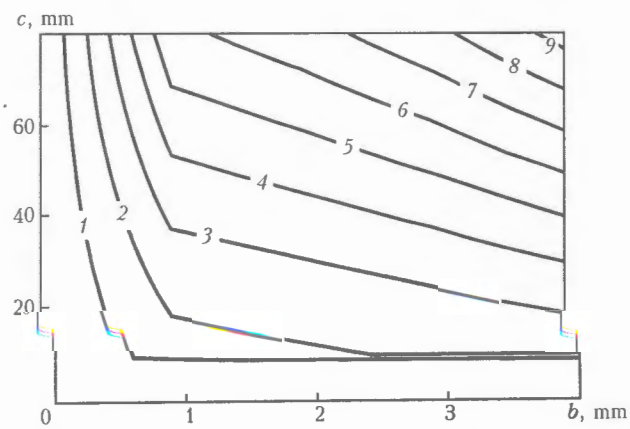

Figure 4. Curves of isometric concentration of stresses on surface of defect of b = 20 mm = const width in the pipe of 219 × 8 mm size obtained during change of its length c and depth d (values of the concentration α_σ of stresses are indicated by figures on the curves)

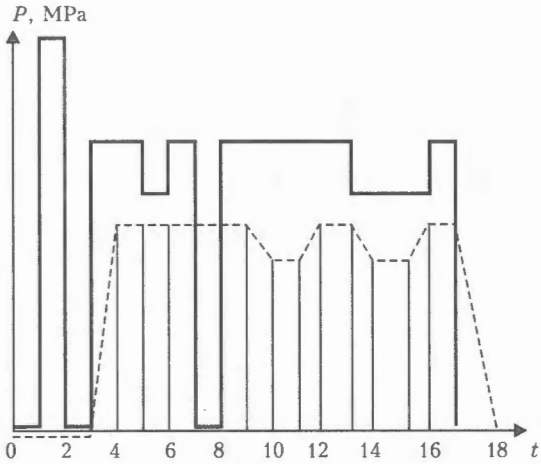

Figure 5. Maine cycles of pipeline loading: solid curves indicate the pressure in pipeline; dash lines indicate the pipeline temperature; t_{1-2} — hydraulic test of the pipeline; t_{3-4}–t_{17-18} — typical start-stop of pumping; t_{5-6} — pressure reduction-increase during pumping; t_{7-8} — emergency (short-term) start-stop of pumping; t_{9-12} — reduction-increase of pumping temperature; t_{13-16} — pumping temperature and pressure reduction-increase

termining ranges (double amplitude) of nominal stress intensity $\Delta\sigma_{ij}$ ($2\sigma_{aj}$) in the loading cycle of the *j*-th type, are calculated:

$$\Delta\sigma_{ij} = 2\sigma_{aj} = \sqrt{\Delta\sigma_{zj}^2 + \Delta\sigma_{\theta j}^2 - \Delta\sigma_{zj}\Delta\sigma_{\theta j} + 3\tau_{z\theta j}^2}.$$

Using value of the stress concentration factor in the defect zone in the elastic area of concentration of stresses α_σ [3], amplitude of maximum stresses σ_{aj}^k in the defect zone is calculated:

$$\sigma_{aj}^k = \sigma_{aj}\alpha_\sigma,$$

where k is the number of the loading cycle;

$$\alpha_\sigma = 1.4\left(1 + \frac{2\frac{b}{d}\left(1.12 - 0.48\frac{b}{c} + 0.13\frac{b}{c}\left(3\frac{b}{c} - 2 - \frac{b}{h}\right)\right)}{1 - \frac{b}{h}\left(1 - 0.75\frac{b}{c}\right)}\sqrt{1 + \frac{5\pi\lambda^2}{32}}\right);$$

λ is the function, which allows for a surface curvature:

$$\lambda^2 = \frac{c^2}{Rh}[12(1-\mu^2)]^{1/2};$$

R is the pipe radius; $\mu = 0.3$ is the Poison's ratio.

If values of calculated elastic stresses $\Delta\sigma_{ij}^k$ exceed yield point σ_y, for further calculation a value of the conditional elastic stress σ_{aj}^{k*} or relative deformation in the defect zone $\bar{e}_{aj}^k$ is used:

$$\sigma_{aj}^{k*} = \sigma_{aj}K_{ej}; \quad \bar{e}_{ij}^k = K_{ej}\frac{e_{aj}}{e_y},$$

where e_{ij} is the amplitude of nominal deformations in the *j*-th cycle of loading; e_y is the intensity of deformation, which corresponds to the yield point; K_{ej} is the deformation concentration coefficient in elastic-plastic area of a material deformation in a defect zone in the *j*-th cycle of loading:

Figure 6. Experimental specimens of 219 × 8 (*a*) and 168 × 7 (*b*) mm size

$$K_{ej} = \frac{\alpha_\sigma^{2/1+m}(\bar{\sigma}_j)^{(1-m)/(1+m)}}{(\alpha_\sigma \bar{\sigma}_j)^{\frac{n(1-m)}{(1+m)}}\left[1-\left(\bar{\sigma}_j - \frac{1}{\alpha_\sigma}\right)\right]},$$

where $\bar{\sigma}_j$ are the relative nominal stresses in the j-th cycle of loading:

$$\bar{\sigma}_j = \frac{\Delta\sigma_{ij}}{\sigma_y};$$

$n = 0.5 = \text{const}$; m is the characteristic of a material strengthening in the elastic-plastic area.

Residual life of the pipeline is

$$T_{res} = \frac{1-a}{a_{year}},$$

where a_{year} is the damage to the pipeline within one year of operation:

$$a_{year} = \sum \frac{f_j}{[N_j]};$$

where f_i is the mean frequency of repeatability of loading cycles of the j-th type per year; $[N_j]$ is the allowable number of the main loading cycles of the j-th type determined on the basis of found values of the amplitude of stresses σ_{aj}^k and σ_{aj}^{k*} or deformation e_{aj}^k in the defect zone using calculated fatigue curves or given below dependence with introduced safety margins for strains (stresses) $\{n_e, (n_\sigma)\}$ and durability n_N:

$$[N_j] = \left[\frac{\ln\dfrac{1}{1-\psi}}{4e_y\left(\bar{e}_{aj}^k - \dfrac{\sigma_{-1}}{\sigma_y}\right)}\right]^{1/n}; \qquad (1)$$

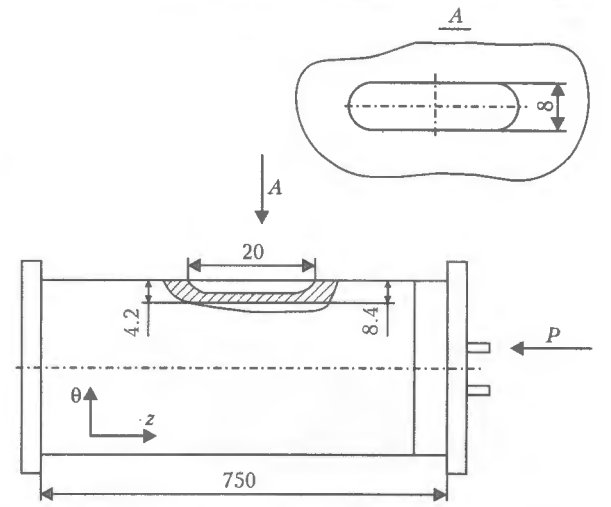

Figure 7. Scheme of 219 × 8 mm specimen with applied on its external surface defect in the form of semi-ellipsoid

$$a = \sum \frac{N_j}{[N_j]}$$

is the total accumulation of damages: N_j is the actual number of main loading cycles of the j-th type in a pipeline having a surface defect.

For the purpose of checking the proposed methodology tests of two full-scale specimens (Figure 6) from pipes of different diameters with mechanically applied recesses in the form of a semi-ellipsoid and a cylinder, which simulated surface damages, were carried out (Figures 7 and 8).

Into the calculation of low-cycle strength of the specimens mechanical property characteristics were introduced, which were determined in standard tensile tests and designed for determining minimal resistance to failure (Table 1).

The experiments were carried out in the PWI Laboratory for Pressure Testing of Welded Joints. In the process of tests specimens were loaded in automatic mode by pulsed internal pressure: from P_{min} to P_{max}

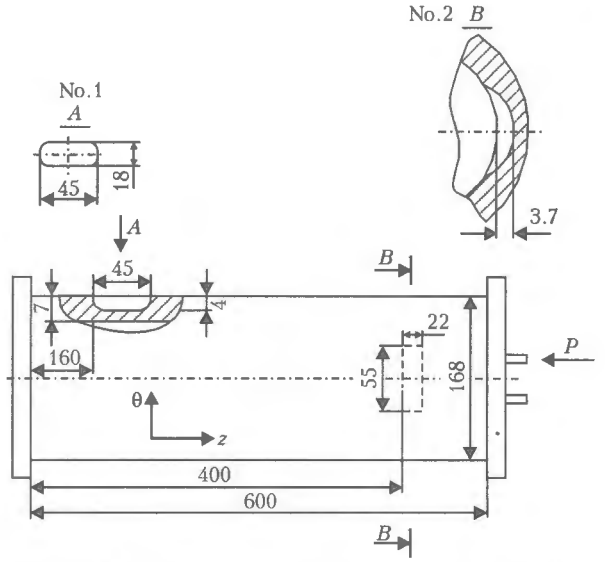

Figure 8. Scheme of 168 × 7 mm specimen with defects applied on its external surface in the form of semi-ellipsoid (No.1) and on its internal surface in the form of cylinder (No.2)

Table 1. Mechanical properties of pipes

Size of pipe, mm	σ_t, MPa	σ_y, MPa	ψ, %
219 × 8	541.3	365.5	55.0
168 × 7	530.6	300.2	55.3

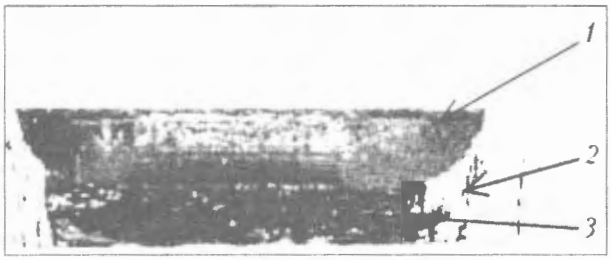

Figure 9. Failure of 219 × 8 cm specimen in the defect zone: *1* — defect in the form of semi-ellipsoid; *2* — base metal; *3* — crack propagation zone

with subsequent drop to P_{min}. The rate of loading was approximately 1 cycle/min.

Data on loading of the specimens are given in Tables 2 and 3. Given in the Tables allowable before failure number of cycles $[N_j]$ was determined using dependence (1) without introduction of safety margin. Tests were continued till depressurization of a specimen was visually determined (Figure 9). As one can see from the Figure, actual failure of a specimen took place after a higher than it was predicted number of cycles. Total accumulation of defects exceeded in both cases 1 that characterizes the carried out estimation as somewhat conservative one. One should, however, take into account that during performance of the experiment influence of the environment, which under real conditions of a pipeline operation reduces its durability, was practically excluded. That's why understating of the service life estimation in the experiment plays in this case positive part, because it is directed at compensation of unaccounted influence of the corrosive environment in the course of operation.

It should be noted that proposed method of calculation in its present interpretation is applicable only for conditions, which were reproduced in the described experiment, i.e. accumulation of damages proceeded after a defect was inflicted, and a size of the defect remained unchangeable in the process of the tests, while in reality from the moment of a defect origination to the moment of its detection certain time passes, within which a significant fatigue damage of a metal may be accumulated in the stress concentration zone. The share of damages, which accumulates in a loading cycle, changes depending upon a defect size. If one does not take into account damages accumulated by the time of defect detection, it may cause overestimation of a pipeline residual life.

After experimental confirmation of suitability of the calculation method for practical application, it should be elaborated in such way that a pipeline residual life be estimated allowing for a change of geometric parameters of a defect, which took place before its detection and will continue to take place, proceeding from the established calculated rate of the corrosion process within the predicted time period.

Data obtained in the course of the experiment showed that in contrast to static loading, in which the ratio of a defect area and a non-reinforced hole is of primary importance [4], determining part in case of a cyclic loading is played by concentration of stresses in a defect zone. Indicative in this respect is defect in the specimen of 219 × 8 mm size and defect

Table 2. Loading characteristics of specimen of 219 × 8 mm size

N_j, cycle	P_{max}, MPa	P_{min}, MPa	K_e at P_{max}	$\bar{\sigma}_j$	$e_a \cdot 10^{-3}$	$[N_j]$, cycle	a
1000	20.0	1	7.78	0.593	3.550	5840	0.171
100	20.5	4	7.92	0.608	3.386	6648	0.015
26	19.0	1	7.49	0.564	3.240	7518	0.003
100	20.0	1	7.78	0.593	3.550	5840	0.017
1114	23.0	1	8.67	0.682	4.593	2983	0.373
30	20.0	1	7.78	0.593	3.550	5840	0.005
70	21.0	1	8.07	0.623	3.878	4610	0.015
1590	24.0	1	9.01	0.712	4.981	2438	0.652
							$\Sigma = 1.251$
Note. $\alpha_\sigma = 4.61$.							

Table 3. Loading characteristics of specimen of 168 × 7 mm size

N_j, cycle	P_{max}, MPa	P_{min}, MPa	$\bar{\sigma}_j$	K_e at P_{max}		$e_a \cdot 10^{-3}$		$[N_j]$, cycle		a	
				No.1	No.2	No.1	No.2	No.1	No.2	No.1	No.2
2400	13	1.0	0.39	5.74	1.88	1.369	0.441	$\sim 2 \cdot 10^5$	$> 1 \cdot 10^6$	0.012	–
6270	17	1.0	0.51	6.65	1.88	2.120	0.588	28130	$> 1 \cdot 10^6$	0.223	–
$1 \cdot 10^4$	15	1.0	0.45	6.18	1.88	1.724	0.514	62640	$> 1 \cdot 10^6$	0.160	–
$1 \cdot 10^4$	17	0.5	0.51	6.65	1.88	2.164	0.607	26170	$> 1 \cdot 10^6$	0.382	–
$7 \cdot 10^3$	21	1.0	0.63	7.66	2.01	3.052	0.788	8912	$> 1 \cdot 10^6$	0.785	–
230	30	1.0	0.90	–	2.43	–	1.387	–	$> 1 \cdot 10^6$	–	0.001
										$\Sigma = 1.562$	$\Sigma \approx 0.001$
Note. For a defect No.1 $\alpha_\sigma = 4.53$, for No.2 — $\alpha_\sigma = 1.88$ (see Figure 8).											

Table 4. Influence of defects on static strength of specimens

Size of specimen with defect, mm	Pipe surface	F, mm^2	F_d, mm^2	M	α_σ	Fracture in experiment
219 × 8	External	88.3	76.4	1.00	4.61	Fatigue
168 × 7, No.1	Same	67.6	120.0	0.83	4.53	Same
No.2	Internal	67.6	81.4	0.89	1.88	Did not occur

Note. F – maximal area of hole, which does not reduce strength of a pipe under internal static pressure action; F_d – area of deepest defect in longitudinal section; M [5] – static strength reduction coefficient P'/P, where P' – allowable internal pressure in a pipeline allowing for availability of defects, and P – estimated pressure in a pipeline.

2 in the specimen of 168 × 7 mm size. In the first case low-cycle failure took place in the absence of weakening in the defect zone, and in the second case fatigue failure didn't take place despite the fact that the defect zone was weakened (Table 4).

So, on the basis of experimental data on durability of full-scale specimens of pipes with surface recesses, which simulated corrosion damages, the developed method of estimating residual life of a pipeline with corrosion damages was checked and its adequacy was confirmed.

1. Vorobiov, V.A., Gumerov, A.G., Sultanov, M.Kh. et al. (2001) Reliability of present systems of pipeline transport and means of its improvement. In: *Work Program of 3rd Congress of Gas and Oil Producers of the Russia* (Ufa, May 22–25, 2001). Ufa: TPPRB.
2. Gafarov, N.N., Goncharov, A.D., Kushnarenko, V.M. et al. (2001) Analysis and evaluation of residual life of pipelines and equipment ONGKM. In: *Abstr. of 3rd Int. Conf. on Diagnostics of Pipelines* (Moscow, May 21–26, 2001). Moscow.
3. Garf, E.F., Netrebsky, M.A., Kobelsky, S.V. et al. (2000) Stress concentration in the areas of corrosion damage of pipelines. *The Paton Welding J.*, **6**, 2–5.
4. Garf, E.F., Netrebsky, M.A. (2000) Assessment of the strength and residual life of pipelines with erosion-corrosion damage. *Ibid.*, **9/10**, 13–18.
5. (1995) *ASME B31.8*. Appendix L: Determination of remaining strength of corroded pipe.

STATIC STRENGTH AND STRESSED STATE OF MECHANICALLY INHOMOGENEOUS BUTT WELDED JOINTS WITH X-SHAPE GROOVE

A.A. OSTSEMIN and **V.L. DILMAN**
South-Ural State University, Chelyabinsk, Russian Federation

Static strength of welded joints comprising a less strong weld on plates with X-groove, compared with base metal, has been estimated by the method of solving the plane problem of the plasticity theory. The stressed state of mechanically inhomogeneous butt welded joints has been studied. The possibility of determining the optimal geometric size of the weld metal is shown.

Keywords: *butt welded joints, relative thickness, soft interlayer, gap, weld root, bevel angle, welded edges, limit tensile force, local strengthening, mechanical inhomogeneity, inhomogeneity coefficient*

Strength and stressed state of mechanically inhomogeneous welded joints are determined by a geometric form and size of soft interlayers, which may be represented by welds, HAZ, and decarburizated zone located near fusion boundary [1] in the oil-and-gas and chemical equipment (pressure vessels, pipes, piping fittings, and cryogenic equipment). Presence in welded joints of soft interlayers, the metal of which has lower in comparison with the base metal yield strength (soft welds), causes localization of plastic deformations in them. In soft welds, as well as in flat soft interlayers, volumetric stressed state occurs and effect of local strengthening takes place as a result of a plastic deformation restrain by a more strong metal over the contact surfaces (fusion boundaries).

By now serviceability of welded joint with flat soft interlayers has been studied in detail [2, 3]. However, geometric form of the latter may be quite different as it is often stipulated by the method of preparation of the edges to be welded, for example, in case of welding plates and pipes of big diameter and significant thickness with X-shape symmetric groove [1].

It is shown in [1] that stressed state of X-shape soft welds may be represented by means of a grid of slip lines. All X-shape symmetric welds may be conditionally divided into three groups, for each of which certain ranges of geometric parameter change are peculiar. However, absence of a mathematical description of static strength dependence upon geometric parameters and degree of mechanical inhomogeneity of

welded joints with the X-shape soft weld significantly reduces possibility of using the theory of local strengthening.

In [4] an approximate method of estimating strength of welded joints with X-shape soft welds based on the method of slip lines is proposed. Distribution of stresses in the considered interlayer is given according to the Prandtl solution.

However, influence of a shape and a size of soft welds on their strength and stressed state from the viewpoint of the plasticity theory is insufficiently studied.

In this work calculated estimation of static strength of welded joints on plates with X-groove (soft weld) is given based on solution of a plane problem of plasticity theory [5], by means of which it is possible to determine optimal gaps h_{opt} in a weld root and bevel angles φ of the edges to be welded (Figure 1).

Theoretical analysis of welded joints on plates was carried out taking into account conditions and assumptions presented in [3, 5]. Static tension (compression) of joints with a soft weld without reinforcement in the ultimate stage of plastic deformation (tough fracture) was considered. Materials in the joint were assumed to be homogeneous, isotropic, and ideally rigidly plastic. It was considered that residual stresses were absent in the presence of significant plastic deformations. In this work besides usual assumptions and simplifying conditions, which are used in theoretical studies of mechanically inhomogeneous welded joints, an assumption [3] was also used, which matches theory of a plastic layer [5] and generalizes known assumption of L. Prandtl, namely tangent stresses τ_{xy} in a soft interlayer linearly depend upon the plane, on which $\tau_{xy}(x, y) = 0$ (see Ox axis in Figure 1).

The purpose of the work is determination of strength and stressed state in mechanically inhomogeneous butt welded joints with the X-shape symmetrical groove.

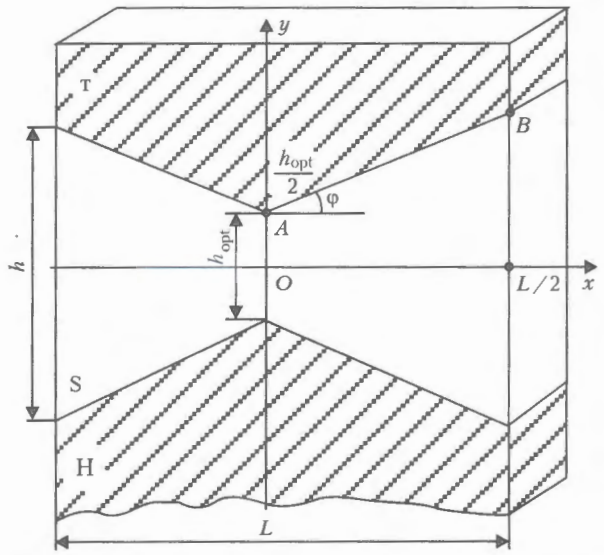

Figure 1. Parameters of soft interlayer of butt welded joints with X-groove: $\nu = h_{opt}/h$; $\chi_0 = h_{opt}/L$; $\chi = h/L$; $y = f(x)$; $0 \le \chi \le \le L/2$

Tangent stresses in a soft interlayer are stabilized near free surfaces. We will obtain on the contact surfaces

$$\tau_{xy}^{con} = \alpha k_w \quad (0 < \alpha < 1), \tag{1}$$

where $\alpha = K_t - 1$ is the parameter, which characterizes involvement of the base metal into plastic deformation, and depends upon mechanical inhomogeneity of a welded joint; $K_t = \sigma_t^{HM}/\sigma_t^{SM}$; σ_t^{HM} and σ_t^{SM} are the ultimate strengths of more strong hard (H) base metal and less strong soft (S) metal of the interlayer; k_w is yield shear strength of the weld metal. If we assume that function τ_{xy} in a soft interlayer depends linearly on y, it allows using together with condition (1) the formula for calculation of normal stresses σ_y [5]:

$$\sigma_y = k_w \times$$
$$\times \left(2 + \frac{1}{2} \ln \operatorname{ch} \frac{4\alpha x}{h} + \frac{4\alpha^2}{h^2} \frac{y^2}{\operatorname{ch}^2 \frac{2\alpha x}{h}} + \frac{1}{2} \ln \operatorname{ch} \frac{4\alpha x}{h} + \frac{\alpha^2}{3} \right). \tag{2}$$

Let $y = f(x)$ is the function, which describes, the contact surface line (curve AB in Figure 1). We assume that linear function $f(x)$ is monotonous within $[0; L/2]$ and does not have inflection points (here L is the thickness of a specimen).

Limit tensile force may be written as $P = P_0 + P_1$, where

$$P_0 = 2\int_0^{L/2} \sigma_y \left(x, \frac{h}{2} \right) dx;$$

$$P_1 = 2\int_0^{L/2} \left[\sigma_y(x, f(x)) - \sigma_y \left(x, \frac{h}{2} \right) \right] dx.$$

As far as $f(x)$ determines contact surface, then

$$P = 2\int_0^{L/2} [\sigma_y(x, f(x))] dx.$$

Integral P_0 is calculated along the line $y = h/2$ like in case of a rectangular interlayer. That's why it is possible to use results of [5] and obtain

$$P_0 = k_w L \left(-\frac{\alpha^2 + 0.2}{2\alpha} \chi + \frac{\alpha}{2\chi} + 2 + \frac{\alpha^2}{3} \right). \tag{3}$$

Having used (2) we calculate the force P_1. At $f(x) = \frac{h_{opt}}{2} + \frac{h - h_{opt}}{L}$ we obtain the following expression (details of the calculation are not given):

$$P_1 = \frac{k_w \alpha}{16} (1 - \nu) L \chi \left[4(1 + \nu) \operatorname{th} \frac{\alpha}{\chi} + (3 + \nu) \operatorname{th} \frac{2\alpha}{\chi} \right], \tag{4}$$

where $\nu = \frac{h_{opt}}{h} = \frac{\chi_0}{\operatorname{tg} \varphi + \chi_0}$; χ_0 and χ are the minimal and the maximal relative thicknesses of a soft interlayer, respectively; $\operatorname{tg} \varphi = (h - h_{opt})/L$.

From expressions (3) and (4) were obtain that limit tensile force equals

$$P = k_w L \left[\left(-\frac{\alpha^2 + 0.2}{2\alpha}\chi + \frac{\alpha}{2\chi} + 2 - \frac{\alpha^2}{3}\right) + \right.$$
$$\left. + \frac{\alpha(1-\nu)\chi}{16}\left(4(1+\nu)\,\text{th}\,\frac{\alpha}{\chi} + (3+\nu)\,\text{th}\,\frac{2\alpha}{\chi}\right)\right]. \quad (5)$$

For mean limit stress we obtain from the formula (5)

$$\sigma_y^{mean} = 2k_w \left[\left(1 + \frac{\alpha}{4\chi} - \frac{\alpha^2 + 0.2}{4\alpha}\chi + \frac{\alpha^2}{6}\right) + \right.$$
$$\left. + \frac{\alpha(1-\nu)\chi}{32}\left(4(1+\nu)\,\text{th}\,\frac{\alpha}{\chi} + (3+\nu)\,\text{th}\,\frac{2\alpha}{\chi}\right)\right]. \quad (6)$$

When the narrowest part of the X-shape interlayer is approached, the level of normal stresses σ_y significantly increases. At $\varphi = 0$ and $\nu = 1$ expression (6) is transformed into the formula for a rectangular interlayer [3] (at $\alpha_1 = \alpha_2$):

$$\sigma_y^{mean} = 2k_w \left(1 + \frac{\alpha}{2\chi} - \frac{\alpha^2 + 0.2}{4\alpha}\chi + \frac{\alpha^2}{6}\right). \quad (7)$$

In order to use expression (7) for welded joints, the weld metal of which is strengthened in the process of plastic deformation, it is necessary to replace $k_w = \sigma_y^{SM}/\sqrt{3}$ (σ_y^{SM} is the yield strength of the weld metal) in the dependences (3)–(6) for $\sigma_t^{SM}/\sqrt{3}$ (σ_t^{SM} is the tensile strength of a soft weld) [2]. By means of the gap h_{opt} reduction, ν also reduces in the weld root and, therefore, mean limit stress σ_y^{mean} increases according to (6). Dependence of the value $\Delta\sigma_y^{mean}$, by which mean limit stress of the X-shape interlayer, calculated according to (6), exceeds similar value of conventional plane-parallel soft interlayer of h width, upon relative depth of the X-shape interlayer (Figure 2) has the form

$$\Delta\sigma_y^{mean} = \frac{\sigma_t^{SM}}{16\sqrt{3}}\alpha(1-\nu)\chi \times$$
$$\times\left[4(1+\nu)\,\text{th}\,\frac{\alpha}{\chi} + (3+\nu)\,\text{th}\,\frac{2\alpha}{\chi}\right]. \quad (8)$$

Increase of the mean ultimate stress $\Delta\sigma_y^{mean}$ by means of the gap h_{opt} reduction at the weld root, while thickness of soft interlayer h remains constant, matches well experimental [6] and theoretical [7] results obtained. The root of the X-shape soft symmetrical welds is the place of the stress concentration and, therefore, may be a center of brittle failure.

Experience of construction of pipelines showed that the most characteristic kind of weld rupture is a through crack, which propagates at a certain length over a circumferential weld axis. It starts from primary defects (undercuts, lack of penetration, and accumulation of pores and slag inclusions), which are located

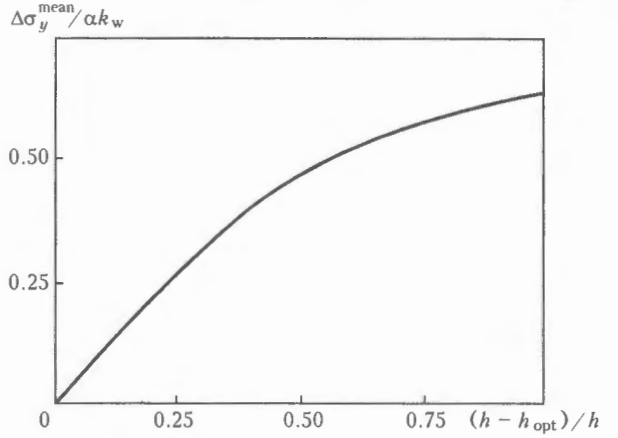

Figure 2. Dependence of correction $\Delta\sigma_y^{mean}$ of mean limit stress upon relative depth of X-groove of $1 - \nu = h - h_{opt}/h$

mainly in the root layer and over fusion boundaries. A butt weld may fail over the whole perimeter or over a blowhole depending upon the level of acting stresses and mechanical properties of a weld metal [8].

Hazard of brittle failure increases by means of reduction of the gap h_{opt} in the weld root because of sharp increase of maximal stresses σ_y^{max}. Proceeding from the value of resistance R_γ^w to the weld material breaking, it is possible to estimate possibility of brittle failure of a welded joint. Dependence of the local strengthening coefficient $K_\chi = \sigma_{mean}/2k_w$ upon relative thickness of the interlayer χ at different bevel angles φ of edges in the welded joints is given in Figure 3. Values K_χ reduce by means of increase of the bevel angle φ and relative thickness χ of a soft interlayer. At $\varphi = 35°$ and $\chi_0 = 0$ (gap in the weld root is absent) $K_\chi = 1$, which means absence of local strengthening in a welded joint. Calculated values of K_χ for

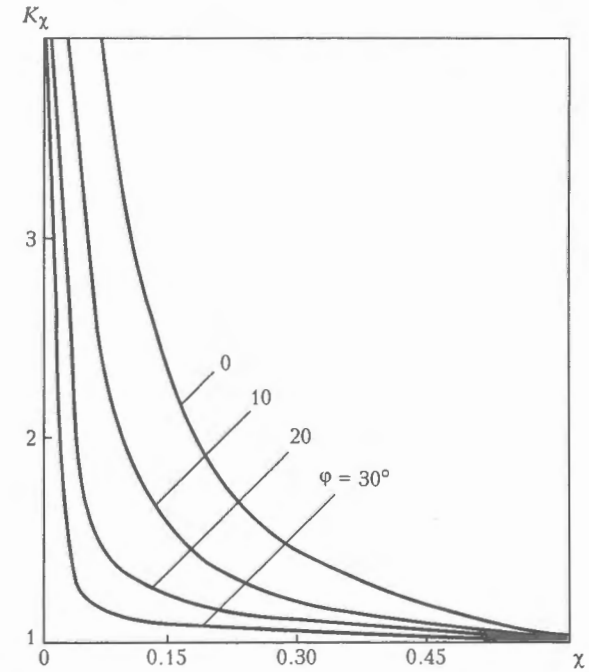

Figure 3. Dependence of local strength coefficient K_χ upon relative thickness of a soft interlayer χ at various angles of inclination φ of X-shape soft interlayer

χ	φ, deg	$\frac{2}{\sqrt{3}} K_\chi^{exp}$	$\frac{2}{\sqrt{3}} K_\chi^{calc}$	$\frac{K_\chi^{exp} - K_\chi^{calc}}{K^{exp}} \cdot 100$ %
0.15	26.0	1.30	1.282	1.4
0.45	12.4	1.29	1.156	10.3
0.10	28.0	1.29	1.298	0.6
0.25	21.0	1.29	1.253	2.8
0.17	22.3	1.32	1.310	0.7
0.25	19.3	1.25	1.268	1.4
0.22	20.8	1.25	1.270	1.6
0.11	27.5	1.25	1.290	3.2
0.09	34.6	1.20	1.256	3.3
0.34	21.0	1.20	1.193	0.6
0.17	30.0	1.20	1.200	0
0.22	25.6	1.22	1.240	1.6
0.25	30.5	1.19	1.200	0.8
0.10	35.7	1.13	1.230	8.8
0.06	36.8	1.11	1.240	11.7
0.54	27.0	1.08	1.060	1.8
0.15	41.3	1.10	1.190	8.4

plates satisfactorily correspond to the obtained on nomograms, given in [1], and experimental data of [6].

In [4] results of experimental data are given. Welded specimens were made from high-strength steel sheets of 16–20 mm thickness. The plates were welded with 1.6 mm diameter wire Sv-10GSMG in CO_2. Tensile strength of the weld metal σ_t^{SM} = 600–700 MPa. Width of the specimens was 100 mm, which ensured plane deformation in soft X-shape welds. The mechanical inhomogeneity coefficient of these joints equal to 2.2–2.4 is rather high, that's why involvement of the base metal into plastic deformation in calculation of estimated values of K_{pl}^{calc} was not taken into account, i.e. $\alpha \approx 1$. Calculated according to (6) and experimental values of parameters [4, 6] obtained by Dr. V.P. Erofeev are given in the Table. Comparison of these data in regard to the carrying capacity of welded joints during change of χ within the range of 0.10–0.54 and bevel angle φ within 12–41° showed their good correspondence. Mean error is 3.5 %. Here $K_\chi^{exp} = \sigma_t^{exp}/\sigma_y^{SM}$ and $K_\chi^{calc} = \sigma_y^{mean}/\sigma_y^{SM}$ are the experimental and calculated values of the local strengthening coefficients, where σ_t^{exp} are the experimental values of tensile strength of welded specimens; σ_y^{mean} are the calculated mean limit stresses.

Proposed relations for static strength of mechanically inhomogeneous symmetrical butt welded joints with the X-groove may be used at the stage of structural-technological designing of welded structures.

CONCLUSIONS

1. The method of estimation of strength of welded joints with the X-shape symmetrical soft welds, developed on the basis of belonging to the authors methodology of a plane problem solution (from the plasticity theory), makes it possible to determine values of limit stresses in welded joints on plates depending upon a gap in the weld root and a bevel angle of welded edges.

2. Experimental values of the local strengthening coefficient match well calculated values (an error about 3.5 %).

3. The data on influence of the gap in the weld root, a bevel angle of edges, and degree of mechanical inhomogeneity allow selecting optimal geometric sizes of less strong welds, thus ensuring strength characteristics of a welded joint metal at the level of the base metal.

1. Bakshi, O.A., Erofeev, V.P. (1971) Stressed state and strength of X-butt weld. *Svarochn. Proizvodstvo*, **1**, 4–7.
2. Bakshi, O.A. (1965) On stressed state of soft interlayers in welded joints at tension (compression). In: *Transact. of Chelyabinsk Polytechn. Inst. on Problems of Welding Production*, **33**, 5–26.
3. Dilman, V.L., Ostsemin, A.A. (1998) Stressed state and strength of welded joints with mechanical inhomogeneity. *Svarochn. Proizvodstvo*, **5**, 15–17.
4. Shakhmatov, M.V., Khmarova, L.I., Tyupyshev, Yu.A. (1985) Assessment of statistical strength of mechanically inhomogeneous X-shaped welded joints. *Ibid.*, **9**, 33–35.
5. Ostsemin, A.A., Dilman, V.L. (1990) Compression of plastic layer by two rough plates. *Problemy Prochnosti*, **7**, 107–112.
6. Erofeev, V.P. (1973) *Investigations of influence of soft interlayer geometry of welded joints on their stress-strained state and strength*. Syn. of Thesis for Cand. of Techn. Sci. Degree. Chelyabinsk.
7. Dilman, V.L., Ostsemin, A.A. (2001) On stress-strained state at tension of plastic layer with two axes of symmetry. *Mekhanika Tv. Tela*, **6**, 115–124.
8. Rakhmanov, A.S., Tarlinsky, V.D., Chaburkin, V.F. (1971) Causes and mechanism of fracture of circular welded joints. *Stroitelstvo Truboprovodov*, **4**, 17.

APPLICATION OF ELECTRIC PULSE TREATMENT OF STRUCTURAL ELEMENTS TO EXTEND THEIR SERVICE LIFE (REVIEW)

L.M. LOBANOV[1], N.A. PASHCHIN[1], V.P. LOGINOV[1] and Yu.V. LOGINOVA[2]
[1]E.O. Paton Electric Welding Institute, NASU, Kiev, Ukraine
[2]NTUU «Kiev Polytechnic Institute», Kiev, Ukraine

Current concepts of the influence of structural material treatment by current pulses on their mechanical properties are generalized. Types of electric pulse impact on current-carrying materials are classified, and prospects for its application to improve the mechanical properties of welded joints are outlined. It is established that electric pulse treatment of welded joints may be promising for extending the service life of metal structures.

Keywords: *welded structures, electric pulse treatment, electric stimulation, electromagnetic field action, structural materials, aluminium alloys, specific treatment energy, current density, corrosion resistance, residual stresses*

Development of modern engineering and technologies necessitates searching for new ways to extend the operating life of welded metal structures in different industries. One of the promising directions of optimization of service properties of new equipment is improvement of mechanical properties of structural materials by their treatment by current pulses. Such is the process, based on the impact of electrodynamic forces on the current-conducting element. By changing the duration and energy of current pulses, acting on an electrically conducting material, it is possible to influence the ductility, hardness, wear resistance and strength of metals and alloys [1–3], as well as their welded joints, as a result of activation of a broad range of dislocation, phase and other mechanisms. The above phenomena can be accounted for by the hypothesis of electron-dislocation interaction [4, 5].

It is known that the electrodynamic forces in electric machines at short-circuiting current, reach the values equal to tens of thousands of newtons [6]. Deformations of the current-conducting contour arise, that may lead to its fracture. Electrodynamic forces depend on current, length, configuration and relative position of the parts of electric machines, as well as pinch effect [7, 8]. If structural elements from sheet conducting materials are part of the current-conducting contour, a change in the mechanical properties of the treated structural elements can be achieved at a certain value of the electrodynamic force.

In keeping with the classification proposed in [3], let us note the following actions of the electromagnetic field on the current-conducting materials.

Induction and contact heating, used to conduct the processes of electrothermal and thermomechanical treatment. This process is based on an integral heating due to scattering of Joule energy, proportional to the electric current density j^2. Duration τ of external current pulse action in such processes is determined by the time of establishment of a uniform temperature field in the treated material volume, as well as characteristic time τ^* of running of physical processes leading to a change of the metal structure and properties [1]:

$$\tau^* = \rho c l^2 / \kappa,$$

where ρ, c and κ are the density, specific heat capacity and heat conductivity of the material; l is the characteristic linear size of the material structure. Current density is $1 \cdot 10^6 \le j \le 1 \cdot 10^8$ A/m^2, and the duration τ of current pulse action is not less than 1 s.

Electrodynamic action of electromagnetic field to increase the ductility. Electric current parameters used in this case were changed in the range of $1 \cdot 10 \le j \le 1 \cdot 10^9$ A/m^2 and $\tau \ge 1 \cdot 10^{-5}$ s. The observed effects of material softening under the impact of an electromagnetic field are accounted for on the basis of the hypothesis of electron-dislocation interaction [4].

Electroplastic deformation of metals at their tension is manifested in tensile stress-strain diagrams in the form of characteristic dropping of the deforming force. It is believed [4, 5] that in the region of elastic deformation of metal the current pulses do not have any influence on metal ductility, but in the region of plastic deformation discrete dropping of the deforming force is observed [9], which increases with increase of current density. This is accounted for both by non-stationary dislocation displacement along slip planes, and the processes of the moving dislocations breaking through the barriers in the form of dislocation clusters, structural inhomogeneities of different type and grain boundaries. The rearrangement of the material dislocation structure under the impact of mechanical deformation during the electric pulse action is found. Absence of active load drop in the plastic region of material deformation before the moment of current pulse running in the above study, is attributable to

the fact that at this value of tensile load all the dislocations are unsurmountably pinned [10, 11]. Activation of relaxation processes of material prasticization directly at the moment of the current pulse running, showed that high-density electric current acts as initiator of dislocation stripping from the pinning sites and their non-stationary motion.

Thermal impact of the electromagnetic field is based on the presence of temperature gradients and electric potential – electric stimulation [12], determined by specific energy $q = 1 \cdot 10^5 - 1 \cdot 10^6$ J/m^3 per a unit of the treated material volume, and duration of current pulse action $\tau = 1-30$ s.

Under the impact of the electromagnetic field ($q = 1 \cdot 10^7 - 1 \cdot 10^{10}$ J/m^3 and $\tau \cong 1 \cdot 10^{11}$ s) an increase of ductility was observed [13] at a slight change of the current-conducting material strength. One of the possible explanations of the mechanism of the above action is local non-uniformity of evolution of energy q, associated with the presence of phases, non-metallic inclusion, concentrators of the electric and magnetic fields in the material structure.

At the current stage of development of mechanical engineering technology investigation of application of various kinds of electric pulse treatments for controlling the mechanical properties of welded structures is of practical interest.

Note that publications on application of welded joint treatment by current pulses are very few at present. On the other hand, investigations in the field of current pulse application for optimization of weld performance can have an important role in extension of the life of both the operating and manufactured welded structures [14]. Permanent joints of metal produced by welding, are characterized by several features compared to materials not subjected to thermal action, namely presence of the cast structure of weld metal, crystallization zones in the HAZ, metal hardness gradients (softening zones) in the joint cross-section, characteristic, in particular, for aluminium alloys. One of the main factors, influencing the item performance, is the stress-strain state of welded joints, with which such phenomena as phase transformations in the weld metal, dimensional stability and residual changes in the structure shape are associated, as well as lowering of the corrosion resistance in the joint zone. In a number of cases the welding processes lead to initiation of the hot and cold cracks in the metal, as well as fatigue strength drop.

Analyzing the work devoted to improvement of mechanical properties of structural materials enables evaluation of the prospects for application of welded joint treatment by current pulses as a method to extend the operating life of metal structures.

Based on the data obtained for different materials, evaluation of the prospects for application of current pulse treatment to improve the mechanical properties of welded joints was performed.

Influence of electric current pulses on the characteristics of aluminium alloys AD-1, D16 and AMg2 was studied in [3]. The alloys were supplied in the form of a sheet semi-finished product 3 to 5 mm thick, which was pre-treated by plastic deformation by cold rolling with the specified degree of reduction (deformation). After such treatment the material was used as initial material. In keeping with the defined problem, testing for static strength and crack resistance at static loading, as well as impact toughness was conducted before and after current pulse treatment.

At material treatment by current pulses, duration τ of the impact and specific energy q were varied. Energy required for the most efficient material treatment was determined theoretically [13], to optimize the range of q values. Energy resulting in sample fracture, was taken as the maximum possible one. Duration τ of current pulse impact and specific energy q was varied in the range of 0.22–0.36 s and $(0.5-1.3) \cdot 10^9$ J/m^3. It is established that current pulse treatment of samples of AD1 alloy leads to ductility increase by 30 % at $q = 0.9 \cdot 10^9$ J/m^3 and by 20–25 % at $q = 0.7 \cdot 10^9$ J/m^3. Ductility of samples of alloy D16 increases. However, if lowering of the material strength characteristics was found in AD-1 alloy samples, in samples of alloys AMg2 and D16 an increase of ultimate strength by 5–8 % was observed under the conditions of treatment in the optimum modes.

It should be noted that for D16 alloy of a limited solubility, susceptible to increased crack formation at local thermal action, increase of material ductility through pre-treatment of welded joints by current pulses may have a positive influence on their performance. Impact toughness testing of samples with a sharp notch was performed in the initial (with preliminary deformation), annealed and treated conditions. Obtained results showed that treatment by current pulses improves the impact toughness by 20 to 50 % relative to the work-hardened material, and by 10–15 % relative to annealed material in a narrow range of values of specific energy, while its maximum and ductility maximum of a specific alloy coincide. While the optimum values of toughness in AD-1 alloy are achieved at $q = 0.9 \cdot 10^9$ J/m^3, in AMg2 and D16 alloys – at $q = 1.4 \cdot 10^9$ and $17 \cdot 10^9$ J/m^3, respectively. Data of study [3] suggest that current pulse treatment of aluminium alloy welded joints may also have a positive influence on their impact toughness. It is established that the electric pulse treatment of alloys AD-1, D16 and AMg2 at q and τ values of $0.92 \cdot 10^9$ J/m^3 and 0.35 s, $1.5 \cdot 10^9$ J/m^3 and 0.37 s, $1.25 \cdot 10^9$ J/m^3 and 0.23 s, respectively, increases the COD value of the crack. Considering that the mechanisms of crack formation in the welded joints are close to the processes proceeding in the base metal, treatment of welded joints by current pulses can be regarded as a promising method of improving the performance of welded structures.

One of the causes for lowering of the welded structure performance during operation is initiation of microcracks in the weld and HAZ and their growing up to fracture. Therefore, investigations of the processes

of microcrack «healing» due to local heating of material in the crack tips are urgent.

In particular, electric processes proceeding on the crack faces and in its tip may have an important role in the mechanism of crack propagation [15]. The rate of crack propagation is due primarily to changes in the metal crystalline structure [2] under the impact of the electric field, that lead to metal strengthening. Pursuing the hypothesis of the change of the crystalline structure [16], a new method of magnetic-pulse strengthening of materials was studied [17], which is also applicable to welded joints. Its essence consists in that a sample is placed into a variable magnetic field and a discharge of a pulsed capacitor battery is applied to it. Use of a variable magnetic field is due to the fact that such values of the magnetic field intensity are achieved in each current pulse, which simulate the start of martensite transformations.

Physical essence of the process of surface strengthening of alloys consists in generation of high-density eddy currents, which results in the surface layer of the metal being heated up to the temperature of phase transformation and developing under the impact of strong magnetic fields and plastic deformation, a structure which consists of fine-needled martensite and finely-dispersed carbides and is characterized by a higher hardness.

From [18] it follows that passage of current pulses through a massive plate with an edge crack is accompanied by a microexplosion in the crack tip, leading to crater formation. The sample proper at a distance from the crack is heated just to several tens of degrees. This phenomenon can be used for blunting the crack tip.

In [19] a method was proposed for «healing» microcracks in the metal, using electric and magnetic fields. Such a possibility was studied on samples of armco-iron and steel 60G. Grain refinement and microhardness increase is found in the metal of the zone of restored continuity, compared to the initial metal.

In a number of studies, for instance [20], it is noted that electric pulse treatment of steels of various classes is the most effective after a certain cycle of structure operation. On the other hand, pre-treatment does not lead to improvement of the item serviceabiliy. It is obvious that purposeful application of this method requires knowledge of the regularities of the impact of current pulses on the structure and phase composition of the treated steels. In [21] such a treatment method was tried out on steel 08Kh18N10T and the possibility of improvement of performance of austenitic steel structures is proved.

It is known that structural elements exposed to alternating loading, may fail through fatigue at comparatively low rated stresses. From a large number of factors, influencing the fatigue resistance, the main one is stress concentration. In most of the cases, fatigue cracks initiate in the zones of cross-section variation or disruption of the surface layer. In welded structures, the locations of weld transition to the base metal and, particularly, defective weld regions, are the sites of fatigue fracture [22].

Several studies [22, 23] underline the need for suppression of initiation of stress microconcentrators in the material due to localization of microdeformations, which is achieved by material processing by powerful current pulses, optimized by frequency, amplitude and time of impact.

Over the recent years, a certain number of studies were devoted to the problem of extension of the fatigue life of steels, alloys and bimetal materials by their processing by powerful current pulses in a certain section of the fatigue curve [24, 25]. Based on analysis of the results of studying the phase composition of steels [26–28], it was established that such an action increases the fatigue life of items by 20 to 30 % and lowers corrosion cracking.

In [29] crack growth in a sample of steel 60GS2 was studied at fatigue testing up to fracture and under the conditions of electric stimulation by applying current pulses to the material. The time of this action was up to 15 s. The width of the zone of fatigue growth of the crack in a material untreated and treated by electric stimulation is 1.25 times larger than in a material fractured without treatment. The size of this zone corresponds to the critical crack length. Therefore, it may be assumed that electric stimulation extends the material operating life. Maximum length of the subcritical crack is also markedly different: in a sample subjected to electric stimulation it is almost 2 times greater than in an untreated sample. Therefore, treatment of steel 60GS2 at the intermediate stage of cyclic testing promotes an essential increase of the subcritical crack length. A positive change of the structure of steel 60GS2 under the conditions of intermediate treatment by current pulses at cyclic fatigue testing is noted [30]. One of the mechanisms, clarifying the nature of improvement of the steel fatigue strength at electric stimulation, is lowering of the level of residual stresses, as a result of local temperature increase in the discontinuity areas in the metal structure, resulting in stress relaxation [31]. This hypothesis was verified on steels 16GS and 09G2 [32, 33]. Duration of electric stimulation cycle was 30 s, and treatment was conducted after every thousand cycles up to material fracture. Analysis of the influence of electric stimulation on the properties of the studied materials shows that an improvement of structure performance by more than 70 % (together with heat treatment) is observed at the above loading cycles both in steel 16GS and 09GS.

Influence of the duration of electric stimulation on improvement of the properties of steel 40 and steel 45 was studied in [34]. Non-destructive testing [35] and optical microscopy methods were used to establish the duration of the current pulse action, at which an increase of ductility is found, and hence, an improvement of the structure performance [36]. Maximum treatment time was 135 s. During fatigue testing of samples treated by current pulses, it was established

that with increase of the duration of current pulse action τ from 30 to 70 s the time to fracture of the studied material increased. Maximum increase of the structure performance was observed at τ = 70 s, and was equal to 28 %. At increase of the duration of current pulse action to 135 s, the time to structure failure is reduced by 10 %. It is assumed that the action of the electroplastic effect [37] is the most clearly manifested at duration of current pulse action of up to 70 s; in case of a further increase of τ the thermal effect starts predominating, which may impair the material characteristics.

In [38–40] the influence of the action of alternating current pulses in a magnetic field on the structure and properties (strength, ductility, fatigue fracture resistance and crack resistance) of bimetal materials 40KhNMA and 38KhN3MFA clad with steels 08Kh19N9F2S2 and 07Kh25N12G2T was studied. The above materials are applied in modern ship-building, the clad steels being used as anticorrosion coatings. In view of that, studying of the influence of current pulse action on the metal corrosion resistance is of interest. Investigation results showed that at current pulse action on the surface of the treated materials, a metal layer with special physical-chemical properties and structure parameters forms — the so-called white layer. Considering that the shipbuilding structures develop electric corrosion, its role can be compared with that of an anticorrosion coating. Metallographic investigations revealed a lowering of the quantity of impurities on grain boundaries of the base steel material 40KhNMA and 38KhN3MFA after current pulse impact, as well as dislocation coming to the metal surface, this practically eliminating development of intercrystalline corrosion, and increasing the fatigue strength of these steels in a corroding environment (sea water).

One of the factors, determining the welded structure performance, are residual stresses, adversely affecting, in particular, the strength, corrosion resistance and geometrical characteristics of the items. Lowering of residual stress level is favourable for extension of the structure fatigue life.

It is established that action of current pulses on the metal subjected to tension up to the ductility level [9], leads to relaxation of the metal stress-strain state. Tensile stresses close to the metal yield point, develop in the weld and HAZ. Weld and HAZ treatment by current pulses can have a positive influence on lowering of the level of the residual stress-strain state of metal structures.

Application of treatment by current pulses to improve the mechanical properties of welded joints on molybdenum and its alloys made by flash-butt welding was studied [41]. High-energy pulses of up to 0.6 s duration were applied to joints of 8 mm diameter rods from molybdenum alloys. This resulted in improvement of mechanical properties of treated joints, compared to untreated joints, which is attributable to acceleration of the processes of diffusion and relaxation of stresses, «healing» of microdefects and formation of a dispersed dislocation structure.

When welds were made by the electroslag process the liquid and cooled down weld metal was treated by a pulsed electromagnetic field [42]. This was followed by mechanical testing, the results of which showed an increase of impact toughness by 30 % and lowering of the cold brittleness limit from –40 to –65 °C. This is attributable to the fact that the impact of the electromagnetic field on the weld pool in the electroslag process promotes an increase of the solidification centers and grain refinement at recrystallization.

CONCLUSIONS

1. Current pulse impact on structural materials causes activation of the dislocation, phase and thermomechanical processes, which results in a change of the mechanical properties of the treated metals and alloys.

2. It is established that different kinds of current pulse action at specified energy parameters of the process have a positive influence on the stressed state, static and fatigue strength, ductility, crack- and corrosion resistance, as well as impact toughness of aluminium alloys, structural steels and bimetal materials.

3. Analysis of the results of research devoted to improvement of the mechanical properties of structural materials shows the good prospects for application of welded structure treatment by current pulses as a method to extend their service life.

1. Beklemishev, N.N., Gorbunov, N.M., Koryakin, N.I. et al. (1989) *Ductility and strength of metallic materials at pulse action of high-energy electromagnetic field*. Moscow: IPM AN SSSR.
2. Troitsky, O.A., Rozko, A.G. (1970) Electroplastic deformation of metal. *Fizika Tv. Tela*, 12(**1**), 203–210.
3. Baranov, Yu.V., Troitsky, O.A., Avramov, Yu.S. et al. (2001) *Physical principles of electric pulse and electroplastic treatments and new materials*. Moscow: MGIU.
4. Spitsin, V.V., Troitsky, O.A. (1985) *Electroplastic deformation of metals*. Moscow: Nauka.
5. Klimov, K.M., Novikov, I.I. (1980) Specifics of plastic deformation of metals in the electromagnetic field. *Doklady AN SSSR*, 253(**3**), 603–606.
6. Aleksandrov, G.I. (1985) *Theory of electric apparatuses*. Moscow: Vysshaya Shkola.
7. Spitsin, V.I., Troitsky, O.A. (1974) Effect of electric current and pulsed magnetic current on creep rate of metal. *Ibid.*, 216(**6**), 1266–1269.
8. Spitsin, V.I., Troitsky, O.A. (1977) Electroplastic effect in metals. *Vestnik AN SSSR*, **11**, 10–15.
9. (2004) Acoustic emission in electric pulse deformation of titanium alloys. *Materialovedenie*, **7**, 29–33.
10. Petrunin, V.A., Chirakadze, D.Z., Tsellermajer, V.Ya. et al. (1997) Synergy of electrostimulated fatigue fracture. *Izvestiya Vuzov. Chyorn. Metallurgiya*, **6**, 46–49.
11. Petrunin, V.A., Tsellermajer, V.Ya., Gromov, V.E. et al. (1999) Mesoscopic level of plastic deformation under the conditions of electrostimulated fatigue fracture. *Fizich. Mezomekhanika*, **4**, 91–93.
12. Klimov, K.M., Novikov, I.I. (1983) Action of electric current pulses on the process of tension of thin metallic wires. *Metally*, **3**, 155–158.
13. Baranov, Yu.V., Tananov, A.I., Koryagin, S.N. et al. (1980) Substructure modifications in copper at pulse action of electromagnetic field. *Fizika i Khimiya Obrab. Materialov*, **4**, 62–68.
14. Benklemishev, N.N., Baranov, Yu.V., Doronin, Yu.L. et al. (1990) Influence of pulse electric current on characteristics

of structural strength of metallic materials. *Ibid.*, **4**, 108–112.
15. Finkel, V.M. (1977) *Physical principles of fracture retardation.* Moscow: Metallurgiya.
16. Finkel, V.M., Golovin, Yu.I., Ivanov, V.M. et al. (1981) On strengthening of metal in the mouth of a crack flown about by a current pulse. *Fizika i Khimiya Obrab. Materialov*, **2**, 42–45.
17. Gajduk, V.V., Rokkel, V.R., Gajduk, D.V. et al. (2004) Surface strengthening of metallic materials using the magnetic-pulse unit. *Stal*, **7**, 87–89.
18. Golovin, Yu.I., Finkel, V.M., Sletkov, A.A. (1997) Formation of a crater in the crack tip at action of high-power local electromagnetic field. *Fizika i Khimiya Obrab. Materialov*, **3**, 18–23.
19. Finkel, V.M., Ivanov, V.M., Golovin, Yu.I. (1983) Healing of cracks in metals by intersecting electric and magnetic fields. *Problemy Prochnosti*, **4**, 54–58.
20. Stepanov, G.V., Babitsky, A.I. (1995) Influence of high-density pulse current on fatigue life of a steel specimen with a concentrator. *Ibid.*, **5**, 74–78.
21. Ivanov, Yu.V., Lychagin, D.V., Gromov, V.E. et al. (2000) Mesoscopic substructure and electric pulse suppression of fatigue fracture. *Fizich. Mezomekhanika*, 3(**1**), 103–108.
22. Panin, V.E. (1998) Principles of physical mesomechanics. In: *Physical mesomechanics*. Vol. 1.
23. Zuev, L.B., Sosnin, O.V., Gromov, V.E. et al. (1997) Possibility of healing of fatigue damages. *Metallofizika i Nov. Tekhnologii*, 19(**8**), 80–82.
24. Kovalenko, V.V., Sosnin, O.V., Ivanov, Yu.F. et al. (2000) Evolution of defective structure and phase shift of steel 18N10T at low-cycle fatigue testing. *Fizika i Khimiya Obrab. Materialov*, **6**, 74–80.
25. Konovalov, S.V., Sosnin, O.V., Ivanov, Yu.F. et al. (2003) Electron-microscopic analysis of steel 45G17Yu3 at electrostimulated high-cycle fatigue. *Izvestiya Vuzov. Chyorn. Metallurgiya*, **10**, 65–69.
26. Ivanov, Yu.F., Sosnin, O.V., Suchkov, E.Yu. et al. (2003) Electroplastification of hardened carbon steel. *Fizich. Mezomekhanika*, **6**, 71–75.
27. Volodin, V.L., Tkhaj, V.D., Konkov, Yu.F. et al. (2002) Study of effect of pulse actions on corrosion resistance of metallic and bimetallic materials. *Izvestiya Vuzov. Chyorn. Metallurgiya*, **6**, 39–43.
28. Konovalov, S.V., Lejkina, O.S., Semukhin, B.S. et al. (2002) Recovery of residual life of steel products at high-cycle fatigue by current pulse actions. *Perspekt. Materialy*, **3**, 45–48.
29. Sosnin, O.V. (2003) Suppression of cracking in steel 60GS2 by current pulses at high-cycle fatigue. *Izvestiya Vuzov. Chyorn. Metallurgiya*, **12**, 30–32.
30. Sosnin, O.V., Ivanov, Yu.F., Gromov, V.E. (2003) Evolution of 60GS2 steel structure at cyclic fatigue testing under the current action conditions. *Ibid.*, **12**, 27–30.
31. Gromov, V.E., Zuev, L.B., Kozlov, E.V. et al. (1996) *Electrostimulated ductility of metals and alloys.* Moscow: Nedra.
32. Konovalov, S.V., Sosnin, O.V., Semukhin, B.S. et al. (2000) Low-cycle fatigue of low-carbon steels 16GS and 09G2S at electric stimulation. *Izvestiya Vuzov. Chyorn. Metallurgiya*, **10**, 55–57.
33. Muraviov, V.V., Zuev, L.B., Komarov, K.A. (1996) *Sound velocity and structures of steels and alloys.* Novosibirsk: Nauka.
34. Troitsky, O.A., Moiseenko, M.M. (1984) On problem of velocity dependence of electron-plastic effect. *Izvestiya AN SSSR. Metally*, **4**, 38–43.
35. Borodina, M.M., Spektor, E.N. (1981) *X-ray analysis of metal and alloy texture.* Moscow: Metallurgiya.
36. Sosnin, O.V., Gromov, V.E., Kozlov, E.V. et al. (2000) *Electrostimulated low-cycle fatigue.* Moscow: Nedra.
37. Gromov, V.E., Zuev, L.B., Kozlov, E.V. et al. (1996) *Electrostimulated plasticity of metals and alloys.* Moscow: Nedra.
38. Volodin, V.L. (1993) Study of the influence of thermal energy actions on the structure and properties of bimetallic joints. *Izvestiya Vuzov. Chyorn. Metallurgiya*, **8**, 74–77.
39. Volodin, V.L., Gajduk, V.V., Maslyakov, A.A. et al. (2001) Study of pulse actions on the structure and properties of bimetallic materials. *Ibid.*, **2**, 45–49.
40. Volodin, V.L., Sarychev, V.D., Gudimova, L.N. et al. (1990) Influence of pulse magnetic fields on the structure and properties of metallic alloys. *Ibid.*, **10**, 77–79.
41. Yaroslavtsev, S.A., Kurochkin, Yu.V., Podolsky, A.Ya. et al. (1988) Improvement of mechanical properties of welded joints. In: *Abstr. of All-Union Conf. on Application of Pulse Technology in Welding Fabrication* (Nikolaev, Oct. 4–6, 1988). Nikolaev: TsNII Lot.
42. Ponomarenko, V.N., Korneev, D.I., Sharchenko, K.I. (1987) Improvement of properties of welded joints at action of pulse electromagnetic fields on ESR process. In: *Abstr. of 1st All-Union Conf. on Action of Electromagnetic Fields on Ductility and Strength of Metals* (Yurmala, 29 Sept.–1 Oct. 1987). Moscow: A.A. Blagonravov IM.

TECHNOLOGY FOR EBW OF PRECISION PARTS AND SEALING OF CASINGS OF ELECTRIC VACUUM DEVICES

The technology is intended for precision electron beam welding of casings of electric vacuum devices and gyro-scopes, as well as sealing of microcircuits in aluminium capsules. The technology is used as a finishing operation in manufacture of high-precision devices.

The technology provides minimal welding distortions (not more than 0.03 mm on a diameter of 100 mm), insignificant (not more than 60 °C) heating of assembly or microcircuit elements located inside a casing, and permits location of the pressure seals on the casing of a device at a distance of up to 2 mm from the weld, which are joined to the casing using adhesive or sealing agents of different compositions.

Application of a package of technical recommendations provides quality welds and high reliability and performance of devices under severe service conditions.

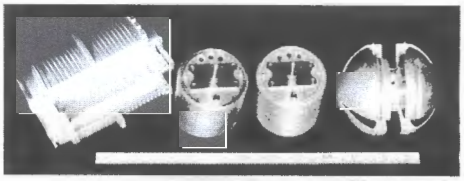

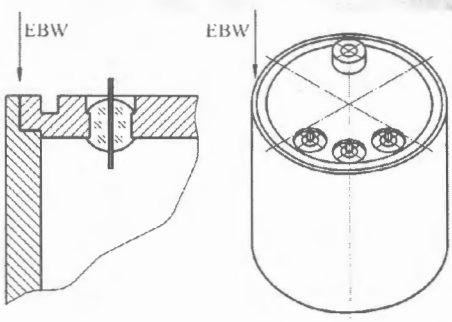

Proposals for co-operation. Development of technical documents, transfer of know-how for the technology, technical consultations and engineering services in commercial application of the technology.

SEALING OF HOT-ROLLED STEEL 20KhN4FA CYLINDER BOTTOMS BY WELDING

A.K. TSARYUK, V.Yu. SKULSKY, A.R. GAVRIK, S.I. MORAVETSKY and G.N. STRIZHIUS
E.O. Paton Electric Welding Institute, NASU, Kiev, Ukraine

Considered are causes of defects formed in hot-rolled cylinder bottoms and peculiarities of their repair. Weldability of steel 20KhN4FA has been evaluated, and recommendations are given on preheating temperature, welding electrodes and manual arc welding procedure. Automatic submerged-arc welding on a backing was tried out as an alternative welding process.

Keywords: *arc welding, hot rolling, cylinder bottom, cylinder manufacture technology, sealing*

One of the methods for commercial manufacture of automotive gas cylinders is hot rolling of necks and bottoms. Sections of seamless pipes 4 mm thick and 215 mm in diameter, made from steel 20KhN4FA, are used as billets. After rolling, thickness of cylinder bottoms increases to 15–18 mm. Because of high-temperature heating to the state of high ductility of metal and rapid recrystallisation under deformation conditions, the ends of pipes become covered with a scale, which is retained on the bottom wall within the rolling zone in the form of interlayers. To guarantee sealing of the resulting spherical bottoms, the joining zones of deformed pipe ends at the top of a sphere are welded up by the fusion arc method. However, as revealed by hydraulic tests of experimental cylinder samples, welding of the bottoms without special machining fails to ensure consistent tightness of the joints. Given below are the results of investigations on selection of method, type of treatment, procedure and parameters of welding to produce welded joints at the tops of rolled bottoms.

Weldability of steel 20KhN4FA and selection of thermal welding conditions. Steel 20KhN4FA belongs to a category of high-strength materials and is usually recommended for manufacture of non-welded parts [1]. The carbon equivalent calculated from the known IIW formula [2] for maximum permissible variations of chemical elements in the composition of steel 20KhN4FA, according to GOST 4543–71 (Table 1), is C_{eq} = 0.64–0.89, which is indicative of a high sensitivity of this steel to cold cracking (the target criterion is C_{eq} = 0.40–0.45; if C_{eq} is higher, the steel is considered sensitive to cracking).

To evaluate weldability of this steel, investigations were conducted to study the character of continuous cooling transformations in HAZ, and the optimal heating temperature in welding was selected on the basis of the results of testing to sensitivity to cold cracking [3].

Results of dilatometric examinations shown in Figure 1 indicate that a purely martensitic structure characterised by high hardness is formed in the HAZ metal at cooling rate $w_{6/5}$ (within a temperature range of 600–500 °C) above 20 °C/s. Slow cooling leads to intensification of diffusion processes and intermediate (bainitic) transformation. As the volume fraction of the bainitic component increases, hardness of metal decreases, although at $w_{6/5}$ > 16 °C/s it is still higher than the target values (*HV* 3500–4000 MPa [2]). Exceeding these values leads to growth of the risk of cold cracking.

Preliminary (concurrent) heating is an efficient method for controlling thermal conditions during welding. It allows affecting both the force and physical-metallurgical (diffusion and phase transformations, hydrogen transport) factors that influence structure of the HAZ metal and technological strength of the welded joints.

Welded joints in steel 20KhN4FA were tested to sensitivity to cold cracking by the implant method in order to identify the optimal temperature of preliminary heating [4]. Welding was performed with preliminary heating from 150 to 300 °C using electrodes providing the concentration of diffusible hydrogen equal to 4.5 cm^3/100 g Me. Heating to above 200–250 °C was found to provide dramatic increase in crack resistance. As seen from the diagram shown in Figure 2, which relates preliminary heating temperature T_{pr}, HAZ metal cooling rate $w_{5/6}$ (under the implant test conditions) and associated bainite content in the bainitic-martensitic structure of the HAZ metal, as

Table 1. Chemical composition of steel 20KhN4FA, wt.%

Material	C	Mn	Si	Cr	Ni	V	Cu	S	P
As-received	0.23	0.38	0.40	0.87	3.96	0.11	0.18	0.010	0.007
GOST 4543–71	0.17–0.24	0.25–0.55	0.17–0.37	0.70–1.10	3.75–4.15	0.10–0.18	< 0.30	< 0.025	< 0.025

well as hardness *HV* 50 (taken from the austenite continuous cooling transformation diagram), welding with heating from 200 to 300 °C provides a sufficient cooling rate for precipitation of 3 to 6 vol.% bainite in the HAZ metal. Hardness of this metal is about *HV* 50-4400–4500 MPa.

Therefore, a high cold crack resistance of welded joints in steel 20KhN4FA is provided at cooling rates that initiate beginning of bainitic transformation in structure of the HAZ metal. This is achieved in preliminary heating to 200–300 °C recommended for welding of cylinder bottoms.

Selection of electrodes and mechanical properties of welded joints. As steel 20KhN4FA has never been used for producing welded joints, no recommendations are available for selection of consumables to weld it. Because this steel is categorised as hardening and hard-to-weld one, it is necessary to limit the transfer of hydrogen to HAZ from the deposited metal, in addition to using preliminary heating, in order to reduce the risk of cold cracking during welding. For this, it is required to apply welding consumables with a basic type of coverings. Also, it is indicated to apply welding consumables providing the weld metal with a lower yield stress compared with the HAZ metal in order to reduce the degree of «rigidity» of a welded joint, which is a factor that leads to accumulation of internal stresses and initiation of cold cracks in HAZ under the thermal-deformation cycle of welding. Growth of stresses and development of plastic strains in shrinkage of the weld, while favouring decrease in the level of internal stresses in a welded joint, lead to cold work hardening of the weld metal and, hence, to increase in its strength properties [5].

Several grades of covered electrodes applied for welding critical structures of low-alloy carbon steels were tried out (Table 2). Metal deposited by using these electrodes has a close chemical composition, wt.%: 0.07–0.09 C, 0.25–0.50 Si, 0.63–1.30 Mn, 0.02–0.03 S and 0.015–0.030 P. However, a combination of increased ductility and sufficiently high strength properties can be provided only with electrodes TMU-21U, Fox EV 50, OK 53.70 and LB-52U. For example, metal of steel 20KhN4FA pipes has the following strength properties: tensile strength — 1334–1520 MPa, and yield stress — not less than 1079 MPa.

Table 2. Mechanical properties of deposited metal in manual arc welding

Electrode grade	σ_y, MPa	σ_t, MPa	δ_5, %	ψ, %	*KCV*, J/cm², at *T*, °C	
					+20	–20
UONI-13/45	360	470	24	57	155	–
TMU-21U	370	520	25	59	155	–
TsU-5	350	500	22	58	147	–
Fox EV 50	450	540	30	65	–	180
OK 53.70	440	530	30	68	–	200
LB-52U	510	600	25	71	–	195

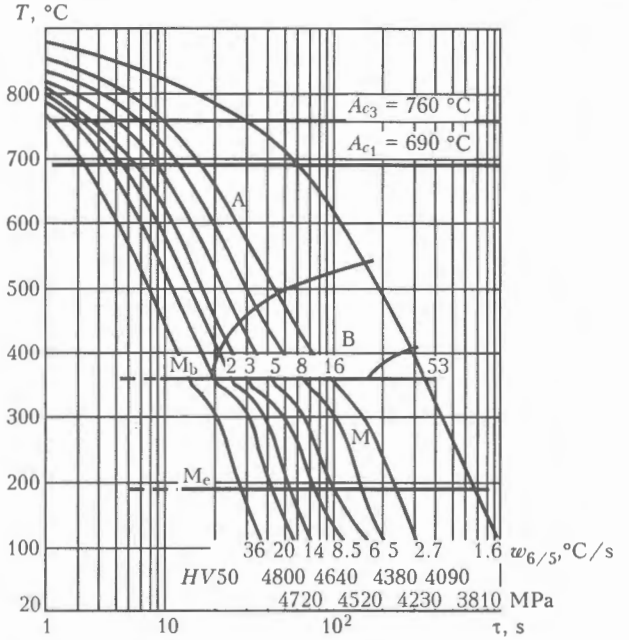

Figure 1. Austenite continuous cooling transformation diagram for steel 20KhN4FA [3]

Electrodes TMU-21U with a 3 mm diameter (produced in Russia) and OK 53.70 with a 3.2 mm diameter (ESAB, Sweden) were chosen to check strength of welded joints in steel 20KhN4FA. Static tensile test specimens (GOST 6996–66) were cut across the butt joints made from pipe steel 5 mm thick and subjected to tempering at 250 °C. Welding was performed under

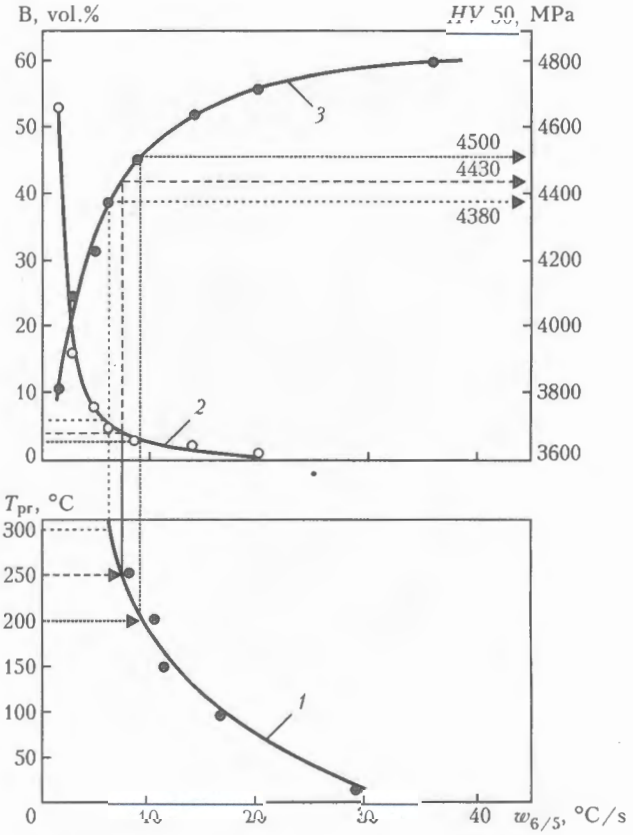

Figure 2. Effect of the temperature of preliminary heating T_{pr} of a plate on cooling rate (*1*) (under the implant test conditions), volume fraction of bainite B (*2*) and HAZ metal hardness *HV* 50 (*3*)

Table 3. Results of testing steel 20KhN4FA welded joints to short-time tension

Sample identification	Electrode grade	$\sigma_{0.2}$, MPa
39-1	TML-3U	915
39-2		1007
21-1	TMU-21U	886
21-2		1086
28-1	OK 53.70	994
28-1		1099

the following conditions: welding current I_w = 110–120 A (direct current of reverse polarity), and arc voltage U_a = 22–24 V. The butt joint edges had a one-sided V-groove. The concentration of diffusible hydrogen (alcohol analysis of «pencil» samples [6]) transferring from welding electrodes to the deposited metal was H_{dif} = 1.25 and 3.3 $cm^3/100$ g Me in the case of electrodes OK 53.70 and TMU-21U, respectively.

The test results are given in Table 3. The chosen electrodes provided sufficiently high and almost identical strength values of the welded joints. No cold cracks formed in this case. Additional tests were conducted on the welded joints produced by using electrodes TML-3U, which are the common electrodes for welding Cr–Mo and Cr–Mo–V heat-resistant steels ($H_{dif} \approx 2.7$ $cm^3/100$ g Me). The level of rupture strength and character of fracture of specimens were similar to those tested earlier. Therefore, electrodes of the grades tested (as well as similar to them) can be applied for welding of non-tight regions of the cylinder bottoms. For this, it is indicated to choose electrodes with a lower concentration of diffusible hydrogen.

Elimination of causes of non-tightness. Pipe ends that converge in zenith of the spherical part of a cylinder in hot deformation form wrinkles containing interlayers of a strongly adhering scale, which may penetrate through the entire wall section in this zone. As shown by metallography, the scale leads to formation of delaminations and cracks in the base metal, while in interaction with the weld the products contained in the scale cause formation of lacks of fusion at the edges of the base metal, as well as pores and cracks in the deposited metal. A typical appearance of defects in macro- and microstructure of metal of the «rolled» zones of the cylinder bottom with the seal welds is shown in Figure 3. Totally, these defects lead to formation of through channels and, hence, loss of tightness of a joint.

As a rule, the «rolled» crack-like layers are concentrated in a narrow zone at the joint edges. To remove them, it is suggested that a defective metal should be machined by drilling a groove. To facilitate access of welding electrode to the future weld root, it is necessary to make a tapered groove in metal. The experimentally optimised angle of bevel in a tapered hole provides a sufficiently effective cleaning of metal from the internal scale and convenient filling up of the hole.

Technique for welding up of holes. Two processes were tried out to weld up the process holes in the cylinder bottoms (using no extra plug): manual arc

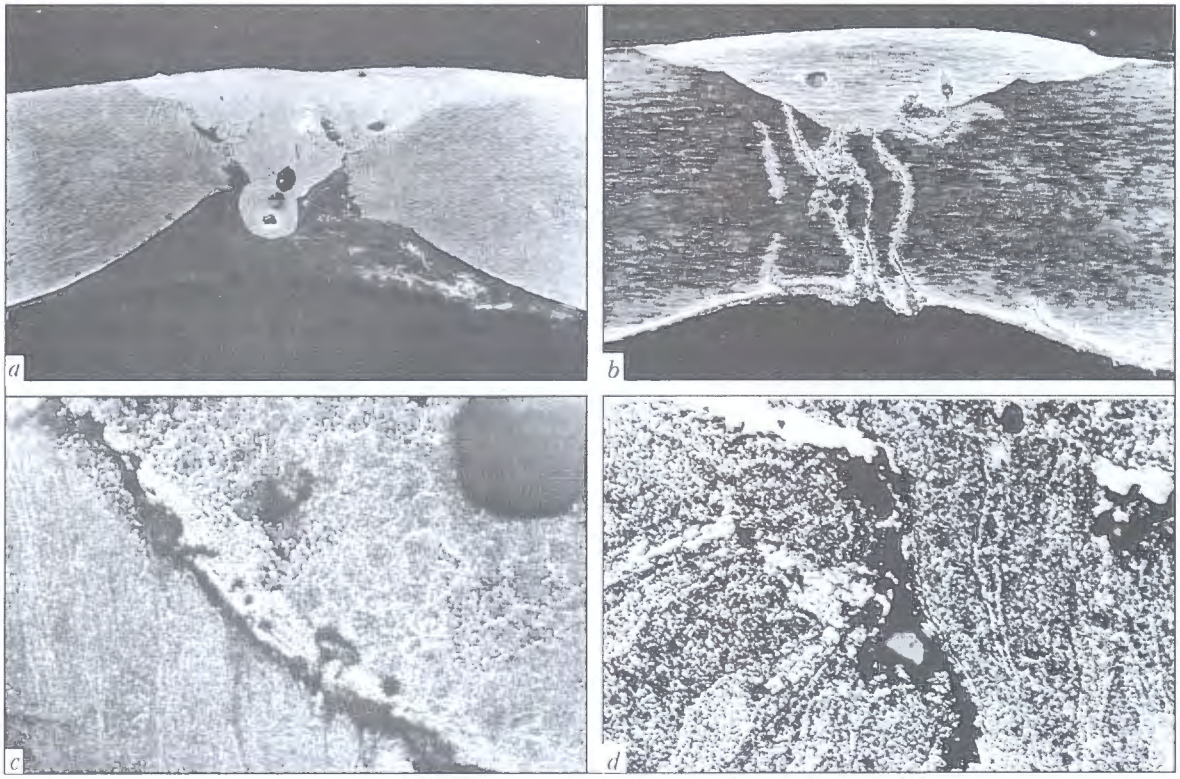

Figure 3. Macro- (*a*, *b*) and microstructure (*c*, *d*) of «rolled» zones of cylinder bottoms with seal welds: *a* — general view of defects in weld (pores in weld metal and cracks in fusion zone); *b* — general view of pores in weld and crack-like defects in base metal; *c* — cracks in fusion zone (×100); *d* — discontinuities formed in cracking of the scale accumulation zone (×200)

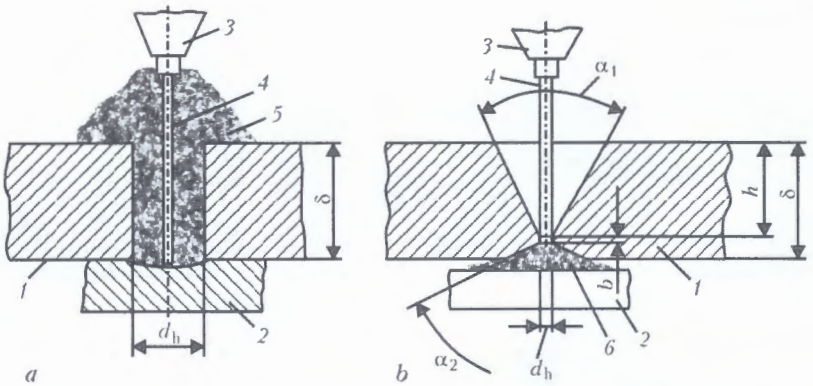

Figure 4. Types of holes made in plates for welding on copper (*a*) and flux-copper backings (*b*): *1* — base metal; *2* — copper backing; *3* — welding torch nozzle; *4* — electrode wire; *5, 6* — welding and backing fluxes, respectively; d_h — cylindrical hole; δ — steel thickness; α_1 — tapered hole opening angle; α_2 — tapered internal groove angle; *h* — tapered hole depth; *b* — root face

welding with covered electrodes used as a baseline process, and automatic submerged-arc welding used as an additional process to check the feasibility of its application. The key peculiarity of manual arc welding is the possibility of performing the process without backing in all spatial positions.

The technological-welding tests show that it is necessary to apply the following welding techniques to provide the sound welds in the cylinder bottoms.

1. When making the root weld, the welding current should be decreased by 10–15 % compared with the rated one; the arc should be ignited in the middle part of the generating line of a tapered groove; after that the arc should be moved to a hole; and the hole should be filled up with a spiral weld, i.e. from the end to centre of the hole, using the short arc.

2. Subsequent passes should be made at a rated welding current, starting the weld at the interface between the base metal and weld of the previous pass and ending at the groove centre; and the weld should be made on a spiral.

3. The quantity of layers depends upon the thickness of metal at the groove location, and thickness of one layer should be 3–5 mm.

4. Slag should be thoroughly removed from the groove after making each pass, by paying a special attention to the weld to base metal transition location.

5. To prevent porosity, welding should be performed using baked electrodes at a short arc by avoiding undercuts at the groove wall.

The above welding technique has the following advantages: lower heat input in each pass provides the weld metal with a finer primary structure and the HAZ metal with a smaller grain; the multi-pass welding method with a small-section beads excludes a transcrystalline structure of the weld metal, leads to formation of a disoriented structure of the weld between layers and refining of grain of the HAZ metal due to phase recrystallisation [7], which has a general positive effect on technological strength of the welded joints; possibility of visual examination of the weld quality after each pass; convenience and simplicity of adjustment of the welding conditions; and mobility.

The drawbacks include a low process productivity. In addition, when making multi-pass welds, if a welder has an insufficient skill, the probability exists of formation of such defects as slag inclusions, pores and lacks of fusion.

With the mechanised process, welding up of the process holes without backing is not permitted, because the weld metal may flow out through its root portion. Therefore, welding was performed using backings, i.e. pure copper backing and copper backing with a flux layer (flux-copper backing). Steel plates 20 mm thick with two types of holes, i.e. cylindrical and tapered, were used for optimisation of the welding conditions and technique. Welding was performed using standard welding equipment: head A1416 and rectifier VDU 1201. The arcing time and welding wire feed speed were selected on the basis of the hole filling conditions.

In the case of using a copper backing, the arc can be ignited directly on the backing, this allowing cylindrical holes to be made in the cylinder bottoms. In the case of a flux-copper backing, the arc is ignited on the base metal of the tapered groove surface.

When increasing metal thickness in the zone of welding up of a hole to the value of an optimal elec-

Table 4. Variants of welding up of holes in bottoms using different backings on steel 20 mm thick

Hole shape	Type of backing	α_1, deg	α_2, deg	d_h, mm	*h*, mm	*b*, mm
Cylindrical	Copper	–	–	10.2	–	–
Tapered	Flux-copper	50	120	2.8 (3.8)*	17	1

*Diameter of electrode wire — 3 (4) mm.

Table 5. Optimal conditions for submerged-arc welding up of holes in bottoms of low-alloy high-strength steel 20 mm thick

d_e, mm	I_w, A	U_a, V	τ, s	Electrode extension, mm
3	400–420	32–34	7–9	48
4	500–520		6–8	64

Note. Size of flux grains in flux-copper backing is less than 0.63 mm.

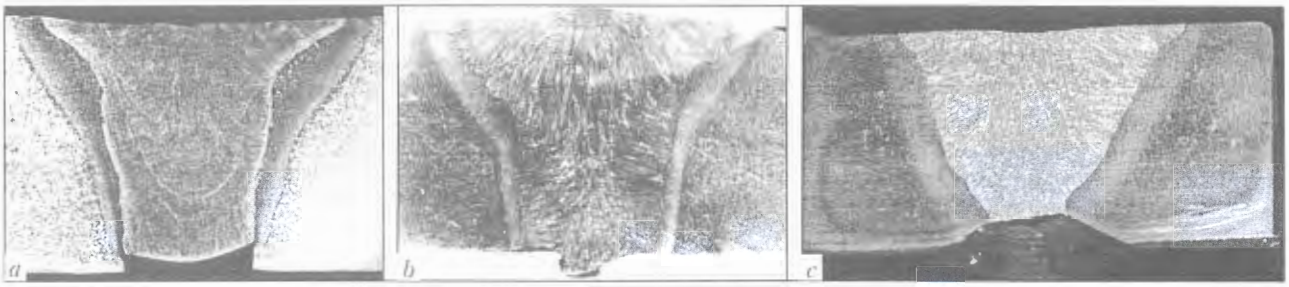

Figure 5. Macrosections of holes filled up by submerged-arc welding using copper (*a*, *b*) and flux-copper (*c*) backings

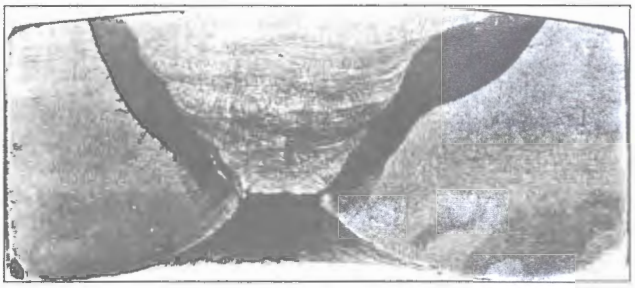

Figure 6. Macrosection of the joint produced by filling up of a process hole in the bottom of steel 20KhN4FA by manual arc welding

trode extension equal to $10d_e$ (where d_e is the welding wire diameter), the extension should also be increased to avoid short-circuiting of the nozzle on a workpiece. Welding in this study was performed with an increased electrode extension ($16d_e$). However, this had no effect on the results of welding up of the holes.

Schematic views of the holes made on plates are shown in Figure 4, and conditions selected for their welding up are given in Tables 4 and 5.

As shown by the experiments, the mechanised process provides a monolithic weld. However, the methods tested are not free from drawbacks. For example, welding on a copper backing is characterised by an unsatisfactory formation of the back side of the weld (Figure 5, *a* and *b*). The lower part of a hole is underfilled (Figure 5, *a*), defects of the type of undercuts are formed, the back side of the weld has an irregular surface (Figure 5, *b*), and crack-like defects near surface irregularities are seen in this case. Irregularities are formed at an unsatisfactory spread of the first portion of molten metal over the backing, the portions being separated by non-melted particles of the spilled flux, which is likely to be related to a substantial heat-removing ability of copper. In addition, the copper backing sticks to the weld metal.

The above drawbacks are excluded when using the flux-copper backing. At a groove with a tapered hole in zenith, the joints with a quality weld formation (Figure 5, *c*) can be produced owing to extra internal bevel α_2, as shown in Figure 4, *b*. Optimal conditions for welding up of the holes selected for welding using 3 and 4 mm diameter electrodes are given in Table 5. To ensure the satisfactory formation of the back side of the weld with an insignificant or zero convexity using the flux-copper backing, it is recommended to apply flux with particles of a small size, which provides its strong adherence to the back side of a workpiece.

Factors that affect formation of the external side of the weld include, first of all, welding current I_w and arcing time τ. The tapered shape of the holes to be welded up is more preferable than the cylindrical one, especially in the case of their increased depth, as it is this shape that provides a more favourable orientation of solidification of the weld metal (absence of zones with transverse growth of crystalline grains), leading to floating of slag inclusions to the surface.

Holes of a cylindrical shape are simpler to make technically. In the case of using the flux-copper backing, the cylindrical groove in the weld root region should be less than d_e in diameter in order to ensure short-circuiting of electrode on a workpiece. However, a small volume of the grooved metal leads to an increased risk of the scale present in it.

Therefore, in the case of employing automatic submerged-arc welding, it is indicated to apply a variant with the flux-copper backing. It is free from the drawbacks characteristic of the pure copper backing. However, mechanised welding requires the use of specialised equipment and extra fixtures for the backing to be introduced through the nozzle and fixed, which makes the entire welding process much more complicated. Moreover, variable wall thickness in zenith of the bottom within the zone of holes requires continuous adjustment of the welding conditions. Therefore, manual arc welding using covered electrodes, where the holes are welded up with preliminary heating, is a better choice. Appearance of the joint made by manual arc welding is shown in Figure 6.

The recommended manual arc welding process provides the high quality of the welded joints. It was comprehensively tested and approved as a method for factory manufacture of standard cylinders with a capacity of 20 and 50 l, designed for a working pressure of 16.9 MPa and meant for storage of automotive fuel.

1. (1989) *Handbook on steels and alloy grades*. Ed. by V.G. Sorokin. Moscow: Mashinostroenie.
2. Hrivniak, I. (1984) *Weldability of steels*. Moscow: Mashinostroenie.
3. Skulsky, V.Y., Tsaryuk, A.K., Vasiliev, V.G. et al. (2003) Structural transformations and weldability of hardening high-strength steel 20KhN4FA. *The Paton Welding J.*, **2**, 17–21.
4. Sawhill, J.M., Dix, A.W., Sawage, W.F. (1974) Modified implant test for studying delayed cracking. *Welding J.*, 35(**12**), 554–560.
5. Zaks, I.A. (1996) *Electrodes for arc welding of steels and nickel alloys*. Refer. Book. St.-Petersburg: Welcome.
6. Kozlov, R.A. (1986) *Welding of heat-resistant steels*. Leningrad: Mashinostroenie.
7. Chew, B., Harris, P. (1979) HAZ refinement in CrMoV steel. Effects of welding position, weld preparation and electrode size. *Metal Construction*, May, 229–234.

REPAIR OF RAILWAY WAGON WHEELS BY CLADDING WITH PRELIMINARY ANNEALING OF ROLL SURFACES

V.V. MATVEEV
Closed Joints Stock Company «Viltrans», Kiev, Ukraine

The set of technological problems to be addressed in the process of repair of railway wheels by cladding is considered. The technology is offered for high-productivity multi-electrode cladding of wheels after annealing of the roll surfaces.

Keywords: *repair, wagon wheels, defects on roll surface, high-frequency heating, HFC annealing, multi-electrode cladding, microstructure*

Wheels having a worn out roll surface after operation (Figure 1, *4*) are subjected to machining to template using wheel-turning lathes in order to restore their initial profile (Figure 1, *1*). Wagon repair factories of Ukraine annually machine 400,000 railway wheelsets, the average decrease in the wheel rim being 4–6 mm. The cost of turning one millimetre of a wheel is estimated at 51 UAH.

To restore one millimetre thickness of a worn out flange of a wagon wheel to bring it to the standard profile with a flange width of 33 mm, measured at a distance of 18 mm from the flange apex, the wheel rim should be decreased by 2 mm. To maintain thickness of the rim, the railway transport enterprises of Ukraine, CIS countries, Sweden, Germany, Czechia, Bulgaria, Poland, Romania and India apply automatic cladding of worn out flanges by the submerged-arc method [1–3] and turning (Figure 1). Known are the efforts on repair of wagon wheels by cladding [1, 2] and turning (Figure 1, *3*). However, for a number of reasons considered below, the regulatory documents in force in the CIS countries [4] make no provision for repair of rims of wagon wheels used in the railway transport.

The purpose of this study is to consider the possibilities of upgrading the technology for repair of railway wagon wheels by cladding, as well as using multi-electrode cladding of the wheel rim after annealing of the roll surface. The following circumstances should be allowed for when addressing the problems of repair of wheels by arc cladding.

Firstly, repair of wagon wheels by cladding is associated with a loss of the level of compressive stresses induced by hardening of the wheels at a manufacturing factory (carbon content of wheel steel is 0.55–0.65 %), as well as revealing and removal of defects of a metallurgical origin [5].

Metallography of wheels with a rim about 30 mm thick, which had come for repair to the wagon repair factories of Ukraine, was carried out by the E.O. Paton Electric Welding Institute. The examinations show that microstructure of the wheel rim metal consists of a sorbite-like pearlite with microhardness *HV* 1-2540–2560 MPa and thin interlayers of ferrite with microhardness *HV* 1-1850 MPa, hardness of the rim metal being about *HRC* 20 and that of the flange — *HRC* 21–23. Manganese sulphides not less than 0.49 mm in size and complex silicates with high hardness, i.e. *HV* 1-7420–7720 MPa, were revealed in the wheel rim metal. The index of contamination of wheel steel with sulphides and silicates, according to GOST 1778–70, was # 3–4. Because of their irregular shape, these inclusions may act as stress raisers, which may lead to formation of cracks and their propagation under cyclic loading during operation. At the same time, according to GOST 10791–89: All-Rolled Wheels, the index of sulphide inclusions and silicates in wheel steel should not exceed # 3.5.

According to GOST 10791–89 and ISO 1005/6, convergence of the rim after radial cutting of a wheel (in the as-received state) should be not less than 1 mm, and no divergence is permitted. In operation of the wheels, under the effect of mechanical loads on the roll surface, convergence of the rim ends after cutting is only –(1–2) mm. In a number of cases, the braking tests caused transformation of compressive stresses into tensile ones of +(1–2) mm [6]. According to our data, wheels with a rim less than 45 mm and more than 30 mm thick, coming for repair after operation to the wagon repair factories, have divergence of the

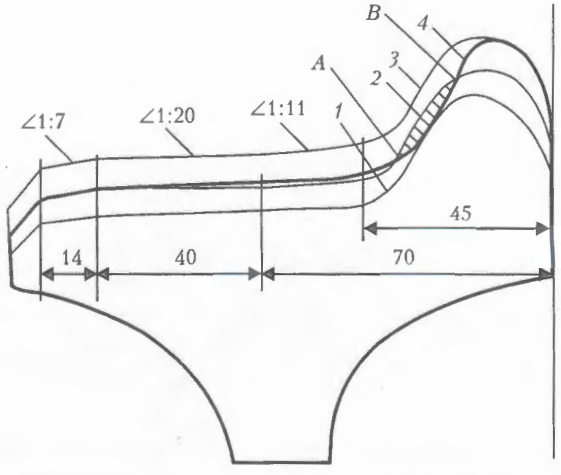

Figure 1. Schematic of restoration of profile of wheel DIIT UZ: *1*, *2* — line of turning before and after flange cladding (*A* — beginning, *B* — end of cladding); *3* — line of turning after restoration of wheels by flange and rim cladding; *4* — line of worn out wheel surface

rim ends after cutting equal to +1 mm. Considering the above-said, one of the most important requirements to be met when developing a technology for repair of wheels is, in our opinion, maintaining of a level of compressive stresses in them, which should be confirmed by a long-time operation of the wheels.

Secondly, as the wheels are made from high-carbon steel, their roll surfaces as a result of operation experience local surface hardening and deep cold working, caused by thermal and mechanical effects. They often have two or three «flats» 1–2 mm deep. «Flats» with metal hardness of more than *HRC* 50 going to a depth of 3 mm, scores going to a depth of 5 mm or more, and defects on the roll surfaces (extrusion of metal to the periphery of the roll surface, exfoliation of metal, cracks, damages of a fatigue character within the zone of wheel and rail contact) are found in about 25 % of the wheels. Prior to cladding of the wheel rim (Figure 1, *3*), it should be turned to a depth of occurrence of defects [7]. Otherwise the latter can act as stress raisers in deposited layers, thus leading to fracture.

Thirdly, wheel steel belongs to a category of hard-to-weld materials. To reduce the risk of hot cracking of deposited metal, cladding of the wheels is usually performed using a low-carbon wire, and special measures are taken to maintain the carbon content of the deposited metal at a level of no more than 0.2 % (increasing the cladding speed, decreasing the welding current, and reducing penetration of base metal and dilution of the deposited metal with the base one) [1]. To eliminate cold cracks, which may be initiated in the HAZ metal as a result of formation of quenching structures or under the effect of welding stresses and diffusible hydrogen, the wheel rim is subjected to preheating prior to cladding and delayed cooling after cladding, and flux is subjected to baking to decrease its hydrogen content [1, 3]. Structural changes take place in the HAZ metal with any cladding method. They lead to coarsening of grain and deterioration of strength properties of the base metal. Increase in thickness of the worn out surface subject to repair, as well as in heating and heat input per unit length (wheel surface area), leads not only to increase in the HAZ width, probability of cracking of both deposited and base metal of the wheel, but also to decrease in the productivity of repair of the wheels (the time of cladding of the rim wear of up to 4 mm is 3.5–4.0 h) [1].

To extend life of a wheel and decrease thickness of the deposited layer required for restoration, it is recommended to subject the roll surface to annealing prior to cladding operations [8]. Annealing of the hardened metal of the wheel roll surface from temperature A_{c_3}, performed prior to cladding, leads to refining of metal grain and reduction of the probability of cold cracking in a zone adjoining the fusion line [7], which allows cladding to be performed without turning out of the defects from the roll surface. In this case, the temperature of preheating of metal prior to cladding can be decreased to a substantial degree. Annealing of the roll surface leads to a more than 2 times decrease in metal hardness. Grinding of deep defects after decreasing hardness of the roll surface, instead of turning on the wheel rolling circle, also adds to improvement of performance of the wheels.

A more cost effective method in repair of wheels, which reduces their distortions during heating and cooling, is the use of high-frequency heating, as the heated layer constitutes a small part of the wheel mass [9]. This heating method is characterised by generation of thermal energy directly in a part heated, which provides a high rate of heating to temperatures at which structural transformations take place in the wheel metal. High-frequency heating of the wheel roll surfaces was performed using the TI2-100/10M unit [7]. At a frequency of 10 kHz and power of 100 kW, structural transformations in metal take place at a depth of about 2 mm. Comparison of microstructures of the wheel rim metal with a worn surface, defects (flats, cracks) and regions with traces of a thermal impact on the rim and flange formed in braking, before and after HFC annealing of the roll surface allowed a conclusion that microstructures of metal within the zone of an acicular martensite structure, as well as region with a structure of grained bainite, undergo transformations to form fine-grained bainite (at a depth of 2.4 mm from the roll surface) and, in general, become more uniform after HFC annealing. The effect of HFC annealing on metal structure through thickness is limited (microstructure and microhardness at a depth of more than 2.4 mm hardly change).

Tensile stresses formed after HFC annealing help to reveal defects in wheels and, thus, discard the defect-containing wheels [5]. As established, divergence of wheels after annealing using the HFC unit is +1 mm, after annealing and one-electrode cladding of flanges it is +2.5 mm, and after annealing, turning out of defects and additional heating using the HFC unit prior to cladding of flanges it is +3.5 mm, which helps to open defects (microcracks) on the wheel surfaces up to sizes that can be detected visually, and up to appearance of cracks in the wheel rim.

Since 1997, the wagon repair factories of Ukraine, owing to annealing of the roll surfaces, detected cracks in rims of 0.2 % wheels that had come for repair. Removal of cracks by turning and subsequent cladding of flanges provided the failure-free operation of about 260,000 repaired wheels with the clad flanges [7]. The experience gained from a long-time operation of repaired wheels allows us to accept divergence of the wheel rims after cutting equal to +3.5 mm, which probably can be used as a criterion of the acceptable divergence of the wheels after their repair by cladding.

Multi-electrode cladding of the wheel rims can be employed to maximise the productivity of repair of wheels by high-quality cladding after annealing of the wheel roll surfaces [10]. The alternate pulsed character of arcing with the arc moving across the rim and uniform distribution of heat input leads to decrease in the penetration depth, content of base metal in the

deposited one and, hence, distortions of the wheels after cladding [11]. Alloying of the deposited layer can provide increase in yield stress, impact toughness and corrosion resistance of the surface layer of the wheel rims, resistance to mechanical wear under high impact loads and deformability of parts, as well as decrease in the risk of cracking. However, in multi-electrode cladding the molten metal pool has a large volume and slowly cools down during solidification. This leads to formation of a coarse-columnar structure of deposited metal, overheating of base metal near the zone of its fusion with the weld metal, and coarsening of grain in coarse-grained regions (CGR) of the HAZ metal. Rolling results in deterioration of mechanical properties, and impact toughness in particular. Higher heat input into a wheel leads to increase in the wheel divergence to +6.5 mm.

Multi-electrode cladding of the wheel rim using 3 mm welding wire Sv-08KhM by the submerged-arc method with flux AN-60, by depositing one or two layers in one weld pool (Figure 3), was performed by using the pilot rim cladding unit UNO-2 (Figure 2). Cladding of flanges was performed with the UNG-2M unit using 3 mm welding wire Sv-08KhM by the submerged-arc method with flux AN-348AM, by successively depositing beads using two electrodes in one weld pool [7]. Cladding was performed using the wire permitted for treatment of wagon wheels at the railway transport enterprises of Ukraine.

It was established that cladding of a 100 mm wide rim of a wagon wheel not less than 850 mm in diameter could be carried out with ten electrodes. The quantity of electrodes depends upon the width of a rim (100 mm) to be clad, and should ensure implementation of the multi-electrode cladding process (distance between the electrodes should be equal to 3–4 electrode diameters [10]). To prevent spread of the weld pool and save welding consumables, the wheelset during cladding was inclined to an angle of not less than 5° in such a way that the wheel profile was parallel to the horizon [12]. The cladding speed and total electric current are interrelated. For example, at a current of 500–600 A the maximal cladding speed is 6–7 m/h and maximal – 4 m/h. At a current of 1200 A the maximal speed is 15 m/h (the time of cladding a rim is 10 min) and minimal cladding speed is 10 m/h (the time of cladding a rim is 16 min). At a high speed of rotation of a wheel the molten metal from the weld pool spreads over the wheel, and at lower speeds the multi-electrode cladding process is interrupted.

Microstructure of deposited metal consists of bainite with microhardness *HV* 1-2850–3230 MPa and hardness *HRC* 23–27. Microstructure of the CGR metal in HAZ consists of bainite with microhardness *HV* 1-2540–3660 MPa and hardness *HRC* 20–31. In this case, the first value of hardness was measured at the multi-electrode cladding surface, and the last – near the fusion line. The carbon content of deposited metal was 0.29 %. No cracks were detected in the deposited and HAZ metal.

Different techniques of multi-electrode cladding were tried out to refine grain of the CGR metal in HAZ. It was found that changing the electrode inclination angle from 50 to 30° led to almost no change in chemical composition of the deposited metal (0.29–0.28 % C, 1.15–1.10 % Mn, 0.56–0.59 % Cr, 0.50–0.35 % Mo), grain of the CGR metal in HAZ having index # 3–4.

Displacement of electrodes forward along the welding direction to 70 mm with respect to zenith, compared with a backward displacement to 70 mm, resulted in reduction of penetration of base metal, which led to decrease in the carbon content from 0.28 to 0.22 % and decrease in hardness from *HRC* 24–27 to about *HRC* 20.

Increasing the speed of one-layer cladding (v_c = = 12 m/h, I = 700–800 A) led to formation of wide ferrite plates, in addition to bainite, in the deposited metal (Figure 4, *a*), decrease of its hardness to values below *HRC* 20 (microhardness of the deposited metal at the rim centre was *HV* 1-2970–3090 MPa), hardness of the CGR metal in HAZ to *HRC* 20–24 (microhardness of the deposited metal – *HV* 1-3060–3220 MPa), and decrease in the carbon content to 0.18 %. The index of grain of the CGR metal in HAZ increased to # 4–6 (Figure 4, *b*). Divergence of a wheel after depo-

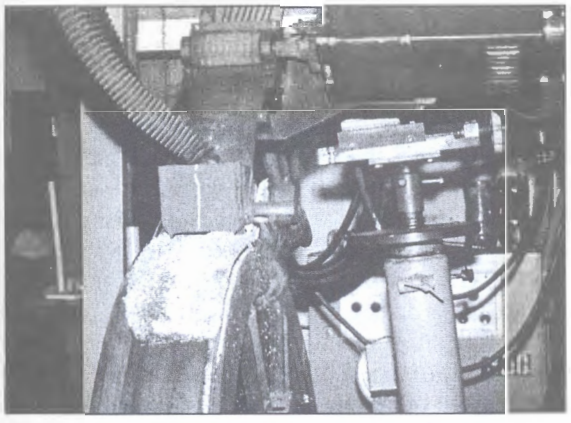

Figure 2. Unit UNO-2 for cladding of wheel rims

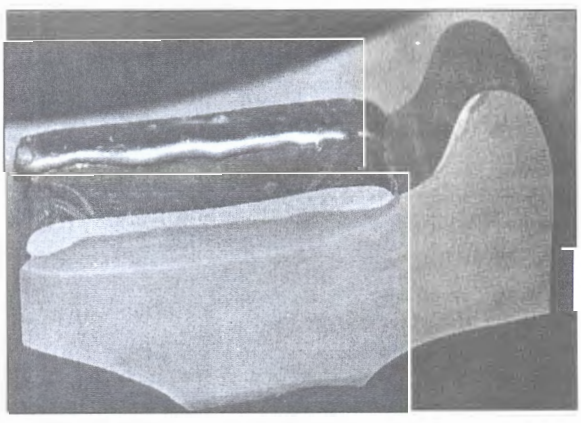

Figure 3. Fragment of wheel rim with clad surface

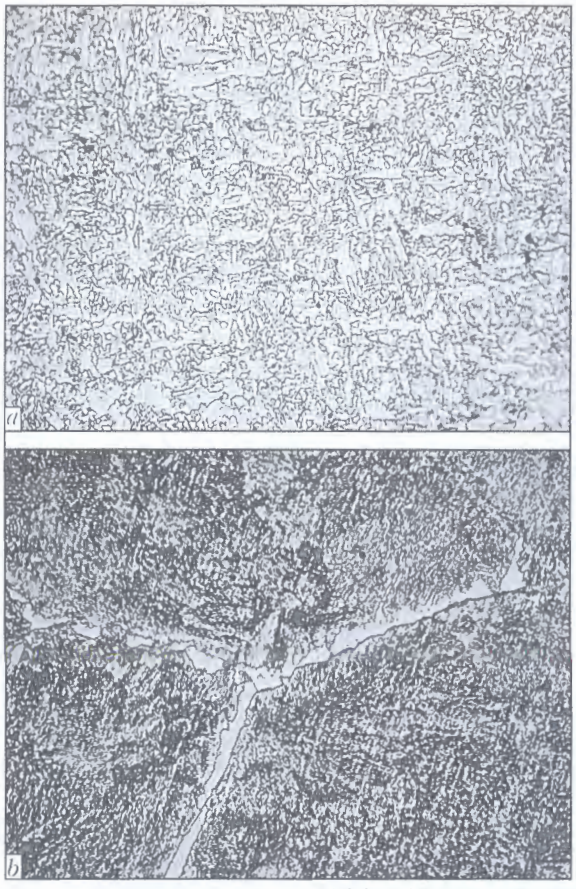

Figure 4. Microstructure of base metal (*a*) and CGR metal in HAZ (*b*) resulting from one-layer 10-electrode cladding of wheel rim using 3 mm welding wire Sv-08KhM by the submerged-arc method with flux AN-60 (×1000)

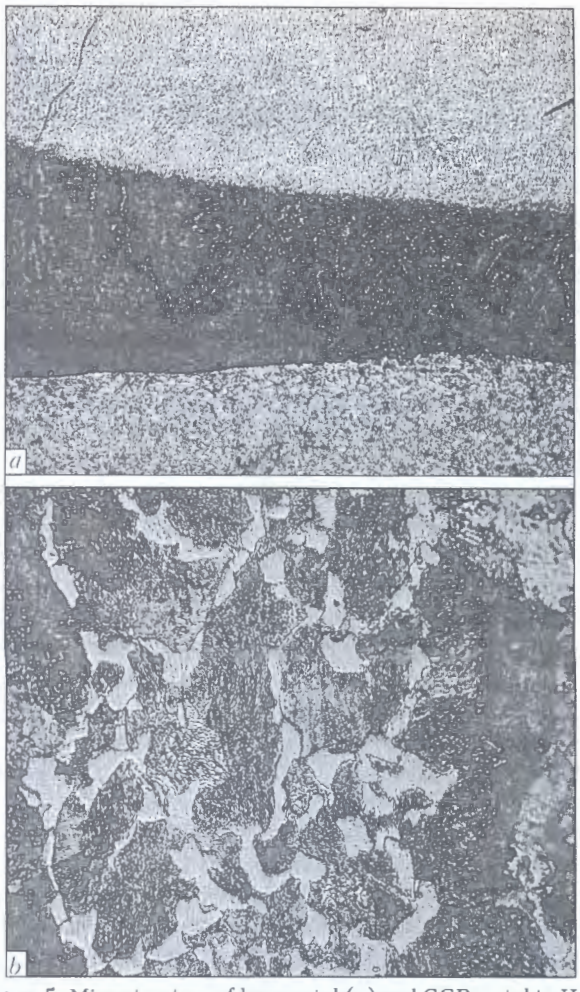

Figure 5. Microstructure of base metal (*a*) and CGR metal in HAZ (*b*) resulting from two-layer 10-electrode cladding of wheel rim using 3 mm welding wire Sv-08KhM by the submerged-arc method with flux AN-60: *a* — ×40; *b* — ×1000

sition of one layer by multi-electrode cladding was +6.5 mm.

Two-layer cladding of the rim (v_{c1} = 10 m/h, I_1 = = 500–600 A; v_{c2} = 14 m/h, I_2 = 800–900 A) (Figure 5) led to increase in size of the ferrite component of microstructure, decrease in hardness of the deposited metal to values of *HRC* 20 and less (microhardness in the first layer at the rim centre was *HV* 1-3090 MPa, microhardness in the second layer was *HV* 1-2740–2970 MPa, and that of the CGR metal in HAZ was *HV* 1-2810–2970 MPa). Chemical composition of the deposited metal was as follows, wt.%: 0.17C, 1.2Mn, 0.79Cr and 0.54Mo. Repeated re-crystallisation of the CGR metal in HAZ resulted in emergence of individual grains with index # 8, in addition to grains with index # 5–7 (Figure 5, *b*). Divergence of a wheel after two-layer multi-electrode cladding of the rim hardly changed (+6.4 mm).

Therefore, penetration of base metal, size of grain of the CGR metal in HAZ and transition of carbon from base metal to the deposited layer can be decreased through decreasing the welding current, manipulating with electrode, increasing the cladding speed and employing two-layer cladding at its maximum possible speed.

It is the opinion of specialists of the Dnepropetrovsk University of Railway Transport, based on research conducted by specialists of the Iron and Steel Institute of the NAS of Ukraine (Dnepropetrovsk), that the noted divergence of wheels does not guarantee the absence of the risk of cracking in operation of the wheels. We found that decrease in divergence of the wheel ends after cutting could be achieved by heating the roll surface after cladding and turning using the TI2-100/10M unit at a rate of 150–160 °C/s to temperatures above A_{c_1}, cooling to a temperature below A_{r1} for 5–6 s, repeated heating for 5–6 s to a temperature below A_{c_1}, and accelerated cooling at a rate of not less than 50–60 °C/s (using inductor with a built-in water sprayer). This heat treatment provides decrease in divergence of a wheel after cutting to +3.5 mm. High-frequency heating of the wheel after multi-electrode cladding (v_c = 6 m/h, I = 500–600 A) and turning on its profile did not change microstructure, index of grain of the CGR metal in HAZ, hardness and microhardness of the deposited metal.

The CGR metal in HAZ contains primarily grains with index # 8, the rest of the grains having index # 5–7. More substantial grain refining can be achieved by raising the speed of deposition of the first layer (v_{c1} = v_{c2} = 14 m/s, I_1 = I_2 = 1100–1200 A) (Figure 6). The carbon content of the deposited metal

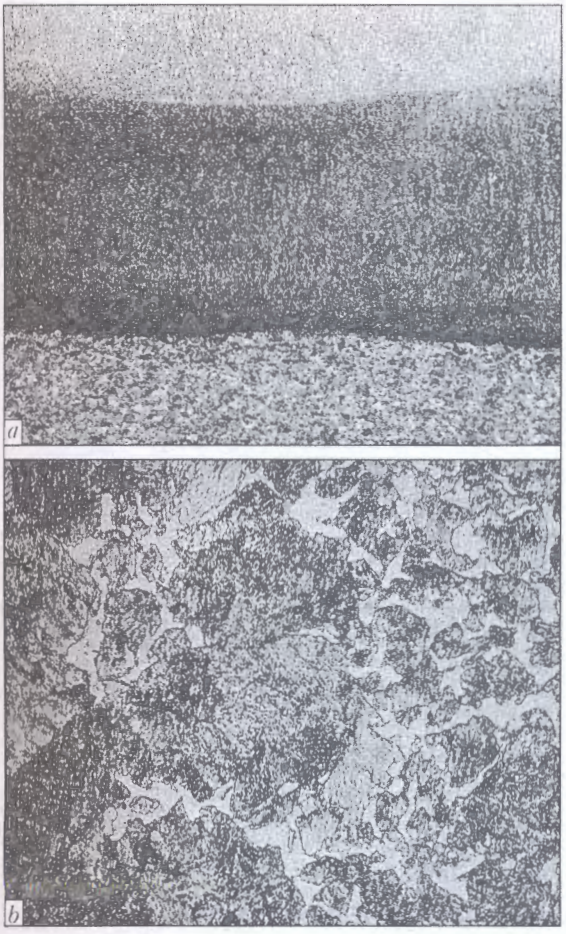

Figure 6. Microstructure of base metal (*a*) and CGR metal in HAZ (*b*) resulting from two-layer 10-electrode cladding of wheel rim using 3 mm welding wire Sv-08KhM by the submerged-arc method with flux AN-60 after heat treatment of the deposited layer turned to the roll profile: *a* — ×40; *b* — ×1000

was decreased to 0.1 % (1.15 % Mn, 0.79 % Cr, 0.54 % Mo), and hardness of the deposited metal did not change. The minimal time of deposition of one layer 9 mm thick on rim of the wagon wheel 850 mm in diameter was no more than 11.5 min. Divergence of the wheel ends after multi-electrode cladding of the rim was +6.5 mm.

Minimal thickness of the rim of wagon wheels in operation is 22 mm, after factory repair it is 28 mm, and after depot repair — 27 mm. At present, the permitted value for a minimal thickness of the rim after turning is 25 mm after depot repair of the wheels. The highest effect can be achieved in repair of thin wheels with a rim thickness of 26–30 mm, which after turning have the rim thickness less than the permitted one and should be subjected to pressing-out. At present, the average service life of such wheels is 8 years. By prolonging it to another two or three years (by achieving an acceptable thickness of the rim in operation), one might expect an extension of service life to 12 years and, ignoring expenditures, an income of not less that 1400 UAH (as of 01.05.2005, the price of a new all-rolled wheel for the «Ukrzaliznytsya» wagon repair factories was about 3000 UAH, not including VAT).

It can be noted in conclusion that the technology for repair of railway wheels due to wear should include:

- annealing of the roll surfaces of wheels using the HFC (10 kHz) unit to a depth of about 2.5 mm, providing the possibility of increasing divergence stresses, detection of defects and discarding of defect-containing wheels, as well as decreasing the probability of cracking after cladding and thickness of the deposited layer necessary for restoration;
- grinding of locations of deep cracks to a depth of more than 3 mm, instead of turning on the wheel rolling circle;
- multi-electrode cladding of the wheel rim with one or two layers (10 electrodes) in one weld pool using alloyed wire, e.g. 3 mm welding wire Sv-08KhM, by the submerged-arc method with flux AN-60 (v_c = 12–14 m/h, I = 800–900 A, U_a = 28–30 V, angle of inclination of welding electrode with respect to zenith — 35–45°, and forward displacement of electrodes to 65–70 mm from zenith in a direction of wheel rotation), providing high productivity and quality of deposited metal (index of grain of the CGR metal in HAZ is not less than # 6–8), and hardness of the roll surface not lower than that of the wheel base metal;
- cladding of worn out flanges [7];
- heat treatment of clad and turned wheels using the HFC unit, providing the divergence level of not more than +3.5 mm.

1. Asnis, A.E., Gutman, L.M., Stepenko, V.P. et al. (1958) *Submerged-arc welding in repair of locomotives*. Moscow: Transzheldorizdat.
2. (2001) ESAB delivers engineered automatic welding station to Ghana in Africa for build-up welding of worn railway wheels. *Svetsaren*, **1**, 20–21.
3. Pavlov, N.V., Kozubenko, I.D., Byzova, I.E. et al. (1993) Surfacing of flanges of railway wheelsets. *ZhD Transport*, **7**, 37–40.
4. (1977) *TsV/3429*: Instructions for examination, inspection, repair and formation of railway wheelsets. Moscow: Transport.
5. Tsyurenko, V.N. (2002) Operational reliability of freight car wheelsets. *ZhD Transport*, **3**, 24–28.
6. Uzlov, I.G. (1985) *Wheel steel*. Kiev: Tekhnika.
7. Matveev, V.V. (2005) Cladding of wagon wheel flanges after annealing of the roll surfaces at wagon repair factories of Ukraine. *The Paton Welding J.*, **6**, 36–41.
8. Matveev, V.V. *Method for restoring of roll surfaces of railway transport wheels*. Pat. 44373 Ukraine. Publ. 15.02.02.
9. Vologdin, V.P. (1974) *Surface induction hardening*. Moscow: Oborongiz.
10. Melikov, V.V. (1988) *Multi-electrode surfacing*. Moscow: Mashinostroenie.
11. Emelianov, N.P. (1962) Multi-electrode submerged-arc and electroslag surfacing. In: *Transact. of All-Union Res. Institute of Railway Transport*. Issue 239.
12. Matveev, V.V., Olshevsky, V.I. *Method for restoration of profiles of railway transport wheel rim surfaces*. Pat. 61794 Ukraine. Publ. 15.07.05.

INFLUENCE OF EXTERNAL ELECTROMAGNETIC ACTIONS ON THE STRUCTURE AND COMPOSITION OF WELDS IN WET UNDERWATER WELDING

R.N. RYZHOV[1], S.Yu. MAKSIMOV[2], E.A. PRILIPKO[2] and V.A. KOZHUKHAR[2]
[1]NTUU «Kiev Polytechnic Institute», Kiev, Ukraine
[2]E.O. Paton Electric Welding Institute, NASU, Kiev, Ukraine

Analysis of microstructures of all the welded joint zones and weld composition was the basis to determine the optimum parameters of the controlling magnetic field, providing maximum improvement of mechanical properties of the joints in wet underwater welding.

Keywords: *wet underwater welding, external electromagnetic actions, composition, weld microstructure*

In study [1] it is established that application of external electromagnetic actions (EEMA) under the conditions of wet underwater welding allows improving the strength and ductility of welds by 10 and more than 60 %, respectively, this being indicative of improvement of the welded joint quality. Improvement of mechanical properties is due to changes in the solidification processes, which is confirmed by microstructures of samples cut out of the central parts of welds. In practice brittle fractures most often occur in the HAZ metal, where the structural changes are considerable. Microhardness lowering by 15 % in this region, achieved due to EEMA, may be related to changes in the secondary microstructures (the latter assumption requires further studies). Also urgent is clarifying the possibility of weld metal composition changing under the conditions of wet underwater welding with flux-cored wire with EEMA, which may also promote improvement of the joint mechanical properties. Proceeding from the above, the objective of this study is evaluation of the influence of EEMA mode parameters on the composition and structure of weld and HAZ metal.

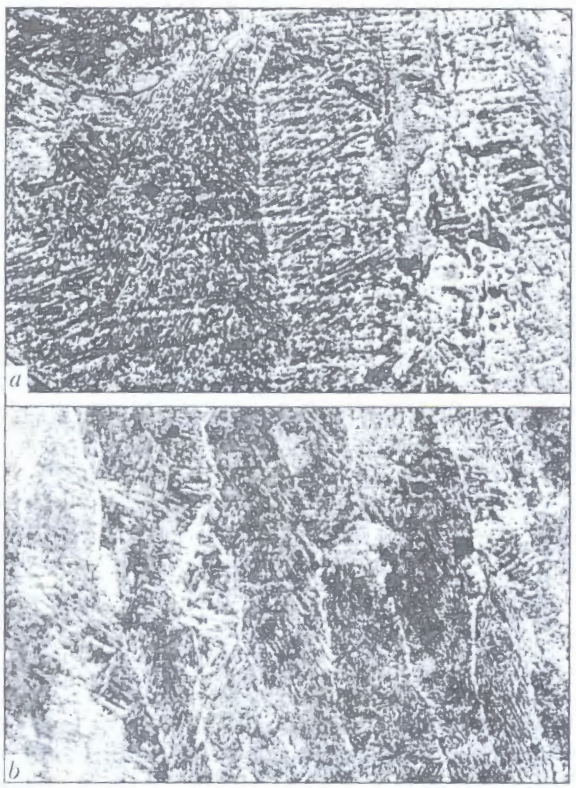

Figure 1. Microstructure of welded joints made without (*a*) and with (*b*) EEMA at reverse polarity current at B = 15 mT (×200)

Samples for investigations were produced under the conditions similar to those in study [1]. Multipass welding of samples of steel 15KhSND 14 mm thick with a V-shaped groove was performed at down to 1 m depth with PPS-AN2 flux-cored wire in the following mode: I_w = 180 A (straight and reverse polarity), U_a = 32 V, v_w = 7 m/h. Reversible axial controlling magnetic field (CMF) in the welding zone was generated using a cylindrical electric magnet placed coaxially to the nozzle. CMF induction B was adjusted using F91 control module [2]. Microstructural and spectral analysis of samples was conducted in planes parallel to the surface of plates being welded.

It is established that the microstructure of the metal of welds made in welding by the standard technology, is a cast structure consisting predominantly of upper bainite (Figure 1, *a*). In welding with EEMA, ferrite fringes form along the cast crystallite boundaries (Figure 1, *b*). EEMA application has an essential influence on the solidification process. Intensive displacement of melt flows in the entire pool volume lead to refinement of the dendrite structure, a higher dispersity being observed in welding with EEMA at reverse polarity current (Figure 1, *b*). This is related to different heat input into the welds and respective changes in the solidification rates. Qualitatively similar results were earlier obtained in welding of structural steels with EEMA in air. In [3] refinement of the structure of welds in the joints of this material class was accounted for by ramification of the protruding hard phase parts during pulsed growth period

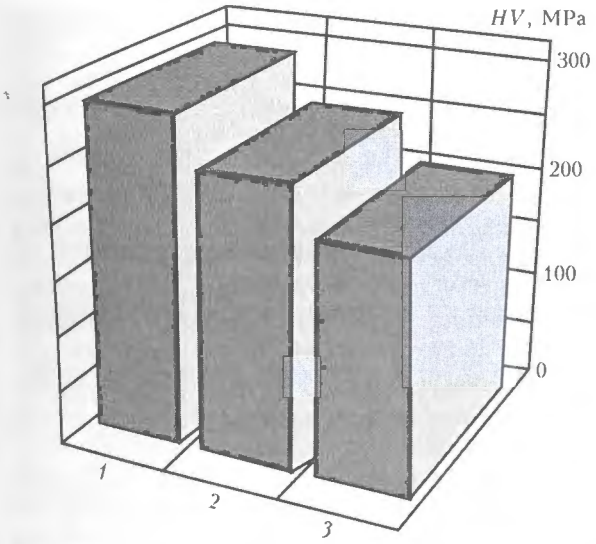

Figure 2. Influence of inductance value on microhardness of the HAZ metal: *1* — B = 0; *2*, *3* — B = 15 mT at straight (*2*) and reverse (*3*) polarity current, respectively

at higher instantaneous rates. This mechanism can also account for microstructural changes in welds under the conditions of wet underwater welding with EEMA.

Structure of HAZ metal is a ferrite-pearlite mixture and it also changes when EEMA are used, depending on the value of CMF induction and I_w polarity. Samples obtained in welding at straight polarity current I_w, are characterized by grain orientation in the heat sink direction, normal to the side surface of the weld pool. Colonies of martensite needles are visible in the structure, this leading to increased microhardness of the HAZ metal [1].

EEMA application in welding at reverse polarity current I_w allows homogenizing the HAZ metal structure, and refining it. No martensite was found in the HAZ metal at CMF induction of B = 15 mT. This is indicative of the fact that this EEMA mode is characterized by maximum intensity of hydrodynamic processes in the pool accompanied by periodical partial melting of the solidification front, and lowering of the HAZ metal cooling rate, this being confirmed by the values of microhardness at different polarity current (Figure 2).

Thus, welding with EEMA application at reverse polarity current is preferable under the conditions of wet underwater welding to produce a homogeneous structure, providing maximum improvement of the ductility and strength properties both in the weld and HAZ metal.

Spectral analysis of the studied samples showed slight differences in the composition of welds, welded

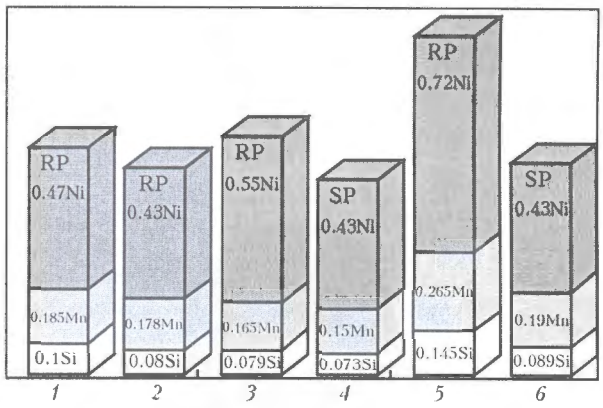

Figure 3. Change of alloying element percentage in welds at straight (SP) and reserve polarity (RP) current: *1*, *2* — B = 0; *3*, *4* — 10; *5*, *6* — 15 mT

by the standard technology (B = 0) and with application of EEMA (B = 10 and 15 mT), when CMF induction was not higher than 10 mT (Figure 3). However, at reverse polarity current increase of induction up to 15 mT was accompanied by more than 50 % increase of the content of alloying elements in the welds, which penetrated into the welds from the flux-cored wire charge. It is known [4] that in welding with EEMA the drops at the electrode tip take the shape of an ellipsoid of revolution. In this case, at increase of CMF induction heat transfer from the arc to the electrode increases exponentially, and the intensity of its melting rises, accordingly. The above effect promotes increase of the coefficient of transfer of the elements from the wire, this accounting for a change in the weld composition. This is particularly important in wet welding, as the highly-oxidizing atmosphere of the vapour-gas bubble markedly limits the possibility of weld metal alloying by elements with a high affinity to oxygen.

Thus, EEMA application under the conditions of wet underwater welding enables making a favourable impact on the weld composition, homogenizing the microstructure of weld metal and HAZ, this being an active factor in improvement of the strength and ductility properties of welded joints.

1. Ryzhov, R.N., Kozhukhar, V.A., Maksimov, S.Yu. et al. (2004) Application of external electromagnetic actions for improvement of mechanical properties of welds in underwater wet welding. *The Paton Welding J.*, **11**, 49–51.
2. Korab, N.G., Skachkov, I.O., Matyash, V.I. (1993) System of control by electromagnetic actions in welding. *Avtomatich. Svarka*, **11**, 52.
3. Yakushin, B.F., Misyurov, A.I. (1979) Increase of technological strength of welds in welding of medium-alloy steel with electromagnetic actions. *Svarochn. Proizvodstvo*, **12**, 7–9.
4. Boldyrev, A.M., Birshev, V.A., Chernykh, A.V. (1991) Specifics of electrode metal melting during welding in the external longitudinal magnetic field. *Ibid.*, **5**, 28–30.

THESIS FOR SCIENTIFIC DEGREE

Priazovsky State Technical University

Arsenyuk V.V. (PWI) defended on the 27th of September 2005 the thesis for a doctor of technical sciences degree on subject «Principles of Formation of Joints in Dissimilar Metals Using Different Pressure Welding Methods»

The thesis is dedicated to analysis and refining of notions on the kinetics and micro mechanisms of plastic deformation, peculiarities of structure formation and technologies for producing sound joints in dissimilar metallic materials at different deformation rates, as well as to development, on the basis of these notions, of recommendations for application of a particular pressure welding method and optimisation of the technological process.

The literature review presents analysis of the state-of-the-art in pressure welding of dissimilar metals. Investigations were conducted using advanced methods of physical metals science. Specific features of the effect of the state of mating surfaces on the formation of pressure welded joints in dissimilar metals are considered. Described are peculiarities and kinetic mechanisms of structural and chemical heterogeneities, phase formation and plastic deformation occurring in the bond zone between dissimilar metals (Al–Fe, Al–Cu, Cu–Ti, Ti–Fe, etc.) in vacuum diffusion bonding, friction welding, vacuum percussion welding, magnetic pulse and explosion welding under the deformation conditions at rate $\dot{\varepsilon} = 1 \cdot 10^{-4} – 1 \cdot 10^{-5}$ s^{-1}. The principles of the processes of accelerated mass transfer in metals under high-rate loading were studied.

It was established for the first time that the rate of deformation is the main factor that determines peculiarities of structure and changes in the deformation mechanisms.

It was found that continuous layers of intermetallics localised on the contact plane are formed at low deformation rates (vacuum diffusion bonding, friction welding). Deformation at a high rate (vacuum percussion welding, magnetic pulse welding, explosion welding) is accompanied by the formation of fine phase precipitates (from ultra fine to those measuring several micrometers). It is shown that the depth of the zone of localisation of plastic strain depends upon the deformation rate and amounts to 25–200 μm, the extent of its localisation varying from about 40 to 1000 %.

New technical approach was developed to analytical evaluation of strength and ductile properties of the joining zone, allowing for structural factors. A new metals science approach to evaluation of weldability of dissimilar metals is offered.

Technological recommendations were worked out, and optimal conditions and techniques were identified for joining various combinations of dissimilar metals by different pressure welding methods, which are commercially applied for the manufacture of components and parts for industrial plants and systems. Applicability of different pressure welding methods for joining dissimilar hard-to-weld materials was estimated, thus allowing selection of an optimal welding method and technological parameters.

ADVANCE BOOK INFORMATION

FORTHCOMING BOOK INFORMATION

Vladimir I. Makhnenko, Viktor E. Pochynok. STRENGTH CALCULATION OF WELDED JOINTS WITH CRACK-LIKE IMPERFECTIONS.

Approx. 300 pp., 165×235 mm, hardback. November 2005. US$ 90

In this manuscript, the idea of the fitness-for-purpose concept is used to improve strength calculations of welded joints with crack-like imperfections caused by structural or technological factors. These include welded joints with fillet, spot, slot and butt welds having sharp fissures brought by geometry of the elements welded and limited sizes of the weld sections. Such joints are widely encountered in modern general-purpose welded structures used in civil building, shipbuilding, automobile industries, etc.

The welded joints just mentioned do not usually cause problems for structures of relatively ductile materials with small-to-medium thicknesses of component sections, and operating under predominantly static loading. However, the use of new structural materials, especially high-strength steels and aluminum alloys, etc., large cross sections of structural elements, and loading with alternate loads, requires a certain caution to be taken. Nonetheless, the technological advantages that these joints produce attract an interest in their use, of course, when it does not cause any harm to the structure safety and its residual service life.

Performing strength calculations based on the fitness-for-purpose criterion for the joints encountered in general-purpose structures, allows ensuring the requirements concerning the service life-time. However, there is a difficulty of implementing such calculations in wide engineering practice. As shown by the authors, a successful implementation of the mentioned concept for general-purpose welded joints and for wide range of users is possible only when it is based on the use of corresponding computer systems with friendly user interface, which do not require a user to have a special knowledge in fracture mechanics, deformation mechanics, numerical methods, etc. Such systems are to be portable and efficient, i.e. calculations of appropriate section sizes or verification of strength of specific joints should be done promptly. In turn, it requires development of numerical procedures and creation of specialized databases that simplify and accelerate calculations.

Viktor Ya. Kononenko. TECHNOLOGIES OF UNDERWATER WET WELDING AND CUTTING.

Approx. 140 pp., 140×200 mm, softback. December 2005. US$ 40

The book deals with the features of arcing, metal transfer and joint formation in consumable-electrode wet underwater welding. Principles of development of coated electrodes and self-shielded flux-cored wires for underwater welding and cutting are established. Characteristics of welding consumables and mechanical properties of weld metal are given. Some types of joints, procedure of preparation and fit-up for welding, possible defects of the joints and methods to prevent their formation are described.

Information on characteristic damage to the underwater metal structures is generalized, and technological solutions are given, which have been implemented during restoration of their performance, using wet processes of underwater welding and cutting. The book gives the characteristics of the equipment for implementation of underwater arc welding process.

The main processes of thermal underwater cutting are presented, and characteristics of consumable materials and equipment for its implementation are described. Examples of work performance using underwater cutting are given.

The book is designed for scientific and engineering-technical personnel, qualified welders-divers involved in design, fabrication and repair of underwater constructions.

The book is written by a specialist, who is developing electrode materials and technologies and has a vast experience of practical work under the water.

ADVANCE BOOK INFORMATION

TITANIUM: Titanium and its alloys. Technologies. Equipment. Production. Electrometallurgy. Welding

Approx. 180 pp., 200×290 mm, softback. December 2005. US$ 50

The collection presents papers on electrometallurgy and welding of titanium and its alloys published between 2002 and 2005 in «Advances in Electrometallurgy» and «The Paton Welding Journal» journals. The authors of the papers are scientists and specialists in the field of titanium and its production, known in Ukraine and abroad. The collection is designed for a broad range of readers dealing with the problems of production, processing and use of titanium.

ORDER RORM

Please return to:

International Association «Welding»,
11, Bozhenko str., Kiev, 03680, Ukraine
Tel.: (38044) 287 6757, 287 6049, 529 2623
Fax: (38044) 287 4677
E-mail: journal@paton.kiev.ua; tomik@mac.relc.com

Please send me:

❑ Vladimir I. Makhnenko, Viktor E. Pochynok «Strength Calculation of Welded Joints with Crack-Like Imperfections». US$ 90, postage included

❑ Viktor Ya. Kononenko «Technologies of Underwater Wet Welding and Cutting». US$ 40, postage included

❑ «Titanium». Collection of Scientific Paper. US$ 50, postage included

How to Pay and Payment Details

❑ By bank transfer (or mail a cheque) into our account
№ 2600801283433
UKREXIMBANK, Kiev, Ukraine
S.W.I.F.T.: EXBSUAUX
CORR. ACC. #04-094-227
Bankers Trust Company,
New York, U.S.A.
S.W.I.F.T.: BKTR US 33

❑ Please Invoice

❑ Your Details
Name _____

Organization _____

Address _____

Signed _____ Date _____

UNIVERSAL KL-115 MACHINE FOR EBW WITH 7-AXIS MOTION SYSTEM

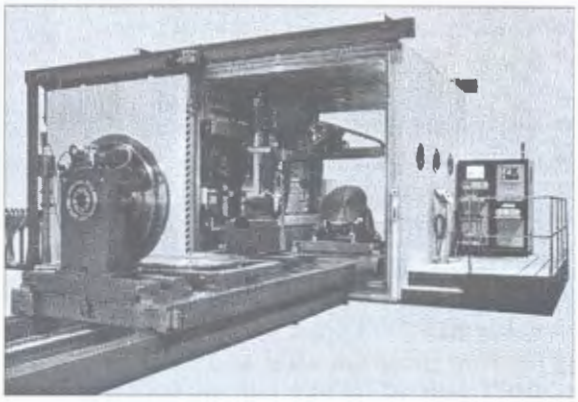

Vacuum chamber and slide doors have two shells, namely a stainless inner shell and outer shell of structural steel connected to each other by frames. The produced box section allows a significant lowering of the structure metal content with preservation of a high rigidity, that guarantees a high accuracy of the displacement mechanisms.

The cantilever mechanism of EB gun displacement allows moving the gun along *X*, *Y*, *Z* axes, as well as rotating it in *X*–*Y* (±90°) and *X*–*Z* (by 90°) planes.

Programmable CNC 7-axes motion control, simultaneous control of 4 coordinates.

Unique high voltage control regulator with vacuum tube detects and suppresses arcing, allowing continuous welding without discontinuties and defects.

Welding control with real time automatic seam tracking by RASTR secondary electron emission system.

Beam analysis system allows the operator to determine actual beam operating conditions prior to welding start and reduce weld parameter development time.

Lanthanum hexaboride cathodes are used for long life of more than 40 h at the power 60 kW, and prevent «beam walking» when the focus position is changed.

PC and programmable controllers are used.

Machine design

The vacuum chamber is a rectangular double-wall welded structure. Two sliding doors are moved letting workpiece to be loaded into the vacuum chamber for the welding. Movement mechanism of the EB gun has three moving axes: *X*–*X*, *Y*–*Y* and *Z*–*Z*. Accuracy of gun linear positioning along *X*–*X*, *Y*–*Y*, *Z*–*Z* axes is not less than ±0.1 mm. EB gun is mounted on the table along *Y*–*Y* axis and has two rotating axes: rotation — *QG* axis and tilt — *VG* axis. Accuracy of EB gun angular movement on *QG* and *VG* axes is better than 0.1°. Screws in ball-and-screw pairs, linear guides of all linear modules are covered by protective shields or encased to protect them from depositions.

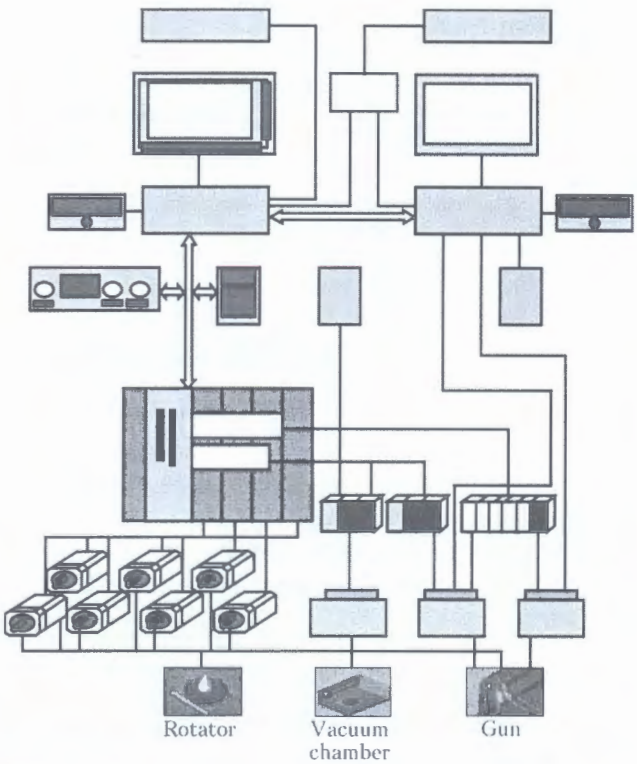

Machine is equipped with three rotators: with horizontal rotation axis, with vertical rotation axis and with tilt rotation axis. Two platforms are functionally designed for the placement of machine mechanisms, mounting of workpieces, their assembling, control of joints to be welded as well as for their transportation into the chamber. This allows assembling and fitting up of workpieces to be done on the one platform while welding of other workpieces is being done on the other platform.

Control system is based on open architecture principles of automation systems for machine tools.

Control system provides implementation of the following features:

- programmable CNC of 7-axes motion (3 linear gun axes, 2 rotary gun axes and 2 rotary rotator axes);
- any 4 axes of the 7 CNC axes selectable for coordinated contouring CNC of motions with linear and circular interpolations;
- full integration of all beam parameters with CNC control;
- operating in a fully automated mode, a semi-automated mode with user defined start and stop locations, and a manual mode including jog function;
- Windows oriented GUI (User Graphic Interface) for programming, system diagnostics, data logging, seam tracking, seam/weld viewing, and real-time process control;
- sequencing blocks of programmed data together into master programs;
- automatic real time teaching and seam tracking via seam tracking system RASTR;
- off-line programming and remote communication;
- PLC control of vacuum system and power supply in all modes;
- diagnostic tools for trouble-shooting faults or errors;
- data logging of process control parameters.

Main technical parameters for KL-115 machine

Overall machine sizes (l × w × h), mm	15960 × 10390 × 3740
Weight, t	48
Vacuum chamber internal sizes (l × w × h), mm	4040 × 2950 × 2950
Working pressure in chamber, Torr	not lower than $1 \cdot 10^{-4}$
Time before working pressure in chamber and gun is obtained, min	max 25
EB gun movements with positioning accuracy of ±0.1 mm along coordinates *X–X*, *Y–Y*, *Z–Z*, mm	3000, 1800, 2000
Gun tilt angle in *X–Z* plane, deg	90
Gun rotation angle with 0.1° accuracy in *X–Y* plane, deg	not less than ±90
EB gun traveling speed along linear coordinates, mm/s	1.66–33.3

Electron beam gun and power supply

Power, kW	60
Accelerating voltage, kV	$60 \pm 0.5 \cdot 10^{-2}$
Beam current, mA	1–1000
Cathode life, h	40
Beam deflection angle, deg	±3.5

Technical parameters provided by the Buyer

Mains	380 V, 50/60 Hz
Consumed power, kV·A	max 250
Cooling water flow rate at temperature of 20 °C and pressure of 4 kg/cm^2, l/h	2630
Compressed air pressure, kg/cm^2	6

UNIVERSAL KL-118 MACHINE FOR EBW WITH 7-AXIS MOTION SYSTEM

Vacuum chamber and slide doors have two shells, namely a stainless inner shell and outer shell of structural steel connected to each other by frames. The produced box section allows a significant lowering of the structure metal content with preservation of a high rigidity, that guarantees a high accuracy of the displacement mechanisms.

The cantilever mechanism of EB gun displacement allows moving the gun along *X*, *Y*, *Z* axes, as well as rotating it in *X–Y* (±90°) and *X–Z* (by 90°) planes.

Programmable CNC 7-axes motion control with the capability of simultaneous control of 4 coordinates.

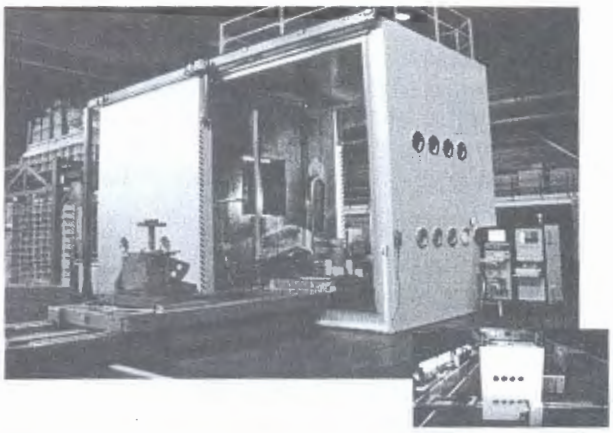

Unique high-voltage control regulator with vacuum tube detects and suppresses arcing, allowing continuous welding without discontinuties and defects.

Welding control with real time automatic seam tracking by RASTR secondary electron emission system.

Beam analysis system allows the operator to determine actual beam operating conditions prior to welding start and reduce weld parameter development time.

Lanthanum hexaboride cathodes are used for long life of more than 40 h at 60 kW power, preventing «beam walking» when the focus position is changed.

PC and programmable controllers are used.

Machine design and parameters

The vacuum chamber is a rectangular double-wall welded structure. Two sliding doors are moved letting workpieces to be loaded into the vacuum chamber for the welding. Movement mechanism of the EB gun has three moving axes: *X–X*, *Y–Y* and *Z–Z*. The accuracy of gun linear positioning along *X–X*, *Y–Y* and *Z–Z* axes is ±0.1 mm. EB gun is mounted on the table along *Y–Y* axis and has two moving axes: rotation – *QG* axis and tilt – *VG* axis. Accuracy of EB gun angular movement on *QG* and *VG* axes is better than 0.1°. Screws in ball-and-screw pairs, linear guides of all linear displacement modules are covered by protective shields or encased to protect them from depositions.

Machine is equipped with three rotators: with horizontal rotation axis, with vertical rotation axis and with tilt rotation axis. Two platforms are functionally designed for placement of machine mechanisms, mounting of workpieces, their assembling, control of assembled butt joints, and their transportation into the chamber. This allows saving the work time during assembling and fit up of workpieces on the one platform due to welding of other workpieces being done on the other platform.

Control system is based on open architecture principles of automation systems for machine tools.

Control system provides implementation of the following features:

- programmable CNC of 7-axes motion (3 linear gun axes, 2 rotary gun axes and 2 rotary rotator axes);
- any 4 axes of the 7 CNC axes selectable for coordinated contouring CNC of motions with linear and circular interpolations;
- full integration of all beam parameters with CNC;
- operating in a fully automated mode, a semi-automated mode with user defined start and stop locations, and a manual mode including jog function;
- Windows oriented GUI (User Graphic Interface) for programming, system diagnostics, data logging, seam tracking, seam/weld viewing, and real-time process control;
- sequencing blocks of programmed data together into master programs;
- automatic real time teaching and seam tracking via seam tracking system RASTR;

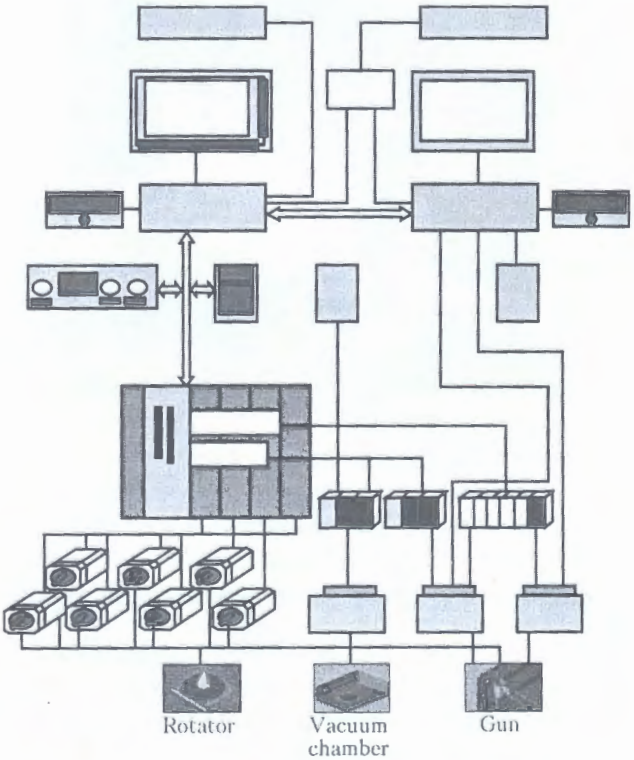

- off-line programming and remote communication;
- PLC control of vacuum system and power supply in all modes;
- diagnostic tools for trouble-shooting faults or errors;
- data logging of process control parameters.

Main technical parameters for KL-118 machine

Overall machine sizes (l × w × h), mm	15070 × 11690 × 6610
Weight, t	51
Vacuum chamber internal sizes (l × w × h), mm	3800 × 3600 × 4800
Working pressure in chamber, Torr	not higher than $1 \cdot 10^{-4}$
Time before working pressure in chamber and gun is obtained, min	max 25
EB gun movements with positioning accuracy ±0.1 mm along coordinates *X–X*, *Y–Y*, *Z–Z*, mm	2800, 2500, 3700
Gun tilt angle in *X–Z* plane, deg	90
Gun rotation angle with accuracy 0.1° in *X–Y* plane, deg	not less than 90
EB gun traveling speed along linear coordinates, mm/s	1.66–33.3

Electron beam gun and power supply

Power, kW	60
Accelerating voltage, kV	$60 \pm 0.5 \cdot 10^{-2}$
Beam current, mA	1–1000
Cathode life-time, h	40
Beam deflection angle, deg	±3.5

Technical parameters provided by the Buyer

Mains	380 V, 50/60 Hz
Consumed power, kV·A	max 300
Cooling water flow rate at temperature of 20 °C and pressure of 4 kg/cm^2, l/h	4566
Compressed air pressure , kg/cm^2	6

UNIVERSAL MACHINE FOR ELECTRON BEAM WELDING *MODEL 101*

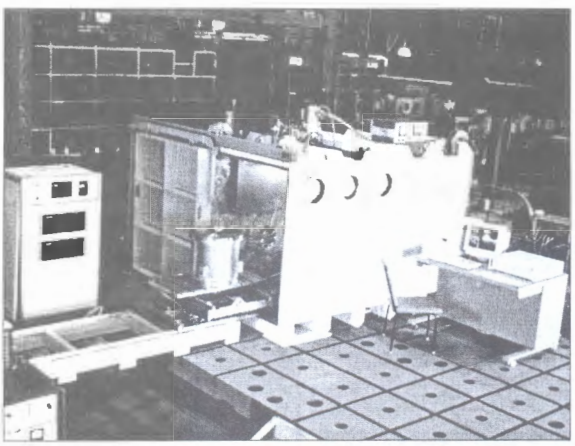

Universal production machine for EBW of a wide range of cylindrical and flat workpieces.

PC and programmable controllers are used.

Real-time seam tracking and monitoring of EBW process by RASTR-3 system on the basis of secondary electron emission.

Power source with the electron tube flashless system.

5, 15, 30 or 60 kW electron beam gun and power source at 60 kV.

Machine design

• Work chamber has two sliding doors. For loading and unloding, the workpiece table is moved out of the work chamber onto the runout platform. This is especially necessary for welding of large heavy workpieces with commensurately large clamping devices. The table accommodates a 2-axis-manipulator for welding of flat workpieces or a rotator for circumferential welding. The electron beam gun with an optical viewing system is mounted in one of the three openings on the upper cover of the chamber.

• The gun has an independent turbomolecular pumping system. The cathode area is isolated by a vacuum valve to keep the gun under vacuum when the work chamber is vented. Precision of the guidance and drive sysems equals that of the high-precision machine tools operation with tolerances in the hundredth-of-a-millimeter range.

Technical data for machine of model 101

Mains	50 kV·A, 380 V ± 10 %, 50–60 Hz
Cooling water flow rate at < 25 °C, l/min	23
Vacuum chamber inner dimensions, m	1.1 × 2.4 × 1.4
Time of pumping down at the vacuum of $2 \cdot 10^{-4}$ Torr, min	8
Workpiece weight, kg	max 500

Application. Welding of high-precision structures; welding and repair in gas turbine engine fabrication; welding of a wide range of power engineering products.

UNIVERSAL MACHINE FOR ELECTRON BEAM WELDING *MODEL 102*

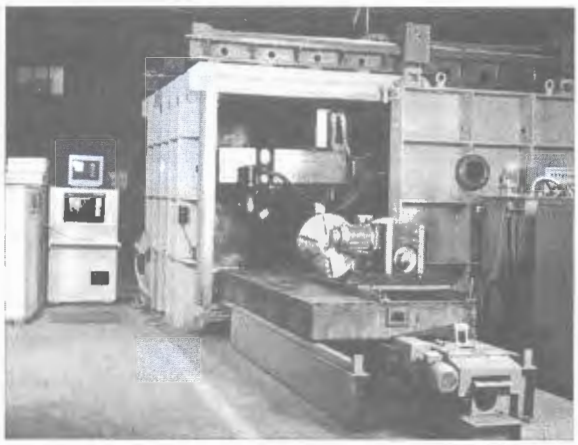

- Universal production machine for EBW of a wide range of cylindrical and flat workpieces.
- PC and programmable controllers are used.
- Real-time seam tracking and monitoring of EBW process by RASTR-3 system on the basis of secondary electron emission.
- Power source with the electron tube flashless system.
- Mobile type 15, 30 or 60 kW electron beam gun at 60 kV.

Machine design

The work chamber has two sliding doors. For loading and unloding, the workpiece table is moved out of the work chamber onto the runout platform. This is especially necessary for welding of large heavy workpieces with commensurately large clamping devices. The table accommodates the universal rotator with horizontal or vertical axis, and back centre. The EB gun 3-axis-manipulator has the travelling distance in X-direction — 2000 mm, in Y-direction — 800 mm and in Z-direction — 800 mm. Precision of the guidance and drive systems equals that of the precision machine tools operation with tolerances in the hundredth-of-a-millimeter range.

The gun can be mounted in any spatial position and has an independent turbomolecular pumping system. The cathode area is isolated by a vacuum valve to keep the gun under vacuum when the work chamber is vented.

Technical data for machine of model 102

Set power	130 kV·A, 380 V ± 10 %, 50–60 Hz
Cooling water flow rate at < 25 °C, l/min	20
Vacuum chamber inner dimensions, m	2 × 2 × 3
Time of evacuation at the vacuum of $2 \cdot 10^{-4}$ Torr, min	20
Workpiece weight, kg	max 1000

Application. Welding and repair in turbine engine fabrication; selection of welding technology for a wide range of workpieces.

MACHINE FOR PRECISE EBW OF SMALL WORKPIECES
MODELS 103/112

Universal production machines for precise EBW of a wide range of small cylindrical and flat workpieces.

PC and programmable controllers are used.

Workpiece visualization by video contron unit (VCU) on the basis of secondary electron emission, magnification ×10, or using RASTR system for real-time seam tracking.

Power source with electron tube flashless system.

Up to 15 kW beam power at 60 kV.

Machine design

• The work chamber has front doors. The main $X–X$ table accommodates the second $Y–Y$ table. Mounted on the table is a universal rotator with horizontal or vertical axis, and back centre.

• Each table has the travelling distance of 200–250 mm. Precision of the guidance and drive systems equals that of precision machine tools operation with tolerances in the hundredth-of-a-millimeter range.

• The gun can be mounted in any spatial position (on upper or side wall), and has an independent turbomolecular pumping system. The cathode area is isolated by the vacuum valve to keep the gun under vacuum when the work chamber is vented.

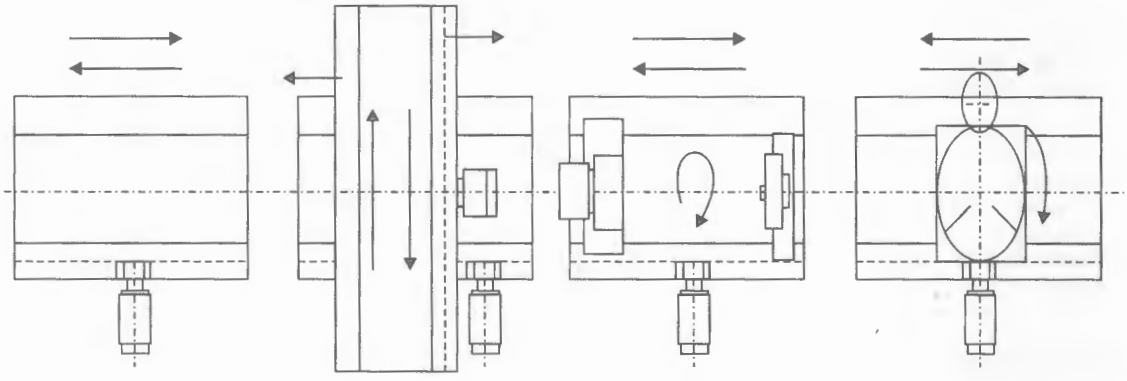

Technical data for machines of model 103/112

Vacuum chamber inner dimensions, mm	500 × 500 × 500
Main vacuum system based on KYKY turbomolecular pump F250/1500	
Time of pumping down to the vacuum of $5 \cdot 10^{-4}$ Torr, min	2
Vacuum in the gun, Torr	$2 \cdot 10^{-5}$
Time of pumping down to the vacuum of $1 \cdot 10^{-4}$ Torr, min	3
Workpiece length (height), mm	up to 200
Workpiece diameter, mm	2–250
Cooling water flow rate at < 25 °C, l/min	4.5

MACHINE FOR EBW OF STEAM GATE VALVES
MODEL 105

- Specialized machine for EBW of steam gate valves with wall thickness up to 90 mm.
- EB cladding of compression surfaces in deep holes.
- PC and programmable controllers are used.
- Real-time seam tracking and monitoring of EBW process by RASTR-4 system on the basis of secondary electron emission.
- Gun and power source with the electron tube flashless system of up to 60 kW power at 60 kV.

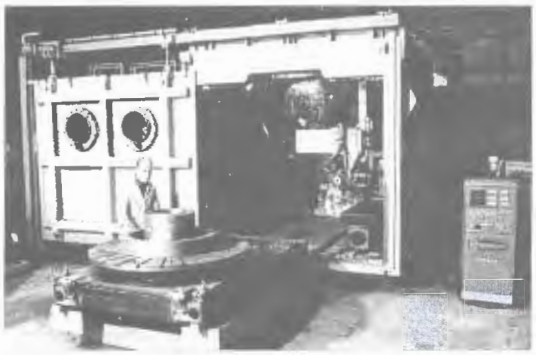

Welded full-scale samples, δ = 90 mm

Machine design

Work chamber has one sliding door. For loading and unloading, the workpiece table is moved out of the work chamber onto the runout platform. This is especially necessary for welding large heavy workpieces with commensurately large clamping devices. The table accommodates a universal rotator with vertical or horizontal axis. The electron gun 3-axis-manipulator moves in X–X', Y–Y' and Z–Z' directions. Precision of the guidance and drive systems equals that of the precision machine tools operation with tolerances in the hundredth-of-a-millimeter range.

The gun can be mounted in any position, has an independent turbomolecular pumping system. The cathode area is isolated by the column vacuum valve to keep the gun under vacuum when the chamber is vented. The gun accommodates the system of powder feed for cladding of compression surfaces.

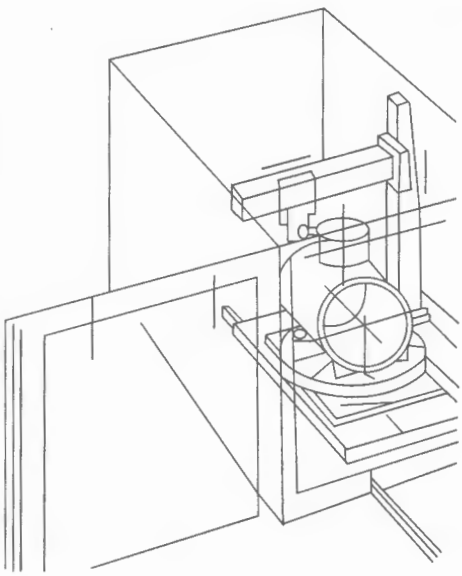

Technical data for machine of model 105

Vacuum chamber inner dimensions, mm	3000 × 2500 × 2700
Operating vacuum, Torr	$2 \cdot 10^{-4}$
Time of chamber pumping down, min	25
Beam power at 60 kV, kW	60
Thickness of welded steels, mm	max 90
Workpiece weight, kg	max 3000
Diameter of workpiece, mm	max 1500
Length of workpiece, mm	max 1700
Gun displacement:	
X–X'	1800
Y–Y'	600
Z–Z'	900

UNIVERSAL MACHINE FOR ELECTRON BEAM WELDING
MODEL 106

- Universal production machine for EBW of a wide range of cylindrical and flat workpieces.
- PC and programmable controllers are used.
- Real-time seam tracking and monitoring of EBW process by RASTR-4 system on the basis of secondary electron emission, accuracy of ±0.2 mm.
- Power source with the electron tube flashless system.
- 5, 15, 30 or 60 kW electron beam gun and power source at 60 kV.

Machine design

The work chamber has a front sliding door. For loading and unloding, the workpiece table is moved out of the work chamber onto the runout platform. This is especially necessary for welding large heavy workpieces with commensurately large clamping devices. The table accommodates a universal rotator with horizontal or vertical axis, and a back centre. The EB gun 3-axis-manipulator has the travelling distance in $X-X'$-direction — 1600 mm, in $Y-Y'$-direction — 800 mm and in $Z-Z'$-direction — 900 mm. Precision of the guidance and drive systems equals that of precision machine tools operation with tolerances in the hundredth-of-a-millimeter range. The gun can be mounted in any position, and has an independent turbomolecular pumping system. The cathode area is isolated by a vacuum valve to keep the gun under vacuum when the work chamber is vented.

Technical data for machine of model 106

Vacuum chamber inner dimensions, mm	2500 × 2500 × 2500
Time of pumping down at the vacuum of $5 \cdot 10^{-4}$ Torr, min	25
Vacuum in the gun, Torr	$2 \cdot 10^{-5}$
Workpiece weight, kg	max 1000
Maximum depth of material penetration at 30 kW power beam, mm:	
steel	75
titanium and its alloys	110
aluminium alloys	150
Machine total weight, kg	24500

Application. Welding and repair a wide range of workpieces.

MACHINE FOR CONTINUOUS ELECTRON BEAM WELDING OF BIMETALLIC SAW BLADE STRIP
MODEL EWS-101

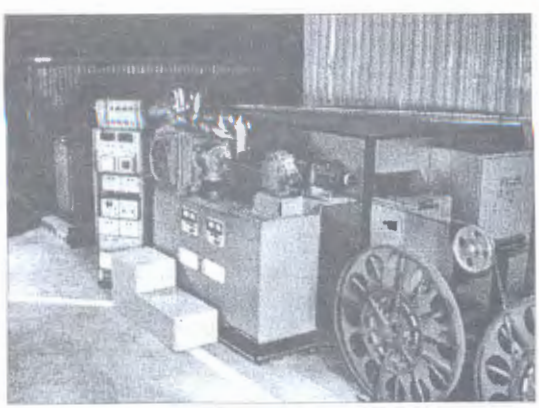

Electron beam with a high power density ensures extremely narrow (0.3 mm) and parallel welds.

High-precision strip alignment device mounted on a movable chamber wall reduces the machine idle period during adjustment operations.

Double-reel unwinding-winding system permits immediate changeover of strip coils while welding.

Two EB guns (of 60 and 120 kV) are intended for making one weld or simultaneous welding of two continuous welds.

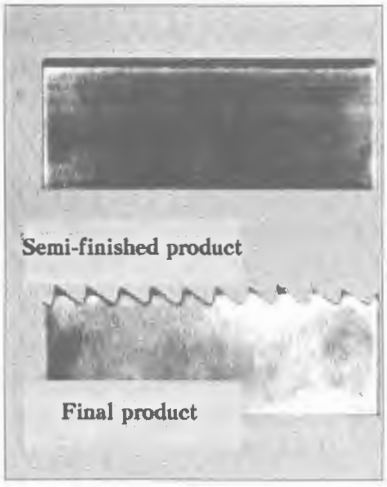

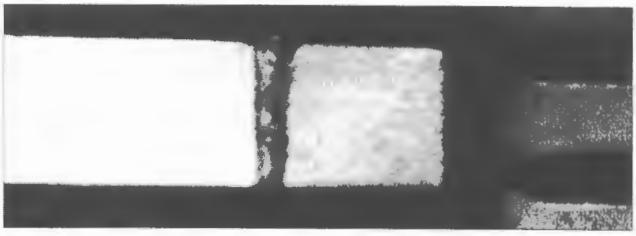

High-speed + alloyed structural steel, 1.2 mm dia.

Machine design

The work chamber of the stripwelder is equipped with a vacuum unit of so-called air-to-air system, which comprises entry and exit vacuum locks. High-precision strip alignment device is mounted inside the chamber on a door, movable along the welding direction. The latter ensures the ease of guiding device adjustment for new strip dimensions, as well as cleaning of the chamber. The EB guns have independent turbomolecular pumping systems. The cathode area is isolated by the vacuum valve to keep the gun under vacuum when work chamber is vented.

Technical data for machine of model EWS-101

Mains	380 V ± 10 %, 50 Hz
Cooling water flow rate at < 25 °C, l/min	20
Thickness of strips, mm	0.6–1.2
Total width of strips, mm	up to 40
Welding speed, m/min	up to 15

Application. Continuous EBW of bimetal strips (high-speed steel + alloyed structural steel) for manufacture of hack and band saws.

MACHINE FOR EBW IN LOCAL VACUUM OF CUT-IN ELEMENTS OF LARGE DIAMETER SHELLS
MODEL EWS-104

Specialized unit for electron beam welding in local vacuum of cut-in elements of large-diameter shells from high-strength aluminium alloys of Al–Cu, Al–Mg–Mn, Al–Mg–Li and Al–Cu–Mg–Si system.

PC and programmable controllers are used.

Visualization of the weld region by VCU system on the basis of secondary electron emission, ×10-magnification.

High stability power source with electron tube flashless system.

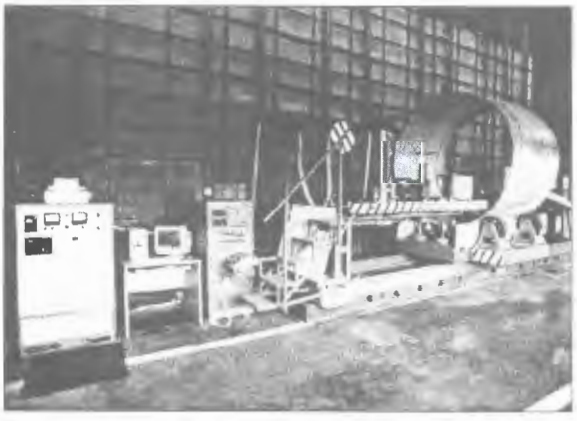

Up to 15 kW beam power at 60 kV accelerating voltage.

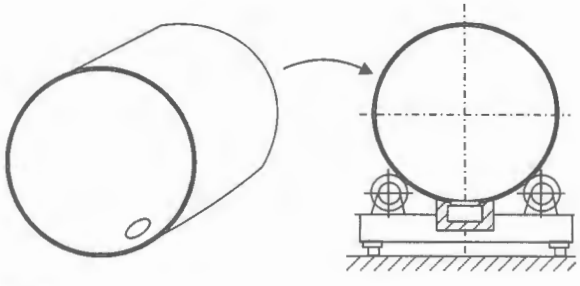

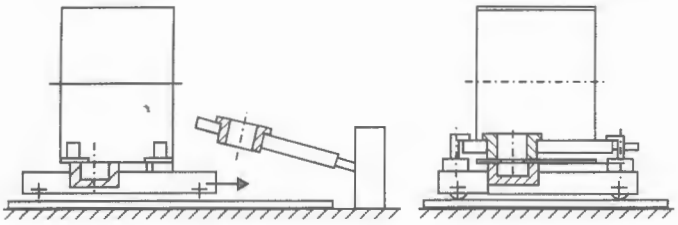

Application of electron beam welding instead of argon-arc welding allows the residual stresses in the cut-in element zone to be lowered by 5 to 6 times.

Machine design

Electron beam machine consists of 4 stations in which the following technological operations are perfomed in succession:

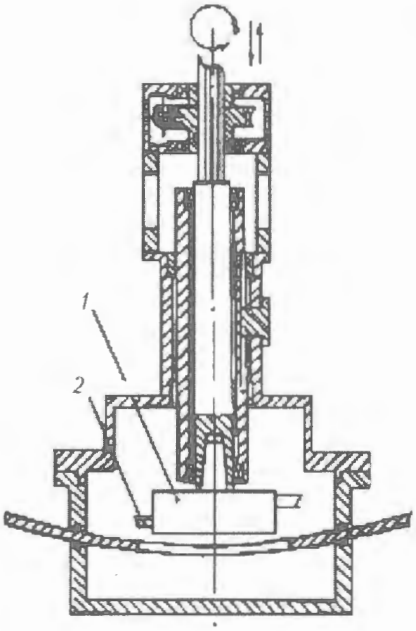

• placing the shell (with the already cut out hole of small diameter in the place of the subsequent welding-in of the cut-in element) on the carriage with the lower vacuum chamber sealed with a circumferential vacuum seal relative to the item;

• movement of the carriage with the shell and lower vacuum chamber under the raised upper vacuum chamber, lowering of this vacuum chamber and pressing of both vacuum chambers to each other and the shell with 2500 kg force using a pneumatic system;

• movement of the shell with the compressed vacuum chambers to the position of the milling head, fastening the milling head relative to the upper vacuum chamber;

• boring with the milling head of the precise final hole in the shell to accommodate the cut-in element. Four cutters *2* are mounted on the rotating mill *1*. By moving the rotating spindle up and down the operator performs manual boring of the hole in the shell to the assigned diameter;

• preparation of the butt edges for welding, mounting and mechanical fastening of the cut-in element *3* in the bored hole in the shell;

• movement of the shell with the cut-in element to the position of welding under the welding module and their fastening relative to each other using a pneumatic device;

• use of the automatic control system to create the working vacuum in the spaces of lower *4* and upper *5* chambers and of electron beam gun *6* mounted on cover *8* rotating around vacuum seal *7*. The speed of revolution of cover *8* around its axis, including the welding speed, is assigned by drive *9*;

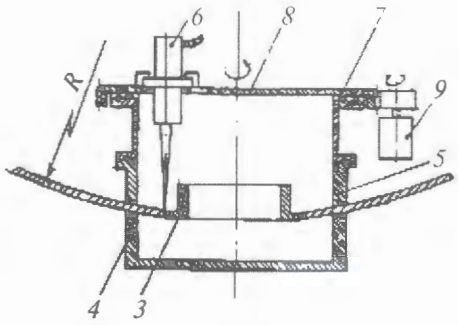

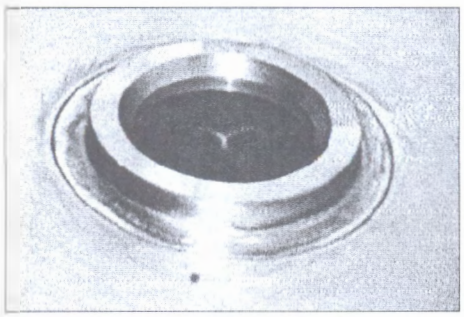

• checking of the accuracy of combining the electron beam with the butt using VCU (×10 magnification);

• successive tack welding of the cut-in element to the shell with control from the ACS, then welding of the circumferential weld around the entire perimeter with overlapping and fading out of the electron beam power at the end of welding, visual control of the quality of weld surface formation using VCU;

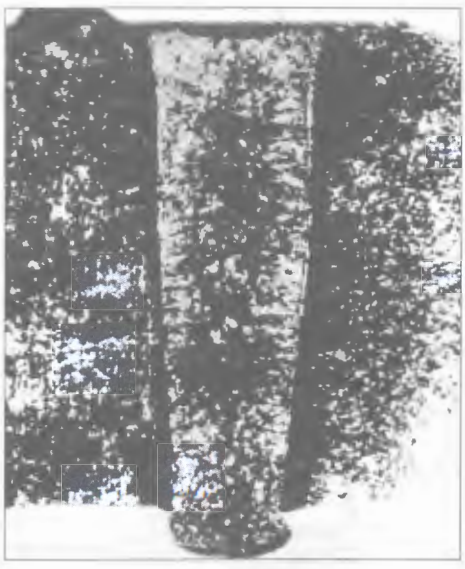

Appearance of a welded cut-in element and transverse macrosection of the welded joint (×20)

• if defects of weld formation are found both with the VCU and after unsealing the cut-in element, repair operations can be performed by programmable secondary electron beam remelting of individual zones or the entire circumferential weld;

• use of replaceable components and fixtures enables readjustment of the machine for welding the cut-in elements in a broad range of diameters from ten to hundreds of millimeters;

• machine design will provide reliable protection of service personnel from X-ray radiation during welding.

Technological results. The developed technology of electron beam welding of cut-in elements of shells from high-strength aluminium alloys provides the formation of welded joints without undercuts, cracks or blowholes.

X-ray control of the circumferential welded joint quality confirms the absence of porosity, microcracks or other defects. The coefficient of welded joint strength is equal to not less than 0.8 without any post-weld heat treatment. The residual strain in the shell after welding does not exceed 0.7 mm against 4 mm for the case of argon-arc welding.

Technical data for machine of model EWS-104

Set power, кВ·А	18
Welding speed, m/h	30–90
Time for preparation and welding of one circumferential butt, min	25
Vacuum in the welding chamber, Torr	$1 \cdot 10^{-4}$
Vacuum in the gun, Torr	$5 \cdot 10^{-5}$
Machine overall dimensions (l × w × h), mm	10000 × 5500 × 2200
Weight, t	not more than 6

CONTINUOUS TRIMETALLIC STRIP WELDER *MODEL EWST*

Two EB guns are intended for two simultaneous welds performance.

Power source with electron tube flashless system.

In-line air-to-air vacuum exhausting system (up to $1 \cdot 10^{-3}$ mm Hg vacuum in the work chamber).

Continuous quality inspection of welds by Foucault current.

Strips alignment device ensures their precise positioning while welding. EB guns have an independent turbomolecular pumping system. The cathode area is isolated by the vacuum valve to keep the gun under vacuum when working chamber is vented. By a special order the stripwelder is supplied with an automatic seam tracking system and CNC of welding parameters.

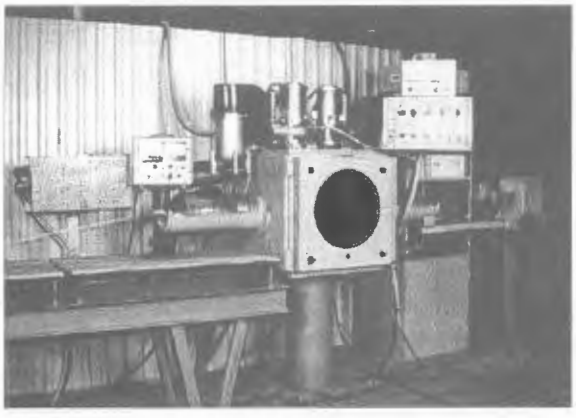

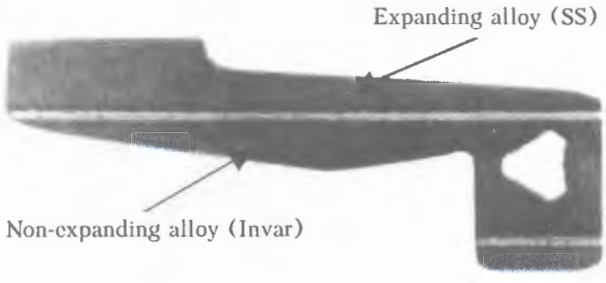

Technical data for machine of model EWST

Set power at 50–60 Hz, V	380 ± 10 %
Cooling water flow rate at < 25 °C, l/min	20
Time of pumping down at the vacuum of $1 \cdot 10^{-3}$ mm Hg, min	8
Capacity:	
thickness of strips, mm	0.8–1.0
total width of strips, mm	up to 80
welding speed, m/min	up to 10

Applications. Continuous EBW of trimetallic strip (stainess steel–Invar–stainless steel) used for positioning of a temperature-independent shadow mask in colour TV telescope tubes.

Final product – thermo-deformable bimetallic support for shadow mask of colour TV telescope tube.